REGULATION OF THE HUNTINGTIN INTERACTING PROTEIN 1 (HIP1) GENE

by

Chiron Wesley Graves

A dissertation submitted in partial fulfillment
of the requirements of the degree of
Doctor of Philosophy
(Cellular and Molecular Biology)
in The University of Michigan
2009

Doctoral Committee:

Associate Professor Theodora S. Ross, Chair
Professor Andrzej A. Dlugosz
Associate Professor John V. Moran
Assistant Professor Peter C. Lucas
Assistant Professor Joann Sekiguchi

To Charles Edward Graves,

my father, my mentor and my inspiration!

ACKNOWLEDGEMENTS

First off, I want to thank my thesis advisor, Theodora S. Ross. She provided me with the encouragement and the intellectual freedom to pursue this project and her patience with me as I "found my way" has been instrumental in my development as a scientist and a scholar. Most importantly, her scientific enthusiasm and sense of humor was a joy to be around. I would also like to thank my thesis committee members, Andrzej A. Dlugosz, John V. Moran, Peter C. Lucas and Joann Sekiguchi for their time and guidance throughout this project.

I would like to thank fellow Ross labmates, Steven T. Philips, Sarah V. Bradley, Katherine I. Oravecz-Wilson, Lina Li and Alice Gauvin, for their contributions to chapter 2 of this thesis, which was published in modified form:

> Graves, C. W., Philips, S. T., et al. (2008) "Use of a cryptic splice site for the expression of huntingtin interacting protein 1 in select normal and neoplastic tissues." Cancer Research 68(4): 1064-1073.

Additionally, I would like to thank them, as well as Heather Ames and Brendan Crawford, for their friendship, additional contributions to other parts of this thesis and support throughout this journey. Thanks to the Day lab for equipment use, cells, samples reagents and friendship when I needed them. Thanks to the Zhang lab for the use of their quantitative PCR machine. Thanks to the Robbins and Lucas labs for allowing me to use their luminometers. Thanks to the Keller lab for allowing me to use their Nanodrop. Thanks to the Dr. Miriam Meisler for her constructive intellectual input and for critical review of the manuscript mentioned above. I would also like to acknowledge the University of Michigan DNA Sequencing Core, which provided excellent sequencing data.

Of course my thesis research would not be possible without funding. I would like to thank all the funding sources that allowed me to pursue my research. They include the

following: The University of Michigan Cancer Biology training grant, the Rackham Merit Scholar fellowship and the Program in Biomedical Sciences predoctoral fellowship. I would also like to thank the administrators associated with these funding sources. Special thanks go to LaCheryl Wicker for her friendship and support in dealing with the multiple issues, such as not getting paid, associated with being a graduate student. Thanks to Tiffany Portes-Stone for her friendship and support, both of which have been extremely value along the way.

Thanks to Dr. Jessica Schwartz and the Cellular and Molecular Biology (CMB) Graduate Program for providing me with the intellectual environment and support to develop as a scientist and future academic scholar. Thanks to CMB administrative assistants, Claire Kolman and Cathy Mitchell for their support in preparing for seminars and recruiting weekends. It was a pleasure to work with both of you. I would also like to thank a few other programs and organizations that played a small but instrumental role in my initial development as a doctoral student. Thanks to the Summer Institute for allowing me to began my doctoral pursuit in the summer prior to my enrollment as a student. The opportunity allowed me to get back into the flow of scientific research after having been away for over 5 years. Thanks to the Association of Multicultural Scientists for providing me with a support group consisting of scientists who shared common experiences with me. Thanks to the Graduate Program in Immunology for providing me with the intellectual base for jumpstarting my doctoral studies

Most importantly, I would like to thank all my family and friends for their unconditional love and support of me through the good and bad times. Very special thanks to the five most important women in my life. To my mother, JoAnn L. Graves, for all the sacrifices she has made and all the heartache she has endured because of me. I would not be here, literally and figuratively, if it were not for her. To my wife, Folake, for allowing me to pursue my dream after our family was established and for "holding down the fort" when I was gone. I know it's been tough, but we're almost there. To my sister, Dr. Shanna L. Graves, the first in our family to earn a PhD. It's not often that a younger sibling serves as a role model for the older sibling but you have definitely been mine. The strength you exhibited during your pursuit gave me the strength and courage to continue pursuing mine. To my two girls, Kyla and Kharis for their patience with me

when we couldn't do things "as a family" because I was busy working in the lab. I hope I can still make it up to you.

Finally, I would like to thank my father, the late Charles E. Graves, who served as the best role model anyone could ever wish for. He taught me how to be a father and a man and all my dreams are a result of his influence.

TABLE OF CONTENTS

LIST OF FIGURES

ABSTRACT

Huntingtin Interacting Protein (HIP1) is a multi-domain clathrin binding protein thought to play a role in receptor-mediated endocytosis. HIP1 contains an adaptor AP180 N-terminal homology (ANTH) inositol lipid-binding domain, specific to endocytic proteins, as well as clathrin- , AP2- and actin-binding motifs. Loss of *Hip1* and its only known mammalian relative *Hip1-related* (*Hip1r*) leads to spinal defects, testicular degeneration, cataracts, adult weight loss, and early death in mice, indicating that the *Hip1* family is necessary for the maintenance of normal adult tissues.

There are conflicting reports concerning the role of HIP1 in cellular survival and proliferation. Our laboratory has found that HIP1 promotes cellular survival and transformation and therefore is involved in supporting tumorigenesis. Others have suggested that HIP1 plays a role in promoting apoptosis and this activity is the cause of neuronal cell death in Huntington's disease patients. This conflict raises the possibility that multiple isoforms of HIP1 exist and these isoforms have contrasting activities. Indeed, I have observed multiple isoforms of HIP1 using many different anti-HIP1 antibodies and western blot analysis in both mouse and human tissues.

To understand the regulation of *HIP1* we have isolated its promoter and characterized it. We have also evaluated the gene for alternative transcripts. The *HIP1* gene is a complex 31-exon gene that spans approximately 250 Kb of DNA. This complexity is highlighted by our first attempt to generate a conditional knockout allele of *Hip1*. Unexpectedly, we found expression of a mutant HIP1 protein in select tissues (lung, brain) due to use of a cryptic splice site. Additionally, we have identified and characterized two alternative *Hip1* mRNA transcripts that comprise distinct first exons, designated *Hip1a* and *Hip1b*. These transcripts are present in human and mouse tissues and may encode for two HIP1 isoforms with distinct cellular functions. The findings

described in this thesis provide a foundation for expanding our current understanding of *HIP1* gene regulation and aberrant expression of HIP1 in cancer.

CHAPTER 1

INTRODUCTION

The Huntingtin Interacting Protein 1 (HIP1) is a fascinating protein with a history as diverse as its suggested roles in normal and aberrant cell biology. HIP1was initially discovered in 1997 by two independent labs through a yeast-two hybrid system [1, 2]. The "bait" used in both these studies was huntingtin (htt), the protein whose gene is mutated in Huntington's disease. Understandably, subsequent studies have investigated the role of HIP1 in the pathology of Huntington's disease [3, 4]. Various studies have also implicated HIP1 in cancer biology [5-11]. Perhaps the most universally-accepted role of HIP1 is that of its involvement in receptor-mediated endocytosis due in large part to its homology with the yeast endocytic protein, Sla2p. Yet one could easily argue that the role of HIP1 in normal biology remains elusive. Indeed, it is quite possible that HIP1 may have multiple cellular functions. The fact that there are conflicting reports on HIP1 involvement in apoptosis-mediated cell death [3, 4, 9] strongly suggests the existence of multiple isoforms of the protein, yet there have been no reports of multiple isoforms of the mammalian HIP1 protein to date. Most studies are directed towards deciphering a role for the HIP1 protein, rather than transcriptional and post-transcriptional regulation of the *HIP1* gene. Given the sheer size and intriguing genomic structure of the *HIP1* locus, the *HIP1* gene is an excellent model for studies in transcriptional and post-transcriptional regulation. This chapter reviews the data demonstrating the ambivalent role of HIP1 as a pro-survival or pro-apoptotic protein. Additionally, we discuss effects of loss of *Hip1* and the possibility of transcriptional regulation leading to multiple isoforms of the HIP1 protein.

HIP1 and Endocytosis

There is considerable evidence suggesting that HIP1 is involved in receptor-mediated endocytosis. HIP1 is a homologue of the yeast protein, Sla2p. Wesp and colleagues showed that Sla2p is required for endocytosis and actin dynamics and that the N-terminus of the protein was important for these functions [12]. Within this region of the protein is an AP180/CALM N-terminal homology domain (ANTH). HIP1 also contains an ANTH domain (Figure 1.1). ENTH/ANTH domains have been found in several proteins with known involvement in clathrin-mediated vesicle trafficking [13]. The ENTH/ANTH domain-containing proteins have been reported to bind specifically to phosphatidylinositol-4,5-bisphosphate [PtdIns(4,5)P_2] and phosphatidylinositol-3,4,5-triphosphate [PtdIns(3,4,5)P_3] [14, 15]. However, Hyun and colleagues have shown that HIP1 preferentially binds to PtdIns(3,4)P_2 and PtdIns(3,5)P_2 [16]. This is significant given that PtdIns(3,4)P_2 and PtdIns(3,5)P_2 are enriched in early endosomes, whereas PtdIns(4,5)P_2 is primarily found in the plasma membrane [17].

In addition to an ANTH domain, HIP1 contains consensus binding sites for the endocytic adaptor protein AP2 (DPF motif) and clathrin heavy chain (LMDMD clathrin-box motif) (Figure 1.1) and has been shown to associate directly with these proteins [18-21]. The central helical domain of HIP1 has been shown to bind directly to the clathrin light chain and stimulate clathrin assembly *in vitro* [22, 23]. Mice that have lost HIP1 due to deletion of the *Hip1* gene show diminished recruitment of HIP1-binding endocytic proteins to liposomes isolated from brain lysates as well as decreased AMPA receptor trafficking [24]. Indeed, there is strong convincing evidence demonstrating the role of HIP1 in endocytosis and most would agree with this role. However, there is disagreement in the field concerning additional roles of HIP1 is pro-survival or pro-apoptotic. There is evidence supporting both roles, which we will review next.

HIP1 and Apoptosis

Because HIP1 was initially identified through its interaction with huntingtin (htt), efforts have been made to determine if it plays a role in the pathology of Huntingtin's disease. HIP1 is expressed at high levels in the central nervous system and colocalizes with htt in neuronal cells [1, 2]. Additionally, HIP1 was shown to interact more strongly

with wildtype htt than with mutant htt. Exogenous expression of HIP1 in neuronal and non-neuronal cells has been reported to induce apoptosis due in large part to a highly conserved phenylalanine at position 398 in a pseudo-death effector domain (pDED) [4]. Co-expression of a wildtype N-terminal htt with HIP1 reduced apoptotic activity. In this report, it was concluded that HIP1-mediated apoptosis occurred in a caspase-8 independent fashion.

A couple of years later, Gervais and colleagues reported that HIP1-mediated apoptosis occurred in collaboration with HIP1 protein interactor (HIPPI) [3]. Both proteins colocalize in the Golgi apparatus of neuronal NT2 cells and interact with each other. Both proteins contain a pDED and loss of this domain in either protein diminished their interaction with each other. However, HIPPI does not contain the essential Phe398 in its pDED. When both proteins were co-expressed in 293T cells that stably expressed mutant htt their interaction was stronger than in cells stably expressing wildtype htt. Additionally, co-expression of HIP1 and HIPPI in both 293 and HeLa cells led to increased caspase 3 activity. In contrast to the earlier report by Hackam *et al.*, HIP1-mediated apoptosis in cooperation with HIPPI occurred in a caspase 8-dependent manner. The proposed model for HIP1-mediated apoptosis provided by Gervais *et al.* states that HIP1 is normally bound and sequestered by wildtype htt. When htt is mutated, HIP1 is freed and allowed to bind HIPPI, leading to a complex that sequesters procaspase 8 and activates it. Surprisingly, an explanation for the difference in apoptotic pathways activated in HIP1-mediated apoptosis was not discussed.

HIP1 as a Pro-Survival Protein

The *HIP1* gene product was first implicated in cellular survival when Rao *et al*. reported that *Hip1*-deficient mice exhibit testicular degeneration due to apoptosis of postmeiotic spermatids [20]. The investigators observed testicular degeneration in *Hip1*$^{-/-}$ mice by hematoxylin and eosin staining as well as decreased numbers of spermatogenic precursors at various stages of development. Additionally, testicular tissue from HIP1-deficient mice displayed more TUNEL-positive cells compared to control mice.

Separately, Rao *et al*. demonstrated that exogenous expression of full length HIP1 does not induce apoptosis [9]. However, exogenous expression of a HIP1 deletion mutant lacking the ANTH domain (termed HIP1-ΔE) did induce apoptosis in 293T cells.

Apoptosis observed with this mutant was inhibited by a dominant-negative caspase-9 mutant, suggesting use of the intrinsic apoptotic pathway. A year later, Rao and colleagues reported that full-length HIP1 has transforming abilities [8]. In this study, NIH/3T3 cells that were stably transfected with a full-length *HIP1* cDNA construct under the control of either a long terminal repeat (LTR) or cytomegalovirus (CMV) promoter exhibited a transformed phenotype as determined by tumor formation in nude mice, anchorage-independent growth in soft agar and growth in low serum conditions. Indeed these data suggest that the full-length form of HIP1 is pro-survival and tumorigenic when exogenously expressed. These data also suggest the possibility of a second naturally-occurring isoform, similar to the the HIP1-ΔE construct, that may be pro-apoptotic when aberrantly expressed.

HIP1 and Cancer

An initial connection between HIP1 and cancer was first reported by Ross *et al.* [10]. The *HIP1* gene was identified as the chromosome 7 partner in a t(5;7)(q33; q11.2) translocation, which also involved the platelet-derived growth factor β receptor (PDGFβR) on chromosome 5, in a patient with chronic myelomonocytic leukemia (CMML). The result is a fusion protein, which contains all but the final 18 amino acids of the HIP1 protein fused to the transmembrane and tyrosine kinase domains of the PDGFβR. The fusion protein has constitutive tyrosine kinase activity and is capable of transforming the interleukin-3 (IL3)-dependent murine hematopoietic cell line, Ba/F3 cells to IL3-independent growth [11].

Since this initial discovery, evidence to bolster the connection between HIP1 and cancers has grown. Rao and colleagues observed that HIP1 is expressed at high levels in multiple cancers [9]. Of 53 cancer cell lines from the NCI60 group [25] derived from solid tumors of various tissue origins (breast, colon, kidney, lung, melanoma, ovarian and prostate), 50 of them expressed high levels of HIP1 by western blot analysis. They confirmed these data with immunohistochemical staining of primary human cancer tissue microarrays, which demonstrated moderate to high staining of HIP1 in most of the cancer types represented in the NCI60 cancer cell line panel. It is worth noting that HIP1 was undetectable in both normal colon and normal prostate epithelium. Additionally HIP1 expression in prostate tumor samples predicted prostate cancer progression. While a lack

of HIP1 expression was observed in the benign prostate epithelium, intermediate expression levels were observed in precancerous prostate lesions and high levels were observed in metastatic prostate cancer. Furthermore, an analysis of linked clinical data for 114 patients with prostate-confined cancer revealed that none of the cases with HIP1-negative tumors relapsed after radical prostatectomy while 28% of the cases with HIP1-positive tumors did. Finally, an analysis of tumors taken from the transgenic mouse model of prostate cancer (TRAMP) displayed high levels of HIP1 expression in 50% compared to benign tissue. Finally, the list of cancers in which HIP1 has been connected has expanded to include brain cancer [5] and both Hodgkin's disease and non-Hodgkin's lymphoma [7].

In addition to HIP1 serving as a prognostic marker in cancer, several pieces of data implicate HIP1 in promoting tumorigenesis. As mentioned earlier, stable exogenous expression of full-length HIP1 transforms fibroblasts [8]. The proposed mechanism of transformation was altered trafficking of receptor tyrosine kinases such as the epidermal growth factor (EGF) receptor, the fibroblast growth factor (FGF) receptor and the platelet derived growth factor (PDGF)-β receptor as the levels of these receptors were elevated in HIP1-transformed cells [8]. In 2004, Hyun *et al*. expanded on this hypothesis by reporting that exogenous expression of full-length HIP1 in 293T cells stabilizes the EGF receptor levels following stimulation with EGF [16]. In 2005, Bradley *et al*. expanded on the previously reported association between prostate cancer and HIP1 with the observation that tumor formation was reduced in TRAMP mice that lacked HIP1 expression [6]. Additionally, they observed increased levels of anti-HIP1 antibodies in patients with prostate cancer, an observation that was also predictive. Given the scope of studies connecting HIP1 with cancer, it appears evident that HIP1 has a functional involvement in cancer.

Complex Phenotypes of *Hip1* Loss of Function Mice

One of the most valuable scientific research tools for determining function of a particular gene is targeted deletion of the gene of interest in mice and extensive analysis of phenotypic abnormalities. This approach is particularly feasible when both the mouse and human proteins are highly conserved, as is the case with HIP1 (the mouse and human HIP1 protein sequences are 87% identical). Indeed this approach, with respect to HIP1,

has been attempted by multiple laboratories using diverse targeting strategies [20, 24, 26]. These studies have provided us with valuable insight yet the complexity of the different phenotypes has prevented complete resolution of the all-important question, "What does HIP1 do?" as we shall see below.

The first knock-out of the *Hip1* locus was reported in 2001 through targeted deletion of exons 2 through 8 [20]. As mentioned earlier, these mice exhibited testicular degeneration due to apoptosis of the postmeiotic spermatids. A couple of years later, Metzler *et al*. reported a separate *Hip1* loss-of-function mouse. They used a promoter-trap gene targeting strategy in which exon 8 and its adjacent intronic sequence was replaced with a SA-IRES-βGeo-pA cassette encoding a bifunctional lacZ-neomycin fusion protein. The resulting mice were born with normal Mendelian distribution and grow similar to wildtype mice early in their lives. However, approximately 12 weeks after birth these mice began to show growth retardation and "thoracolumbar kyphosis" with as secondary condition of "wasting, tremor and a gait ataxia". The thoracolumbar kyphosis was observed as early as 9 months of age with greater than 85% of the mice demonstrating this phenotype by one year of age. A block in ligand-induced AMPA receptor internalization was also observed in the brain cells cultured from these mice. Interestingly, there were no observable defects in gross brain morphology despite the fact that HIP1 is highly expressed in this organ.

In 2004, Oravecz-Wilson and colleagues reported two new independently generated mutant HIP1 mice [26]. One of the mutant mice was generated "serendipitously" by attempting to knock-in a human HIP1/PDGFβR fusion protein cDNA into the *Hip1* locus. This resulted in a loss of normal HIP1 expression so the mice were studied as nulls (referred to as $Hip1^{null/null}$). Similar to the mutant mice reported earlier by Metzler *et al*., these mice displayed degenerative spinal defects with 100% of the mice studied developing this phenotype after one year of age. Unlike the mutant mice reported on by Metzler *et al*., $Hip1^{null/null}$ mice were born in significantly decreased numbers compared to expected Mendelian ratios, suggesting partial embryonic lethality. Additionally, $Hip1^{null/null}$ mice were infertile (males only), developed cataracts, and exhibited stunted growth and hematopoietic abnormalities, including resistance to 5-fluorouracil- (5-FU) induced lethality. Surprisingly, no observable defects in the

endocytic machinery were found in embryonic fibroblasts. Both spinal defects and growth abnormalities were accelerated when the only other known mammalian family member of *Hip1*, Hip1-related (*Hip1r*) was disrupted [27]. The spinal defects, growth defects and cataracts were rescued with heterologous expression of full-length HIP1, indicating that these phenotypes were indeed associated with a loss of *Hip1* [28].

The second mutant mouse reported in the study (termed $Hip1^{\Delta 3\text{-}5/\Delta 3\text{-}5}$ mice following recombination of the alleles) was generated by targeted and conditional deletion of exons 3 to 5 of the *Hip1* locus [26]. Although these mice were not as extensively studied as $Hip1^{null/null}$ mice, comparisons of the two mutant mice were made. $Hip1^{\Delta 3\text{-}5/\Delta 3\text{-}5}$ mice were born at normal Mendelian ratios. Eighty percent of $Hip1^{\Delta 3\text{-}5/\Delta 3\text{-}5}$ mice developed spinal defects by one year of age. Similar to $Hip1^{null/null}$ mice, $Hip1^{\Delta 3\text{-}5/\Delta 3\text{-}5}$ mice were infertile, exhibited testicular degeneration and were also resistant to 5-FU treatment. No cataracts were observed in $Hip1^{\Delta 3\text{-}5/\Delta 3\text{-}5}$ mice. The differences between these various targeted *Hip1* mutants may be due to incomplete null status. Alternatively, some of the defects observed in the $Hip1^{null/null}$ mice may be the result of disruption of Hip1-neighboring genes due to the presence of the neomycin selection cassette.

Although HIP1 was discovered over 10 years ago, we know very little about the regulation of *HIP1* gene expression. The *HIP1* gene structure is complex. The mouse *Hip1* gene maps on chromosome 5 at position 5qG2 in humans, and covers over 139 Kb. The human gene maps to chromosome 7 at position 7q11.23 and covers over 204 Kb. Both genes contain disproportionately large first introns relative to the rest of the gene (Figure 1.2). Intron 1 of the human *HIP1* gene comprises over 139 Kb (roughly 68% of the gene) while intron 1 of the mouse *Hip1* gene consists of over 89 Kb (about 64%). The existence of such a large intron suggests the possibility of an alternative promoter leading to expression of an additional transcript. Both human and mouse mRNA transcripts consist of 31 exons, which suggests the possibility of multiple *HIP1* transcripts through alternative splicing. Large 3' untranslated regions (3' UTR) of over 6kb in both mouse and human (Figure 1.3) suggest additional regulatory mechanisms. Given this data it appears that the HIP1 gene may be highly regulated at the transcriptional and post-transcriptional levels.

A Case for Multiple HIP1 Isoforms

There is reason to believe multiple forms of HIP1 protein exist. The presence of multiple bands within the range of 100 to 120 kDa in western blot analysis of HIP1 expression has been noted repeatedly in studies involving HIP1. Initially, Chopra *et al* reported the presence of alternative *HIP1* transcripts following their 5' rapid amplification of cDNA ends (RACE) analysis of human brain RNA [29]. These alternative transcripts differ at their 5' ends and were attributed to alternative splicing of exons 1, 2 and 4 (labeled as *HIP1-1*) or exons 1, 3 and 4 (*HIP1-2*). Further characterization of these transcripts has not been performed to date.

Recently Moores and colleagues identified two variant cDNA clones in *Drosophila* that have homology to *HIP1* [30]. Sequence analysis of these clones revealed that the two variants have alternative first exons and an identical six core exons from 2 to 7 followed by different transcriptional termination sites in a final eighth exon. The first clone (labeled CG10971-RA) represents a 3881-bp transcript with a predicted protein product of 1124 amino acids, including a complete ANTH domain (dubbed full-length *Hip1*). The second clone (CG10971-RB) represents a 3983-bp transcript and a predicted protein product of 1026 amino acids. Most notably, the predicted protein product does not include a complete ANTH domain (*Hip1ΔANTH*). Excluded from the truncated ANTH domain are the consensus sequence of (K/G)A(T/I)X_6(P/L/V)KXK(H/Y) necessary for lipid binding [31]. Interestingly, the two proteins display contrasting roles in neurogenesis. Full-length *Hip1* decreased sensory bristle density, whereas *Hip1ΔANTH* led to an increase in sensory bristle density. The authors conclude that plays a dual-regulatory role in neurogenesis based on the correlation between bristle density and the number of sensory neurons formed [32, 33]. The idea that Hip1 plays a dual-regulatory role in development is an interesting one considering apoptosis plays a prominent role in early organism development and over-expression Hip1 that lacks the ANTH domain induces apoptosis. However, one would predict that *Hip1ΔANTH* would decrease bristle density.

As indicated earlier in this chapter, Rao *et al.* reported similar contrasting roles of a full-length human HIP1 construct and a mutated construct (HIP1ΔE), which lacks the ANTH domain [9]. Exogenous expression of HIP1ΔE in cells led to a much higher

percentage of apoptotic cells compared to exogenous expression with full-length HIP1. The increase in cell death observed was attributed to a "dominant-negative" behavior of the ANTH domain-lacking HIP1 protein. Although a transcript representing the mutated human construct has not been reported to date, this data does present an intriguing explanation for the contrasting reports the role of HIP1 in cellular survival versus its role as an inducer of apoptosis.

The major focus of this thesis project is to investigate the existence of an additional HIP1 isoform primarily through examination of transcriptional and post-transcriptional regulation of the *HIP1* gene. In chapter 2, we began to explore the necessity of HIP1 in prostate and breast cancer using a conditional *Hip1* knockout strategy. Unexpectedly we discovered a novel cryptic splice site in the *Hip1* gene, which uses the rare U12 minor-class pathway to maintain expression of a partially functional protein [34]. Chapter 3 explores the possible expression of multiple *HIP1* mRNA transcripts in both mouse and human and their potential connection with the different HIP1 isoforms seen by western blot analysis. Finally, in chapter 4, we examine the putative promoter of the human *HIP1A* transcript for its general activity and possible involvement in aberrant HIP1 expression in lymphoma.

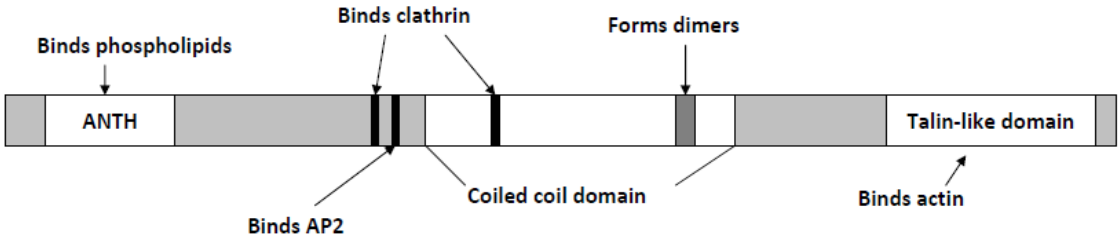

Figure 1.1: Diagram of the HIP1 protein. The human HIP1 protein consists of 1037 amino acids while the mouse HIP1 protein comprises 1031 amino acids. The HIP1 protein has a number of functional domains that suggest a role in endocytosis. At the N-terminus of HIP1 is an AP180 N-terminal homology domain, which preferentially binds to 3-phosphoinositides. HIP1 also has clathrin and AP2 binding motifs. The central portion of the protein is comprised of a coiled coil domain with a leucine zipper. This allows HIP1 to form homodimers and heterodimers with HIP1-Related (HIP1-R). The C-terminus is comprised of a talin-like domain involved in binding to F-actin.

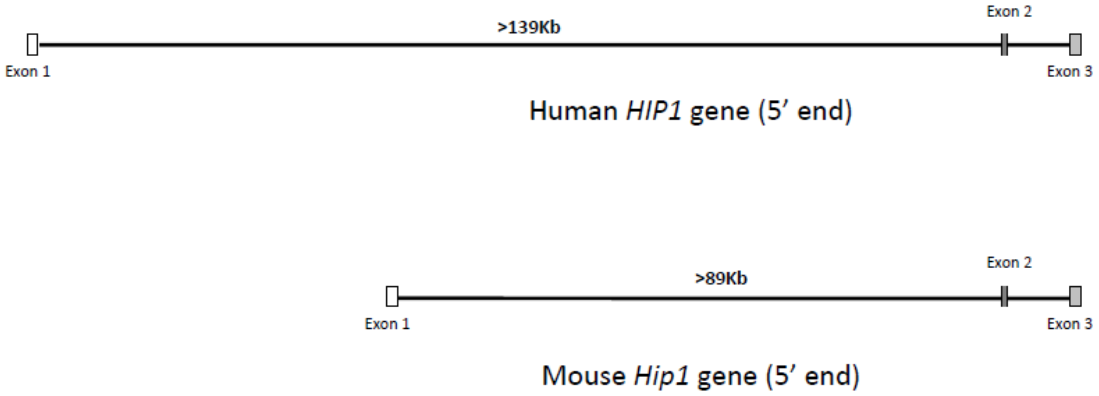

Figure 1.2: Comparison of the 5' end of the HIP1 gene in human and mouse. The *HIP1* gene in both mice and humans consists of a relatively large intron 1. Intron 1 of the human *HIP1* gene is over 139 kilobases while intron 1 of the mouse *Hip1* gene is 89 kilobases. Multiple expressed sequence tags (EST) have been generated that contain starting exons located within intron 1 in both species. However, no alternative promoters or alternative transcripts have been reported.

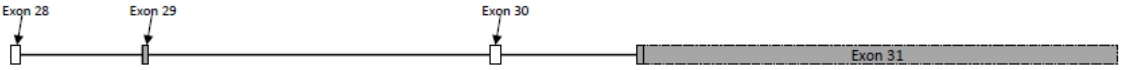

Figure 1.3: Diagram of the 3'end of the HIP1 gene. The HIP1 gene has a total of 31 exons. The last exon, exon 31, is over 6 kilobases in size but only 53 of these bases are part of the coding sequence.

CHAPTER 2

USE OF A CRYPTIC SPLICE SITE FOR THE EXPRESSION OF HUNTINGTIN INTERACTING PROTEIN 1 IN SELECT NORMAL AND NEOPLASTIC TISSUES

Summary

Huntingtin Interacting Protein 1 (HIP1) is a 116 kDa endocytic protein that is necessary for the maintenance of several adult tissues *in vivo*. Its complete deficiency, due to homozygosity of a null *Hip1* allele, leads to degenerative adult phenotypes. HIP1 deficiency also inhibits prostate tumor progression in the prostate cancer prone TRAMP mouse model. To better understand how deficiency of HIP1 leads to such phenotypes, we carefully analyzed tumorigenic potential in mice homozygous for a *Hip1* mutant allele, designated *Hip1*$^{\Delta 3\text{-}5}$, which is predicted to result in a frame-shifted, nonsense mutation in the N-terminal region of the coding sequence. In contrast to our previous studies using the *Hip1* "null" allele, an inhibition of prostate tumorigenesis was not observed as a result of the homozygosity of the "nonsense" Δ3-5 allele. Also, it did not inhibit breast tumorigenesis in the MMTV-Myc breast cancer-prone background. To more closely examine the contrasting results from the two different *Hip1* mutant mice, we cultured tumor cells from homozygous Δ3-5 allele bearing TRAMP and MMTV-myc mice and discovered the presence of an approximately 110 kDa form of HIP1 in tumor cells. Upon genomic DNA and cDNA sequencing of *Hip1* from these tumors, we determined that this 110 kDa form of HIP1 is the product of splicing of a cryptic U12-type AT-AC intron. This event results in the insertion of an AG dinucleotide between exons 2 and 6 and restoration of the original reading frame. Remarkably, this mutant protein retains its capacity to bind lipids, clathrin, AP2, and EGFR providing a possible explanation for why tumorigenesis was not altered following this "knockout" mutation. The expression and activities of this mutant form of HIP1 provide clues for future studies

investigating the contribution of HIP1 to the homeostasis of specific normal and neoplastic tissues at different developmental stages.

Introduction

Huntingtin Interacting Protein 1 (HIP1) was first identified by its ability to interact with huntingtin, the protein encoded by the gene that is mutated in Huntington's disease [1, 2]. HIP1 and its only known mammalian relative, HIP1-related (HIP1r), were subsequently shown to specifically interact with clathrin, AP2 [4, 18-22, 35, 36], and epidermal growth factor receptor (EGFR) [5]. Thus, the HIP1 family is widely thought to be involved in the regulation of growth factor receptor endocytosis and signaling. Additionally, HIP1 and HIP1r contain AP180 N-terminal homology (ANTH) inositol lipid-binding domains, which are specific to endocytic proteins [14, 15]. Finally, deficiency of HIP1 leads to spinal defects, testicular degeneration, cataracts, adult weight loss, and early death [26, 37]. Heterologous expression of full-length *HIP1* cDNA rescues most of these phenotypes confirming that the phenotypes are due to a loss of *Hip1* [28]. These *in vivo* phenotypes indicate that HIP1 is necessary for fundamental cellular and organismal homeostasis. Despite their clear necessity in the maintenance of adult cells and tissues, the precise cellular and biochemical function(s) of this protein family are yet to be determined. In fact, several attempts at understanding the effects of HIP1/HIP1r deficiency on receptor endocytosis either in cultured cells or *in vivo* have not been successful [26-28].

In addition to its function in normal tissue maintenance, HIP1 has been widely implicated in tumorigenesis. HIP1 was discovered to be an amino-terminal partner of PDGFβR, in the leukemogenic fusion resulting from a t(5;7) chromosomal translocation [10]. HIP1 protein also has been found to be up regulated in multiple human tumor types including prostate, colon [9], breast [38], brain [5], and lymphoid [7] cancers. Additionally, HIP1 over-expression is prognostic in prostate cancer [9]. Furthermore, heterologous human HIP1 over-expression can transform mouse fibroblasts [38], an effect that we propose to be due to altered growth factor receptor endocytosis and subsequent signal transduction cascades.

To examine the role of HIP1 in prostate cancer, we have previously used mutant mice that are deficient in HIP1 due to a spontaneous targeting event ($Hip1^{null}$). When

these HIP1-deficient mice were crossed with the transgenic adenocarcinoma of mouse prostate (TRAMP) mice [39], the HIP1-deficient progeny mice contained fewer and less aggressive prostate tumors than their littermate TRAMP control mice [6]. We have expanded these studies by using a different tumor model system (MMTV-MYC model of breast cancer) and a "third generation" *Hip1* knockout mouse allele (the $Hip1^{\Delta 3\text{-}5}$) that does not provide the confounding issues associated with the above-described spontaneous "null" allele [26], such as possible altered expression of *HIP1*-neighboring genes caused by the neomycin cassette. In the present study, we report the surprising result that $Hip1^{\Delta 3\text{-}5/\ \Delta 3\text{-}5}$ are equally, if not more, prone to the development of prostate and breast tumors than *Hip1* wild type mice. Furthermore, we found that the tumor cells from the $Hip1^{\Delta 3\text{-}5/\ \Delta 3\text{-}5}$ genetic background express a truncated form of the HIP1 protein that is the result of a novel cryptic splicing event. These results have important implications not only for the role of HIP1 and its interacting proteins in normal and neoplastic cell biology but also for the development and analysis of mouse model systems with specific targeting events. Our data emphasize the value of how sequencing the transcript that is actually produced by an engineered knock-out allele can reveal novel types of molecular compensation at the level of splicing.

Materials and Methods

Mice

Mx1cre (B6.Cg-Tg(Mx1-cre)1Cgn/J, The Jackson Laboratories), $Hip1^{null}$, $Hip1^{loxp}$, $Hip1^{\Delta 3\text{-}5}$ [26], TRAMP ([39], C57BL/6, The Jackson Laboratories) and MMTV-myc ([40], MammJ/FVB, Gift from Lewis Chodosh) allele-containing mice were maintained and bred under SPF conditions as per UCUCA guidelines at the University of Michigan. The TRAMP and MMTV-myc allele-containing mice were maintained on pure genetic backgrounds. Since the other alleles were maintained on a mixed C57BL/6;129svj background, all experiments were performed using the appropriate littermate controls.

Tumor analysis in MMTV-myc mice

MMTV-myc transgenic mice were mated onto $Hip1^{null/null}$ and $Hip1^{\Delta 3\text{-}5/\Delta 3\text{-}5}$ backgrounds and were palpated for breast tumors weekly. Tumor size was measured

with calipers. The mice were sacrificed at one year of age or if a tumor impeded movement or ulcerated.

Tumor cell culture

Fresh tumor samples from MMTV-myc and TRAMP mice were cut into 1 mm sections, added to DMEM containing 2.2 mg/ml collagenase (Sigma), and incubated for 1 hour at 37^{o}C with agitation every 10 minutes. The digested samples were filtered through a 100 μm nylon cell strainer (Falcon) then centrifuged at 1,000 rpm for 10 minutes. The supernatant was removed, and the remaining cells were suspended in DMEM/10% FBS and plated onto 10 mm dishes. Cells were passaged every 3 days into fresh media.

Survival analysis in TRAMP mice

The *Hip1*$^{null/null}$ and *Hip1*$^{\Delta 3\text{-}5/\Delta 3\text{-}5}$ mice were maintained on a mixed C57BL/6;129svJ background, and the TRAMP mice were maintained on a pure C57BL/6 background. Intercross matings of TRAMP and *Hip1*$^{null/null}$ and *Hip1*$^{\Delta 3\text{-}5/\Delta 3\text{-}5}$ mice were performed as previously described [6]. Fourteen TRAMP;*Hip1*$^{\Delta 3\text{-}5/\Delta 3\text{-}5}$, 13 TRAMP;*Hip1*$^{+/\Delta 3\text{-}5}$, 18 TRAMP;*Hip1*$^{+/null}$, and 15 TRAMP/*Hip1*$^{null/null}$ littermates were analyzed for tumors at 6.5 months. Prior to these necropsies, a group of mice from these cohorts either unexpectedly died or became moribund and required euthanasia. This survival data for each of these observation groups was compared.

Genomic DNA sequencing

High-fidelity PCR amplification of the 3 kb genomic region between exons 2 and 6 of *Hip1* from a MMTV-myc;*Hip1*$^{\Delta 3\text{-}5/\Delta 3\text{-}5}$ tumor was performed. The resulting products were cloned, and single-run complete sequencing was performed on two independent clones.

Sequence analysis

The alignment of sequences from wild type *Hip1* cDNA or MMTV-myc;*Hip1*$^{\Delta 3\text{-}5/\Delta 3\text{-}5}$ tumor genomic DNA was analyzed using a combination of Sequencer version 4.5 (GeneCodes) and the NCBI BLAST program.

RNA isolation

Total RNA was isolated from cultured tumor cells, tissues, and early passage mouse embryonic fibroblast (MEF) extracts using the TRIzol reagent (Invitrogen).

Reverse-transcriptase PCR (RT-PCR)

RT-PCR was performed on total RNA using the SuperScriptTM One-Step RT-PCR system (Invitrogen) and primers specific to *Hip1* exon 1 (5'-ATGAAGCAGGTATCCAACCCGCTGCCC-3', forward primer) and the exon 14/15 junction (5'-ATTAGCCTGGGCCTTTCTTTCTATCTC-3', reverse primer) of murine *Hip1* cDNA. Resulting products were separated on 0.8% agarose gels. Products were extracted from the gel and amplified by nested PCR using primers specific to the exon 1/2 junction (5'-TTCGAGCGGACTCAGACGGTCAGCGTC-3'-forward primer) and the exon 13/14 junction (5'-ATGGCCCGCTGGCTCTCAATCTTCATG-3' reverse primer) of murine *Hip1* cDNA. Products were again run on 0.8% agarose gels, extracted, and directly sequenced using the PCR primers that were used for the amplification. PCR products that did not yield readable sequence were cloned using the TOPO TA Cloning Kit for Sequencing (Invitrogen). Multiple clones were selected, and plasmid DNA was isolated and sequenced.

Northern blot analysis of mouse embryonic fibroblast (MEF) mRNA

Poly (A) RNA was isolated from total RNA using the Poly(A) Purist MAG protocol (Ambion). Then, 5ug of this poly(A) RNA was separated on a 1% agarose gel with 6% formaldehyde, stained with ethidium bromide, transferred to Nytran membrane (Schleicher & Schuell), and cross-linked. The membrane was prehybridized in a buffer containing 5X SSC, 5X Denhardt solution, 1% sodium dodecyl sulfate (SDS) (wt/vol), and 100 μg of denatured salmon sperm DNA/ml for 3 h at 65°C. For the mouse *Hip1* Northern probe, an 850-bp *Eco*R1 and *Not*1 digested fragment encoded by m*Hip1* exons 10-14 was used. The probe was ^{32}P labeled using a random-primed labeling kit according to manufacturer's directions (Roche). The blot was hybridized overnight at 65°C, washed twice in 2X SSC for 20 min, once in 1X SSC for 10 min, and twice in 0.1X SSC for 10 min. The blot was exposed for 4 to 5 days on Kodak Biomax film. The mRNA abundance was normalized with the signal for glyceraldehydes-3-phosphate dehydrogenase (GAPDH).

Tissue preparation and western blot analysis

Tissue harvesting, preparation, and immunoblotting of tissues was performed as previously described [27]. A polyclonal anti-HIP1 (1:5,000, UM354) antibody was used to detect HIP1 expression in MMTV-myc, TRAMP and Mx1-Cre mice, and polyclonal anti-actin (1:1000, Sigma) antibody was used as a control.

polyIpolyC (pIpC)-treatment of Mx1-cre mice

Mice were injected intraperitoneally with 250 ug/mouse of polyinosinic-polycytidylic acid (pIpC, Sigma, St. Louis, MO) every other day for 7 or 14 days as previously described [41, 42].

Bone marrow culture

Mouse bone marrow cell monocytic culture was carried out as previously described (Bradley, 2007), except that RPMI-1640 media and M-CSF (1 ng/ml, Sigma, St. Louis, MO) was used and femur bone marrow was plated onto 100 mm dishes. One week later, cells were directly lysed in the dishes and collected for protein analysis.

Co-immunoprecipitation of HIP1 and EGFR and endocytic factors

Full-length and mutant EGFR and HIP1 cDNA constructs in pcDNA3 have previously been described [5]. A 15-cm dish of 70% confluent 293T cells was transfected with 20 μg of HIP1 cDNA and 20 μg of EGFR cDNA using Superfect reagent (Qiagen). Twenty-four hours post-transfection, the cells were lysed using an all-purpose lysis buffer [50 mmol/L Tris (pH7.4), 150 mmol/L NaCl, 1% Triton X-100, 1.5 mmol/L MgCl2, 5 mmol/LEGTA, 10% glycerol, Complete EDTA-free protease inhibitor tablets (Roche), 30 mmol/L sodium pyrophosphate, 50 mmol/L sodium fluoride, and 100μmol/L sodium orthovanadate]. Five milligrams of protein were incubated with pre-immune serum, polyclonal anti-HIP1 serum (UM323), or sheep polyclonal anti-EGFR (Upstate). One hundred microliters of a 3:1 slurry of protein G-sepharose beads (GE Healthcare) in lysis buffer were then incubated with the lysate-antibody mixture at 4ºC for 60 min with rotation. The protein G pellets were washed four times with 1 mL of lysis buffer. The entire pellet was dissolved in SDS sample buffer, boiled for 5 min, separated on 7% SDS-PAGE, and transferred to nitrocellulose membranes. Antibodies used for western blot analysis were the anti-HIP1/4B10 antibody (mouse monoclonal, human anti-HIP1

immunoglobulin G1, 400 ng/mL), anti-adaptin-α antibody (rabbit polyclonal, BD Biosciences), anti-clathrin heavy chain TD-1 antibody (kind gift of Linton Traub, University of Pittsburgh), and an anti-EGFR antibody (sheep polyclonal antibody, Upstate Biotechnology, Charlottesville, VA).

Generation of HIP1 expression constructs

Generation of the pcDNA3/FL HIP1 expression construct was reported previously [9]. PCR mutagenesis using pcDNA3-FL HIP1 as a template was used to generate the insert for the pcDNA3/hHIP1Δ3-5/insAG expression construct. Two initial PCR products were generated using two separate pairs of primers. The first primer pair consisted of a forward primer specific to exon 1 (5'-AGGGAGACCCAAGCTTGGTA-3'including a *Kpn*I restriction site) and an engineered reverse primer (5'-GGGATTCTTTCTGGCGTGTTTTTCCTT-3') consisting of sequence from exon 2, an AG dinucleotide, and sequence from the 5' portion of exon 6. The second primer pair consisted of an engineered forward primer (5'-AACACGCCAGAAAGAATCCCAGGTTCC-3') consisting of sequence from the 3' portion of exon 2, an AG dinucleotide, and sequence from exon 6 and a reverse primer specific to exon 14 (5'-TTCTATCTCAGACAGGCTCC-3'; just 3' of the *Eco*RI restriction site at position 1290 of the coding sequence). The resulting PCR products were used as templates in a second PCR reaction to generate the hHIP1Δ3-5/insAG insert. The hHIP1Δ3-5/insAG insert was cloned into pcDNA3-FL HIP1 using the *Kpn*I and *Eco*RI restriction sites.

Generation and purification of GST-fusion proteins

The 5' portions of pcDNA3/FL HIP1 and pcDNA3/hHIP1Δ3-5/insAG were cloned into pGEX4T.1 to generate GST-HIP1wt (amino acids 1-430) and GST-HIP1Δ3-5 (amino acids 1-337) expression constructs, respectively. The HIP1wt and HIP1Δ3-5 inserts cloned into the pGEX4T.1 vector were generated by PCR amplification using the forward primer, 5'-CCGGAATTCATGGATCGGATGGCCAGC-3', and the reverse primer, 5'-CCGCTCGAGACAGTCGTCGGCCGCCTGC-3' and pcDNA3/FL HIP1 and pcDNA3/hHIP1Δ3-5/insAG as templates. Constructs were verified by sequencing. The GST-HIP1wt and GST-HIP1Δ3-5 fusion proteins were expressed in *E. coli* strain BL21 following induction with 0.1mM isopropyl-β-D-1-thiogalactopyranoside (IPTG) for 2 h

at 37^{o}C. Bacteria were pelleted and resuspended in PBS containing protease inhibitors (Roche Diagnostics). Resuspended cells were lysed by sonication, and Triton X-100 was added to a final concentration of 2%. The mixture was centrifuged at 12,000 x g for 10 min. Following centrifugation, the supernatant was added to glutathione sepharose 4 beads (50% slurry) and incubated at room temperature for 30 min. The beads were washed 3 times with PBS and elution buffer (50mM Tris-HCL, 10mM reduced glutathione [pH 8.0]) to elute the fusion proteins. Eluted proteins were dialyzed in PBS at 4^{o}C for 2 h and again overnight. Dialyzed proteins were concentrated using Aquacide (Calbiochem), and protein concentrations were determined by SDS-PAGE and Coomassie blue staining. Proteins were further analyzed by western blot analysis using an anti-GST antibody (Cell Signaling Technologies) and an anti-HIP1 antibody (UM354).

Lipid-binding assay

Lipid-binding assays using PIP strips and PIP arrays (Echelon) were performed according to manufacturer's protocol. Briefly, either PIP strips or PIP arrays were incubated overnight at 4^{o}C with 12.5 µg of purified protein in TBST with 1% milk. Binding was detected using anti-GST antibody (1:5000) or UM354 (1:2000) in TBST with 1% milk. Anti-rabbit secondary antibodies conjugated to horse radish peroxidase (HRP) were used at 1:5000 (for anti-GST) or 1:2000 (for UM354) in TBST with 1% milk.

Survival analysis in TRAMP mice

The *Hip1*$^{null/null}$ and *Hip1*$^{\Delta 3\text{-}5/\Delta 3\text{-}5}$ mice were maintained on a mixed C57BL/6;129svJ background, and the TRAMP mice were maintained on a pure C57BL/6 background. Intercross mating of TRAMP and *Hip1*$^{null/null}$ and *Hip1*$^{\Delta 3\text{-}5/\Delta 3\text{-}5}$ mice were performed as previously described [6]. Fourteen TRAMP; *Hip1*$^{\Delta 3\text{-}5/\Delta 3\text{-}5}$, 13 TRAMP; *Hip1*$^{+/\Delta 3\text{-}5}$, 18 TRAMP;*Hip1*$^{+/null}$ and 15 TRAMP;*Hip1*$^{null/null}$ littermates were analyzed for tumors at 6.5 months. Prior to thes necropsies, a group of mice from these cohorts either unexpectedly died or became moribund and required euthanasia. This survival data for each of these observation groups was compared.

RNA isolation and northern blot

Total RNA was isolated from cultured tumor cells, tissues, and early passage mouse embryonic fibroblast (MEF) extracts using the TRIzol reagent (Invitrogen). Poly (A) RNA was isolated from total RNA using the Poly(A) Purist MAG protocol (Ambion). Then, 5µg of this poly(A) RNA was separated on a 1% agarose gel with 6% formaldehyde, stained with ethidium bromide, transferred to Nytran membrane (Schleicher & Schuell), and cross-linked. The membrane was prehybridized in a buffer containing 5X SSC, 5X Denhardt solution, 1% sodium dodecyl sulfate (SDS) (wt/vol), and 100µg of denatured salmon sperm DNA/mL for 3 hours at 65^{o}C. For the mouse Hip1 Northern probe, an 850-bp *EcoR*1 and *Not*1 digested fragment encoded by m*Hip1* exons 10-14 was used. The probe was ^{32}P-labeled using a random-primed labeling kit according to manufacturer's directions (Roche). The blot was hybridized overnight at 65^{o}C, washed twice in 2X SSC for 20 min, once in 1X SSC for 10 min, and twice in 0.1X SSC for 10 min. The blot was exposed for 4 to 5 days on Kodak Miomax film. The mRNA abundance was normalized with the signal for glyceraldehydes-3-phosphate dehydrogenase (GAPDH).

Tissue preparation and western blot analysis

Tissue harvesting, preparation, and immunoblotting of tissues was performed as previously described [27]. A polyclonal anti-HIP1 (1:5,000, UM354) antibody was used to detect HIP1 expression in MMTV-myc, TRAMP and Mx1-Cre mice, and polyclonal anti-actin (1:1,000, Sigma) antibody was used as a control.

Co-immunoprecipitation of HIP1 and EGFR and endocytic factors

Full-length and mutant EGFR and HIP1 cDNA constructs in pcDNA3 have previously been described [5]. A 15-cm dish of 70% confluent 293T cells was transfected with 20µg of EGFR cDNA using Superfect reagent (Qiagen). Twenty-four hours post-transfection, the cells were lysed using an all-purpose lysis buffer [50 mmol/L Tris (pH7.4), 150 mmol/L NaCl, 1% Triton X-100, 1.5 mmol/L $MgCl_2$, 5 mmol/L EGTA, 10% glycerol, Complete EDTA-free protease inhibitor tablets (Roche), 30 mmol/L sodium pyrophosphate, 50 mmol/L sodium fluoride, and 100µmol/L sodium orthovanadate]. Five milligrams of protein were incubated with pre-immune serum, polyclonal anti-HIP1 serum (UM323), or sheep polyclonal anti-EGFR (Upstate). One

hundred microliters of a 3:1 slurry of protein G-sepharose beads (GE Healthcare) in lysis buffer were then incubated with the lysate-antibody mixture at 4^{o}C for 60 min with rotation. The protein G pellets were washed four times with 1 mL of lysis buffer. The entire pellet was dissolved in SDS sample buffer, boiled for 5 min, separated on 7% SDS-PAGE gel, and transferred to nitrocellulose membranes. Antibodies used for western blot analysis were the anti-HIP1/4B10 antibody (mouse monoclonal, human anti-HIP1 immunoglobulin G1, 400 ng/mL), anti-adaptin-α antibody (rabbit polyclonal, BD Biosciences), anti-clathrin heavy chain TD-1 antibody (kind gift of Linton Traub, University of Pittsburgh), and an anti-EGFR antibody (sheep polyclonal antibody, Upstate Biotechnology, Charlottesville, VA).

Results

Germ line deletion of Hip1 exons 3 thru 5 leads to a phenotype similar to that of Hip1null mice

The *Hip1* gene has a complex structure consisting of 32 exons spread over 220 kilobases. To examine the role *Hip1* plays in development and disease, we have generated a series of *Hip1* [26] and *Hip1r* [27] mutant alleles. The original *Hip1*^{null} allele was serendipitously generated in an attempt to knock the human HIP1/PDGFβR fusion cDNA into the mouse *Hip1* genomic locus [26]. Using this null allele, we previously reported that HIP1 deficiency leads to a complex degenerative mouse phenotype [26] and impaired tumor progression in transgenic adenocarcinoma of the mouse prostate (TRAMP) mice [6]. Because of the complex structure of this original allele and the resultant multi-tissue phenotype, we generated a conditional *Hip1* mutant allele (*Hip1*^{loxp}). To do this, we generated a targeting vector to introduce loxP sites flanking *Hip1* exons three through five, which encode a significant portion (80%) of the ANTH domain. As predicted, cre-mediated recombination of these loxP sites resulted in the deletion of exons 3-5 as well as the neomycin selection cassette [26]. The resulting allele (*Hip1*$^{\Delta 3\text{-}5}$) contains not only a deletion of most of the ANTH domain sequences but also a frame-shifted, nonsense mutation that fuses exon 2 to exon 6. Protein expressed from this mutant allele is predicted to be a truncated amino terminal 10 kDa protein lacking the ANTH, clathrin-binding, AP2-binding, coiled-coil, and Talin homology domains (domains that span the remaining 90% of the coding sequence; Figure 2.1).

Previously, mice homozygous for the Δ3-5 allele were found to exhibit degenerative phenotypes similar to the *Hip1*$^{null/null}$ mice (*e.g.*, kypholordosis and testicular degeneration/infertility). However, there were two differences in the phenotypes associated with these mice. First, the *Hip1*$^{\Delta 3\text{-}5/\Delta 3\text{-}5}$ mice did not have cataracts. Second, the *Hip1*$^{\Delta 3\text{-}5/\Delta 3\text{-}5}$ mice did not display perinatal lethality [26]. These differences suggested that either the *Hip1*$^{\Delta 3\text{-}5}$ allele is not a complete null allele or that the serendipitous *Hip1*^{null} allele affects neighboring genes and that those effected genes (rather than *Hip1*) are necessary for embryogenesis and lens homeostasis.

Breast and prostate tumorigenesis is not inhibited in Hip1$^{\Delta 3\text{-}5/\Delta 3\text{-}5}$ mice

Since HIP1 is known to transform mouse fibroblasts [38] and is over-expressed in multiple human cancers [9], it has been hypothesized to play a role in tumorigenesis. We have previously demonstrated that HIP1 deficiency inhibits prostate tumor progression in TRAMP mice [6]. To examine further the involvement of HIP1 in tumor development, we analyzed the effect of HIP1 deficiency on breast tumorigenesis using the MMTV-myc mammary tumor model [40]. Because of its less complex structure but similar phenotype to the *Hip1*^{null} allele, we have used the *Hip1*$^{\Delta 3\text{-}5}$ allele in our subsequent studies of the role of HIP1 in tumorigenesis. MMTV-myc and TRAMP transgenic mice were generated in both the *Hip1* "null" and Δ3-5 genetic backgrounds. The MMTV-myc mice were sacrificed prior to or at 12 months of age and analyzed for the appearance and progression of breast tumors (Figure 2.2). Consistent with our previous results using the TRAMP mice, the HIP1 "null" background inhibited tumorigenesis induced by the MMTV-myc transgene [6] such that none of the 6 *Hip*$^{null/null}$;MMTV-*myc* mice (0%) analyzed developed breast tumors. In contrast, 3 of 16 *Hip*$^{+/null}$;MMTV-*myc* mice (18.8 %) analyzed developed breast tumors. This trend supports the hypothesis that HIP1 deficiency inhibits breast tumorigenesis (Figure 2.3A).

The use of the Δ3-5 allele (compared to the null allele) to generate a HIP1 deficient background resulted in a different effect on tumorigenesis. For the MMTV-myc mice, 8 of 18 (44%) *Hip1*$^{\Delta 3\text{-}5/\Delta 3\text{-}5}$ mice and 19 of 37 (51%) *Hip1*$^{+/\Delta 3\text{-}5}$ mice developed palpable breast tumors (Figure 2.3A). This level is significantly higher than the 19% breast tumor incidence in MMTV-myc mice with the *Hip1*$^{+/null}$ backgrounds and the 0% incidence in the *Hip1*$^{null/null}$ background (Figure 2.3A). Additionally, we only observed

breast tumor metastasis in mice that contained the Δ3-5 allele (Figure 2.3B). Both multiple synchronous primary breast tumors (Figure 2.3C) as well as multiple metastatic foci (Figure 2.3D) were observed in *Hip1*$^{+/\Delta 3\text{-}5}$ and *Hip1*$^{\Delta 3\text{-}5/\Delta 3\text{-}5}$ mice.

The TRAMP;*Hip1*$^{\Delta 3\text{-}5}$ mice produced similar results with a smaller cohort of mice available for tumor analysis (Figure 2.4). We initially planned to compare larger groups of 6-month-old heterozygous and homozygous TRAMP;*Hip1*$^{\Delta 3\text{-}5}$ mice. This plan was based on the results of three independent prior TRAMP experiments that demonstrated that *Hip1*$^{null/+}$ and *Hip1*$^{+/+}$ mice developed prostate cancer at a similar frequency and to a similar extent in the TRAMP background and survived to at least 6 months of age. As expected, when we performed this fourth TRAMP experiment we observed that 84 % (15/18) and 93% (14/15) of the TRAMP mice that were heterozygous and homozygous for the null allele, respectively, survived to 6 months of age (Figure 2.5A). Unexpectedly, *Hip1*$^{\Delta 3\text{-}5}$;TRAMP mice (both heterozygotes and homozygotes) began to die spontaneously by 4 months of age and only 35% (5/14) of the homozygotes and 69% (9/13) of the heterozygotes survived to the 6 month point (Figure 2.5A). This reduction in survival associated with the *Hip1*$^{\Delta 3\text{-}5}$ allele was not due to the effects of the *Hip1*$^{\Delta 3\text{-}5/\Delta 3\text{-}5}$ degenerative phenotype (*e.g.*, kypholordosis, dwarfism, etc.) as it was observed in both the heterozygotes and the homozygotes. In the TRAMP mice that were available for tumor analysis we found that 4 of the 5 surviving homozygous *Hip1*$^{\Delta 3\text{-}5}$ allele bearing TRAMP mice had gross prostate tumors (80%) and 3 of those 4 tumor bearing mice displayed gross evidence for multiple synchronous primary tumors in different lobes of the prostate (Figure 2.5B). In comparison, there was no evidence for multiple primary tumors in the *Hip1*$^{\Delta 3\text{-}5/+}$ (7 of these 9 (75%) mice had prostate cancer), *Hip1*$^{null/+}$ (6 of the 18 (33 %) mice had prostate cancer) or *Hip1*$^{null/null}$ (5 of the 15 (33%) had prostate cancer) TRAMP mice.

A novel cryptic splicing event allows for expression of a large mutant HIP1 protein

The difference in tumor incidence in the *Hip1*$^{null/null}$ mice and the *Hip1*$^{\Delta 3\text{-}5/\Delta 3\text{-}5}$ mice suggests either that (1) the original null allele alters the expression of neighboring genes and that it is those genes that influence tumorigenesis or (2) the Δ3-5 allele is not a completely null allele. To investigate these two possibilities, we examined normal and tumor tissues from TRAMP and MMTV-myc mice with the Δ3-5 allele for the

expression of polypeptides that react with HIP1-specific antibodies. Extracts from these tissues were analyzed by western blotting for the presence of either full-length or truncated HIP1 protein using a polyclonal rabbit antibody (UM354) specific for the amino-terminal end of the HIP1 protein (Figure 2.6A, lanes 5-10). Additionally, tumor tissue was dissociated and cultured so that tumor cells from these mice could be analyzed. Results of this analysis indicated that a truncated protein approximately 10 kDa smaller than the wild type HIP1 protein was expressed in the *Hip1*$^{\Delta 3\text{-}5/\Delta 3\text{-}5}$ tumor-derived cultured cells (Figure 2.6A, lanes 1 and 2 versus lanes 3 and 4). Extracts derived from the bulk of the tumor as well as other select tissues from these mice showed the expected lack of expression (Figure 2.6A, lanes 5-10).

In the construction of the Δ3-5 allele, exons 3 through 5 were deleted not only to disrupt the ANTH domain but also to ensure that the splicing of exon 2 with exon 6 or any of the other exons downstream of exon 6 would result in a frame shift that would lead to premature truncation at the amino terminal end of the protein. Therefore, the presence of a truncated HIP1 protein in these tumor cells that is only 10 kDa smaller than the wild type protein was quite surprising (Figure 2.6A, lanes 3 and 4). To identify the mRNA that encodes for this truncated HIP1 protein, we performed reverse transcriptase polymerase chain reaction (RT-PCR) using total RNA derived from TRAMP and MMTV-myc tumor-derived cultured cells. Primers specific to the exon 1 and the exon 14/15 junctions of the HIP1 cDNA sequence (NCBL BLAST-Accession # NT_039314) were used in the initial RT-PCR reaction. We detected a PCR product of the expected size (1.6 kb) in tumor-derived cells generated from wild type mice and from mice heterozygous for the Δ3-5 allele (Figure 2.6B, lanes 2, 4, 6-8 wt arrow). An additional band approximately 300 bp smaller (*i.e.*, 1.3 kb) than expected was observed in both heterozygous and homozygous mice. These bands were excised from the gel, PCR amplified using nested primers, and the products were sequenced. The cDNA sequence for the nested 1.6 kb product was identical to that of the wild type *Hip1* cDNA. Interestingly, the sequence of the nested 1.3 kb product contained exon 2 fused to exon 6 with a dinucleotide AG insertion in the junction. This dinucleotide insertion put the exon 2/6 fusion in frame (Figure 2.7) such that it encodes for an only slightly truncated HIP1 protein (Figure3c, “observed” sequence).

To examine further the above-described HIP1 mutant protein, we sequenced the *Hip1* gene from genomic DNA derived from cultured tumor cells. Surprisingly, we did not detect a mutation. However, careful analysis of the genomic sequence revealed two unique findings to explain the aberrant protein and transcript expression. First, we found that intron 2 uses a rare "AT-AC" U12 dependent splicing mechanism (Figure 2.6C). This type of intron, which represents approximately 1% of the introns in the mammalian genome [43], consists of 5'AT and 3'AC splice sites. Second, we found that the intron 5 splice acceptor (a typical AG) is immediately preceded by an AC. This ACAG sequence allows for the incorporation of an AG dinucleotide into the coding sequence of the mRNA transcript and serendipitous maintenance of the original reading frame. The predicted size of this mutant protein is 106 kDa (Figure 2.1 schematic), which is very similar to the size of the observed protein product (Figure 2.3A, lanes 3 and 4).

Mutant HIP1Δ3-5insAG protein expression in embryonic and adult lung and brain tissues

The presence of this AG dinucleotide insertion that placed exons 2 and 6 in frame in both Δ3-5 heterozygous and Δ3-5 homozygous cells led us to re-evaluate whether or not *Hip1* protein is expressed in normal tissues. We isolated select normal cells and tissues from wild type, Δ3-5 heterozygous, and Δ3-5 homozygous mice and analyzed them for the presence of the HIP1Δ3-5insAG protein product. Using northern blot analysis of embryonic fibroblast RNA (Figure 2.8A), we found that the truncated message was evident in homozygous mice (lane 2) when analyzed beside wild type RNA (lane 1). Using RT-PCR, we also found that tissue from the brains, lungs, and kidneys of Δ3-5 heterozygous and homozygous mice contained the Hip1Δ3-5insAG mRNA (Figure 2.8B). No PCR product representing the Hip1Δ3-5 mRNA was observed in wild type mice (Figure 2.8B, lanes 3, 6 and 9). We also found that extracts from cultured, early passage embryonic fibroblasts and embryonic brain contained easily detectable truncated HIP1Δ3-5insAG protein product (Figure 2.9). In contrast, nearly all adult tissues, with the exceptions of the lung and brain (Figure 2.8C, lanes 6 and 8), displayed very low levels of HIP1 polypeptide expression (Figure 2.8C, lanes 2, 4 and 10; use of an amino-terminal polyclonal antibody UM354). Either the diminished expression or the lack of function of the HIP1Δ3-5insAG product could explain why these mice display a

degenerative phenotype similar to that of the original homozygous "null" mice. In addition to the altered expression levels of the HIP1 peptides in various tissues, we noted that the migration of the HIP1 protein in the embryonic brain was quite different from that in the adult brain. Analysis of the *Hip1* protein product in embryonic, newborn, pre-weaned, and adult mice indicated that this differential expression correlates with developmental stage, with the product in the adult brain migrating distinctly slower or co-migrating with the wild type form of HIP1 (Figure 2.8D, lanes 2, 4 and 6). The molecular explanation of this striking developmental correlation remains to be determined.

Next, using the original *Hip1*$^{loxp/loxp}$ mice [26], we generated a tissue-specific Δ3-5 recombinant allele. By crossing the *Hip1*^{loxp} mice with mice carrying an interferon inducible Mx1-Cre transgene, we generated mice that expressed the Δ3-5 allele only in cells of the adult hematopoietic system, liver, and kidney following pIpC-mediated induction of Cre expression [42, 44]. With these mice, we examined whether the gross phenotype of the germ line Δ3-5 mouse could be recapitulated only in the isolated adult tissues. Interestingly, western blot analysis of extracts from the spleen, liver, kidney (Figure 2.10A), and bone marrow (Figure 2.10B) of Mx1-Cre induced mice demonstrated that the expression of the truncated HIP1 protein was most prominent in the spleen (Figure 2.10A, lanes 9-11) and bone marrow (Figure 2.10B lanes 3, 5, 7, 8) and loss of HIP1 expression altogether was frequently observed in the normal liver (lane 4-6, panel 1) and kidney (Figure 2.10A, lanes 9-11, panel 4) but as expected not in brain, heart, eye (Figure 2.10A), uterus, ovary or the GI tract (data not shown). It is of interest that in the two tissues, liver and kidney, where we observed HIP1 protein deficiency due to a complete recombination event did not display the degenerative phenotype observed in the germ line recombined Δ3-5 mice. We therefore conclude that tissue specific HIP1 deficiency in the liver and kidney does not induce the knockout phenotype. Unfortunately, we could not make this conclusion in the hematopoietic system as despite repeated attempts to induce interferon with pIpC, the complete recombination of the *Hip1*^{loxp} allele in the Mx1-cre mice was not achieved in hematopoietic tissues (Figure 2.10B, lane 7) and, therefore, a significant amount of wild type Hip1 expression remained in the homozygotes.

These findings also suggest the possibility that the truncated HIP1 protein may be preferentially expressed in dividing cells, including tumorigenic cells. This prediction is supported by the finding that Δ3-5insAG protein was present in the fibroblasts and brains of Δ3-5 mouse embryos at E17.0 day (Figure 2.8C, lanes 5, 6, 11, 12). Furthermore, we discovered a gross liver tumor in an Mx1Cre;*Hip1*$^{loxp/+}$ mouse (Figure 2.10C). The tumor from this mouse expressed a truncated Δ3-5 protein product while the surrounding "normal" liver did not. Additionally, we identified a trend in which the spleen sizes of the *Hip1* floxed, Mx1cre, pIpC-treated mice increased, although frank hematopoietic malignancies were not observed (data not shown).

The HIP1Δ3-5insAG protein retains its ability to bind lipids, clathrin, AP2, and EGFR

We have observed some slight phenotypic differences between the *Hip1* $^{\Delta 3\text{-}5/\Delta 3\text{-}5}$ mice and the *Hip1*$^{null/null}$ mice [26]. These differences included absence of cataracts or perinatal death in the *Hip1* $^{\Delta 3\text{-}5/\Delta 3\text{-}5}$ mice, increased mortality from tumors in the TRAMP;*Hip1*$^{\Delta 3\text{-}5}$ mice relative to the TRAMP;*Hip1*$^{null/null}$ mice (Figure 2.5A), no decrease in breast or prostate tumorigenesis in *Hip1*$^{\Delta 3\text{-}5}$ allele bearing backgrounds (although there was a trend toward more tumors; Figure 2.3A), and a liver tumor in a young, conditional *Hip1*$^{\Delta 3\text{-}5}$ heterozygous mouse (Figure 2.10C). Given these differences, we examined whether the Hip1Δ3-5insAG protein product possesses all or a subset of its cellular activities that promote normal and neoplastic cell proliferation/survival by assessing its ability to bind to lipids, endocytic factors, and EGFR.

Because this truncated protein retains its clathrin-, AP2-, and EGFR-binding regions, we predicted that the Hip1Δ3-5insAG protein product would have the ability to bind these proteins. To test this hypothesis, we expressed the *HIP1*$^{\Delta 3\text{-}5/insAG}$ cDNA in 293T cells, immunoprecipitated the mutant protein with an anti-HIP1 polyclonal antibody (UM323, bleed 8/2002), and immunoblotted the precipitates to determine the presence or absence of the endocytic proteins and EGFR. As expected, the truncated mutant protein bound EGFR, clathrin and AP2 (the alpha subunit) (Figure 2.11A, lanes 11 and 15). In contrast, expression of a human HIP1 mutant cDNA construct that lacks the AP2- and clathrin-binding domains did not bind these endocytic proteins (Figure 2.11A, lanes 12

and 16). Also, it should be noted that the interaction between HIP1 and EGFR was apparently enhanced by the deletion of either the sequences encoded for by exons 3-5 (Figure 2.11A, lanes 11 and 15 compared to 10 and 14) or the domains that bind to endocytic proteins (Figure 2.11A, lanes 12 and 16), suggesting that the interaction of HIP1 with EGFR is not indirectly mediated by the its binding with clathrin and/or AP2.

Since 80% of the sequence of the lipid binding ANTH domain is deleted from the HIP1Δ3-5insAG protein (Figure 2.1), we predicted that this mutant would likely not retain its lipid binding activity. Interestingly, most of the key residues that are important for the direct binding of the ANTH domain-containing proteins to $PI(4,5)P_2$ were retained in the Δ3-5 protein product (key residues are bold in Figure 2.1) [14, 15]. However, one key residue (homologous to K76 of epsin) that has been shown to be important in binding to the $Ins(1,4,5)P_3$ head group [15] is deleted in the truncated Δ3-5 protein. To determine whether the Δ3-5 protein product retained its lipid-binding capacity, we examined lipid binding using recombinant GST-$HIP1^{wt}$ and GST-$HIP1^{\Delta 3\text{-}5/insAG}$ fusion proteins. We generated and glutathione-sepharose purified GST-fusion proteins that contained the first 430 and 370 amino acids of the $HIP1^{wt}$ and $HIP1^{\Delta 3\text{-}5/insAG}$ proteins, respectively (Figure 2.11B). The purified proteins were separated by SDS-PAGE and Coomassie stained to quantitate the amount of recombinant protein. The purified recombinant proteins were also analyzed by western blot to ensure interaction with anti-GST and anti-HIP1 antibodies (Figure 2.11B). Next, the purified proteins were incubated with Echelon-generated PIP strips to examine whether the fusion proteins were capable of binding lipids. Both the wild type and the $HIP1^{\Delta 3\text{-}5/insAG}$ mutant fusion proteins bound PtdIns(3)P predominantly (Figure 2.12). These results were confirmed using PIP arrays (Echelon), which were used to further examine the differential abilities of these proteins to bind to lipids. Interestingly, these truncated fusion proteins displayed a higher specific binding to PtdIns(3)P than to polyphosphorylated inositol lipids. On the other hand, our previous studies using the full-length HIP1 expressed in 293T cells indicated that its lipid binding preference was polyphosphorylated 3-phosphoinositides [16]. Our contradictory results may be due to either the absence of the carboxyl-terminal end of the protein, differences in proteins expressed in bacteria versus mammalian cells or differences in the materials used in the various assays. Additional biochemical analyses are necessary to clarify this

issue. Nevertheless, the specific inositol lipid binding capacity of the ANTH domain is retained in the Hip1Δ3-5insAG protein.

Discussion

We have previously demonstrated that the HIP1 family of proteins are biologically important since both single *Hip1* [26, 37] and double *Hip1/Hip1r* [28] knockout mice have adult degenerative phenotypes and HIP1 protein expression is altered in multiple cancers [9]. However, the exact function of this protein family remains unclear, and more detailed cellular and biochemical analyses are needed to validate predicted functions and identify novel ones. In the current study, we describe a novel form of HIP1 that is expressed *in vivo* as the result of a novel cryptic splice event between a 5' AT-AC intron (intron 2) and a 3' GT-AG intron (intron 5). These results are important for both technical and functional reasons. First, it illustrates an unpredicted cryptic splicing event in a previously predicted "loss of function" gene targeting event, and, second, this type of cellular natural selection may provide clues to the function of HIP1 in normal and neoplastic cells.

The technical aspects of these findings have provided us a very important lesson. The targeting event that we initially designed led to a mutation in the AT-AC intron 2. The rare splicing event that we observed reflects preferential splicing between splice sites of the same class. The identification of rare U12-dependent intron splicing sites or AT-AC introns will be important for all proteins with similar genetic structures [43]. This finding has also raised an intriguing possibility that such splicing events might occur in normal cells leading to the expression of unexpected polypeptides. Interestingly, the rare AT-AC intron 2 is conserved in both the human and mouse *Hip1* genes. This observation is consistent with previous reports that U12-type introns are usually conserved phylogenetically [45]. It has been reported previously, that genes with nonredundant, crucial cellular activities may have strong selective evolutionary pressure against the conversion of U12- to U2-type introns and, therefore, have retained them. HIP1 supports this assertion as HIP1 clearly has nonredundant, crucial activities as evidenced by the fact that its deletion in mice leads to dramatic adult phenotypes [26, 28, 37].

In terms of HIP1 function, it is evident that the expression of the truncated mutant protein in adult lung and brain tissue does not prevent the adult degenerative phenotypes, such as kypholordosis or testicular degeneration. The discovery here of concomitant expression of HIP1 sequences in the Hip1Δ3-5 homozygous mice and the degenerative phenotype suggests that this mutant protein may not be completely functional in normal cells. In contrast, the presence of the truncated mutant protein in tumor cells may explain why tumorigenesis is not inhibited by the homozygosity of this allele. This proposal is supported by the finding that this mutant protein retains some of its functions (*i.e.*, the ability to bind to lipids, clathrin, AP2, and EGFR). These findings illustrate a prototypical example that provides insights into how mouse modeling may lead to insertion mutations and unpredicted, active protein products.

The maintenance of AP2-, CHC-, EGFR- and lipid-binding functions in the truncated mutant HIP1 protein suggests that another HIP1 cellular function must contribute to the gross phenotype of the mutant mice. This unknown function likely explains why we were unable to identify endocytic defects in either of the mutant mouse systems. Future studies are required to understand the molecular modifications and sequences of the various forms of HIP1 that are expressed in different tissues at different times during mammalian development and how these different forms affect HIP1 functions.

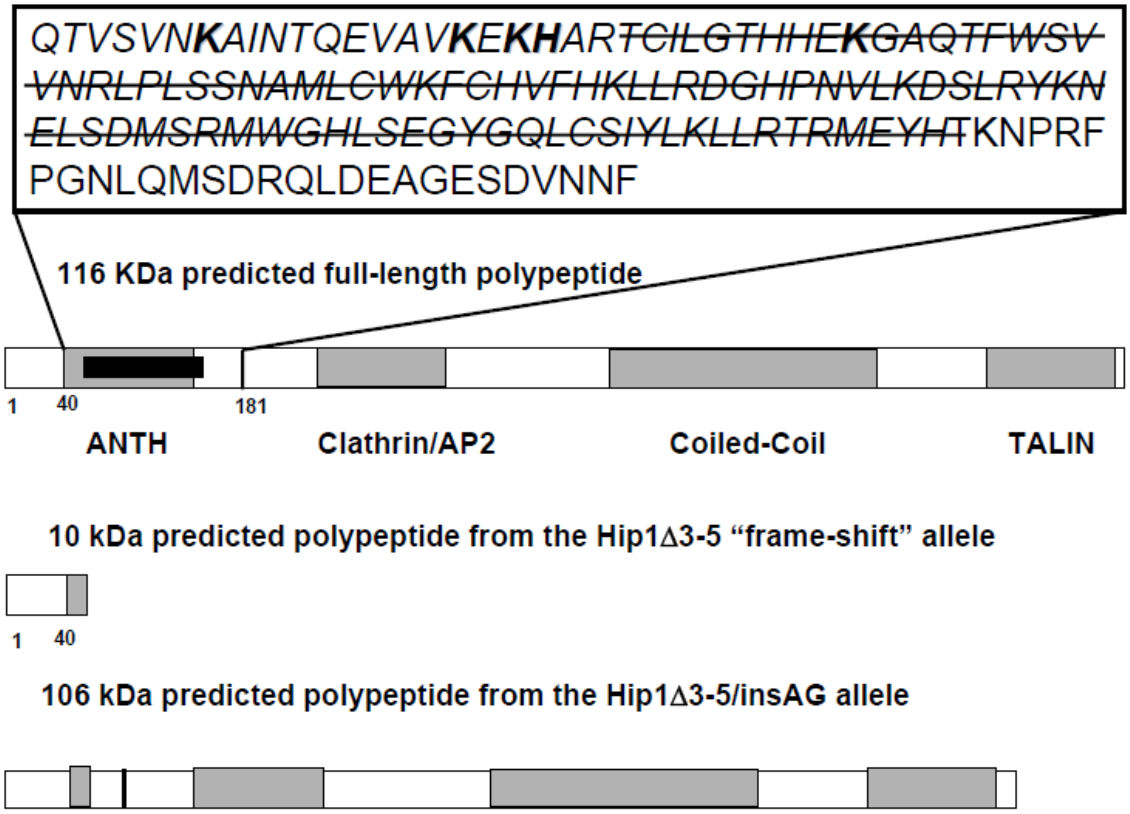

Figure 2.1: Amino acid sequence of the HIP1 ANTH domain and schematic diagram of the HIP1 domain structure. The majority of the mouse ANTH domain is encoded by exons 3 to 5. The amino acid sequence of the mouse ANTH domain (italicized, [14, 15]) and a few additional carboxyl amino acids are shown in the box above the schematic diagram of the full-length protein. A line is drawn through the amino acids that are encoded by exons 3 to 5. Residues in bold (K, K, KH, K) share homology with AP180 and epsin and are considered to be critical inositol lipid-binding residues. The predicted protein product encoded by the *Hip1*$^{\Delta 3\text{-}5}$ allele is 10 kDa and is shown schematically below the full length HIP1 diagram. The predicted protein product from the *Hip1Δ3-5insAG* cDNA is 106 kDa and is also shown schematically.

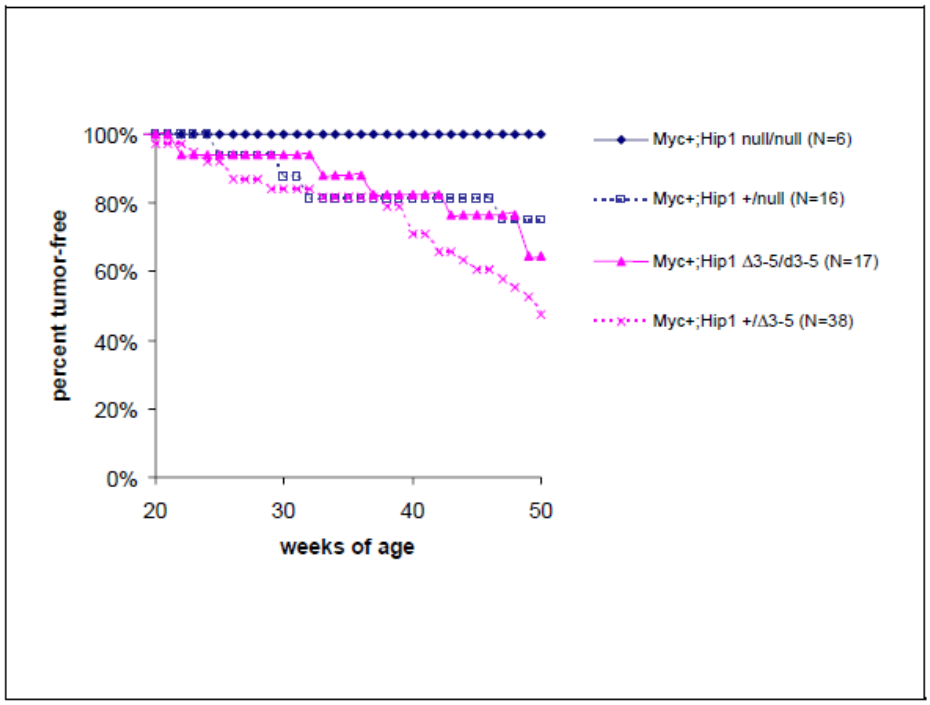

Figure 2.2: Tumorigenesis in MMTV-myc mice in the absence of HIP1. Percent tumor-free survival out to 5 weeks of age is shown for MMTV-Myc+ mice on various HIP1 knockout backgrounds. Mice were sacrificed when the tumor ulcerated or impeded movement.

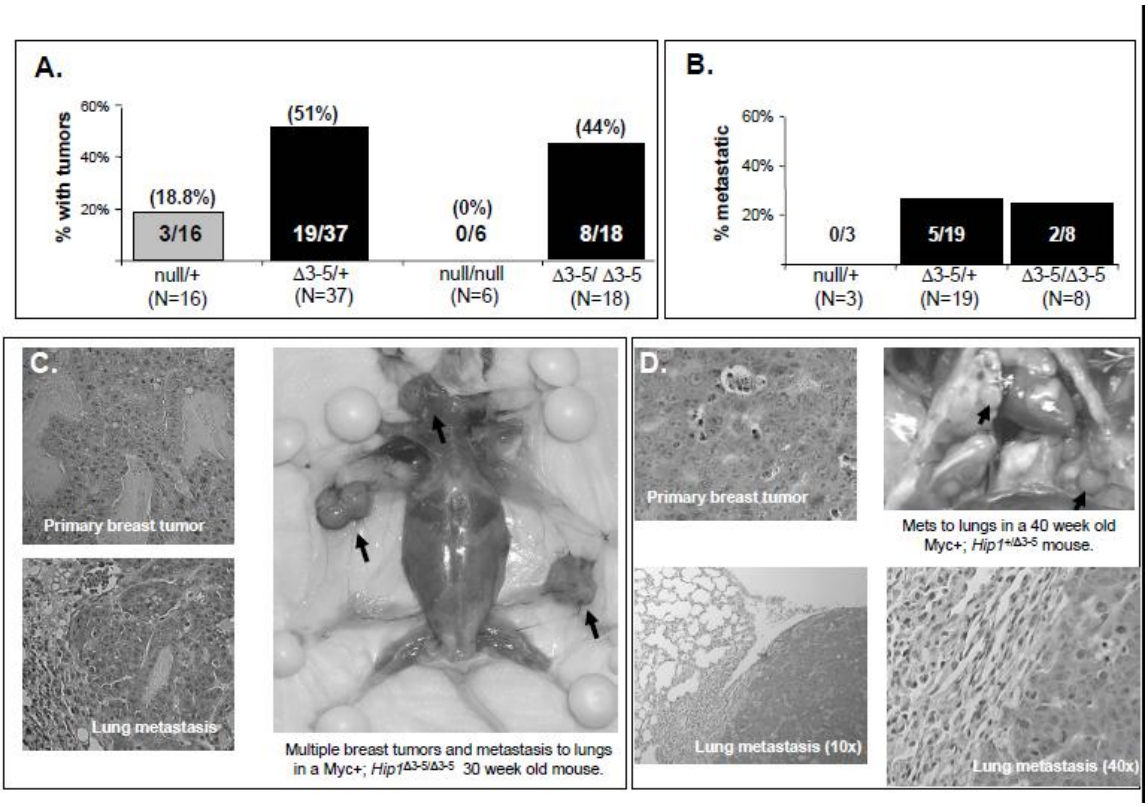

Figure 2.3: Breast tumorigenesis in the presence of the Hip1Δ3-5 allele.
A. MMTV-myc transgenic mice were mated on to *Hip1*$^{null/null}$ and *Hip1*$^{\Delta 3\text{-}5/\Delta 3\text{-}5}$ backgrounds. Mice were dissected at one year of age, or earlier if a tumor was found. 44% of *Myc+;Hip1*$^{\Delta 3\text{-}5/\Delta 3\text{-}5}$ mice developed breast tumors, compared to none of the *Myc+; Hip1*$^{null/null}$ mice. 51% of *Myc+; Hip1*$^{+/\Delta 3\text{-}5}$ mice developed breast tumors, compared to 19% of *Myc+; Hip1*$^{+/null}$ mice.
B. None of the *Hip1*$^{+/null}$ mice with tumors (N=3) exhibited metastasis of the breast tumors. 25% of *Myc+;Hip1*$^{\Delta 3\text{-}5/\Delta 3\text{-}5}$ mice with tumors (N=8) and 26% of *Myc+; Hip1*$^{+/\Delta 3\text{-}5}$ mice with tumors (N=19) had metastasis of the breast tumors to organs including the lungs, liver, spleen and salivary gland.
C. Multiple breast tumors and metastasis to lungs of a *Myc+; Hip1*$^{\Delta 3\text{-}5/\Delta 3\text{-}5}$ mouse at 30 weeks of age.
D. Metastasis of a breast tumor to the lungs of a *Myc+;Hip1*$^{+/\Delta 3\text{-}5}$ mouse at 40 weeks of age.

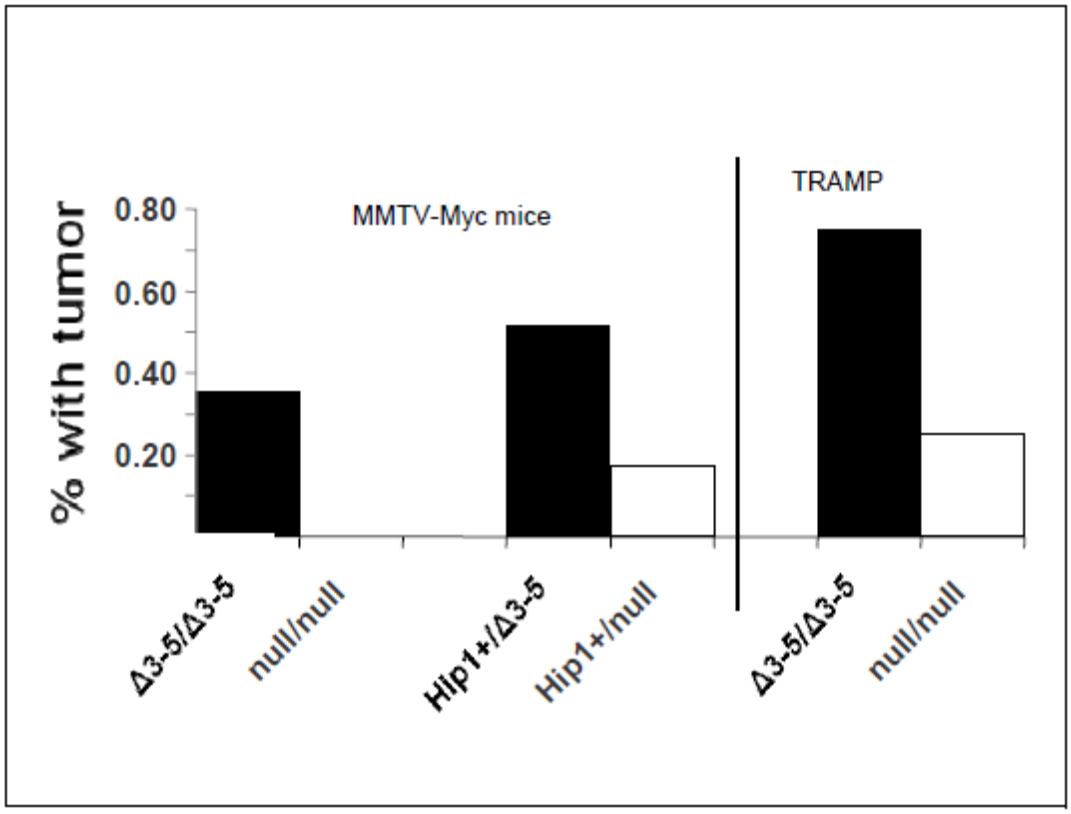

Figure 2.4: Tumor incidence in mice with *Hip1*Δ3-5 and *Hip1*null alleles. MMTV-myc transgenic and TRAMP mice were mated on the *Hip1*$^{null/null}$ and *Hip1*$^{\Delta 3\text{-}5/\Delta 3\text{-}5}$ backgrounds and analyzed for tumor incidence. TRAMP mice that survived to 6 months of age were scored for gross prostate tumors. In each case the mice with the Δ3-5 allele were afflicted with more tumors.

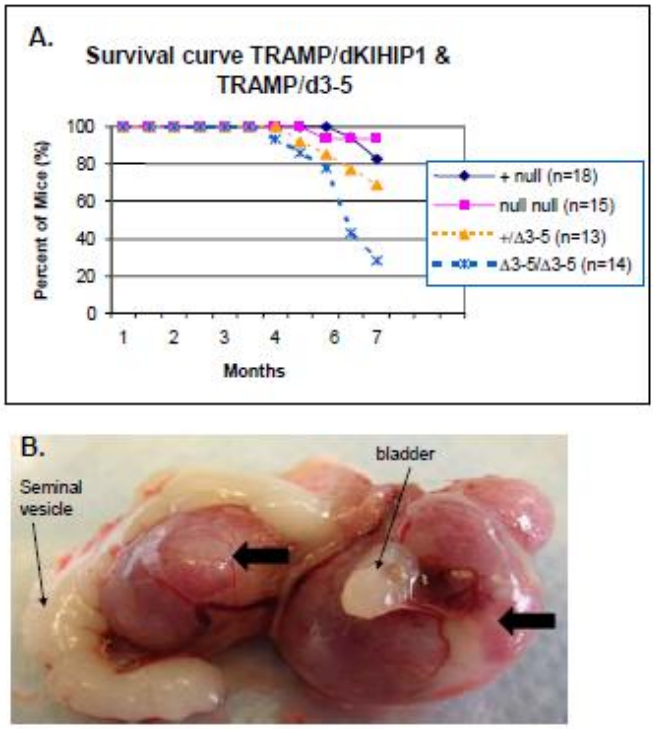

Figure 2.5: TRAMP mice on different *Hip1* mutant backgrounds.

A. Survival curve of TRAMP mice in different *Hip1* mutant backgrounds.

B. Examples of bilateral synchronous prostate tumors.

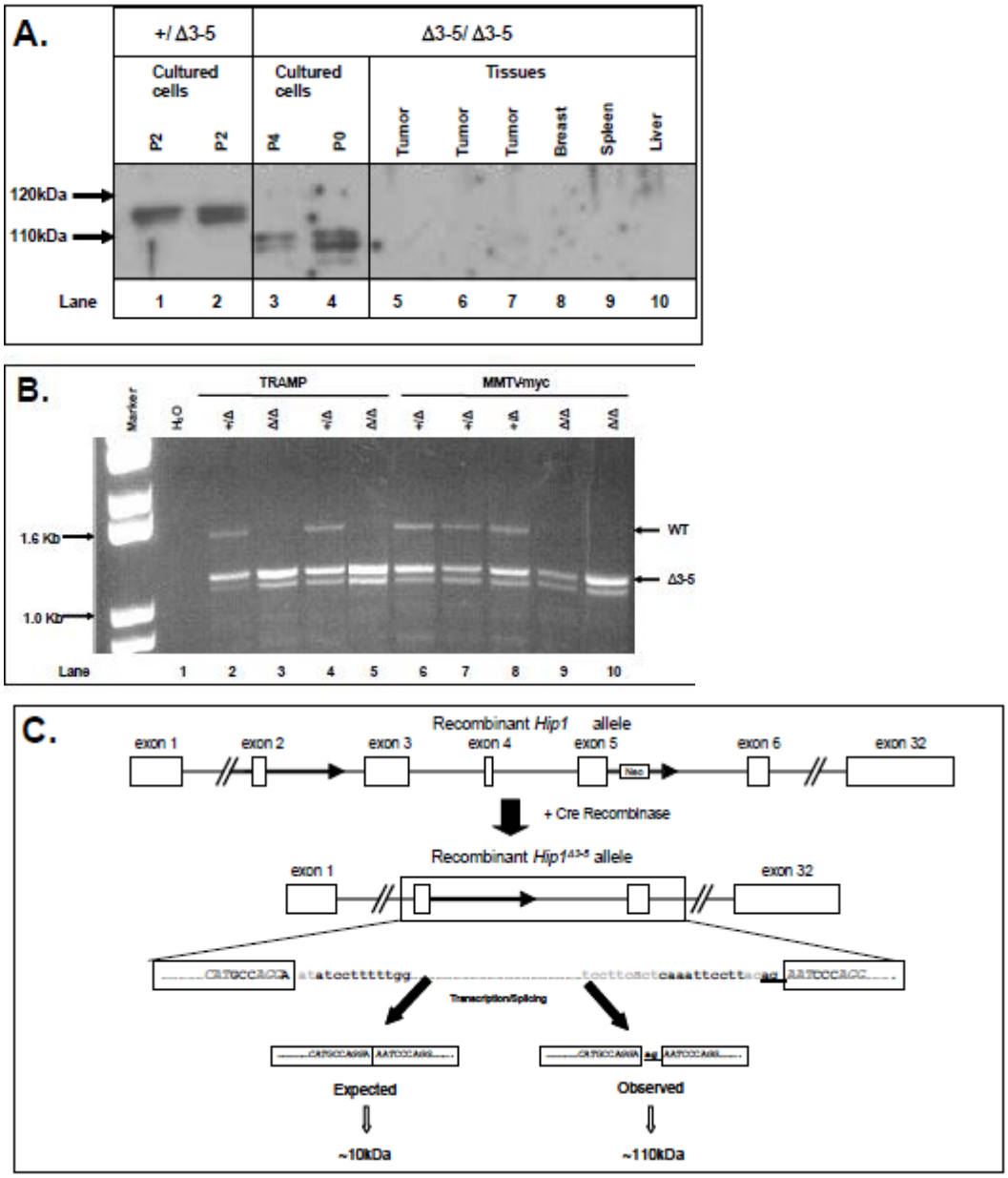

Figure 2.6: Expression of Hip1 sequences in Hip1Δ3-5 mice.

A. Tumors from mice with breast (MMTV-myc) and prostate (TRAMP) cancer were grown in culture and analyzed by western blot for the presence of HIP1 polypeptides. Results from an MMTV-myc breast tumor sample are shown. P=passage number. Even at zero passages (P0), the cultured cells from Δ3-5/Δ3-5 tumors expressed a slightly truncated form of HIP1 (Lane 4). This product was not detected in the bulk tumor tissue, in the normal tissues tested of these mice, or in any cell types derived from mice heterozygous for the Δ3-5 allele (lanes 5-10).

B. RT-PCR of total RNA extracted from Δ3-5 allele-containing tumor-derived cultured cells resulted in the generation of wild type (WT) and mutant (Δ3-5) bands of expected sizes.

C. Partial *Hip1Δ3-5* cDNA sequence alignment with wild type mouse *Hip1* cDNA demonstrated an AG dinucleotide insertion between exons 2 and 6 of the *Hip1Δ3-5* cDNA sequence. This insertion maintains the open reading frame of the transcript. Tumor cell line genomic DNA contains a recombined "AT-AC" intron. Genomic DNA isolated from a Myc breast tumor-derived cell line was sequenced in the region where the recombination occurred (box). The sequence was compared to wild type *Hip1* genomic DNA and no additional mutations were observed. Note the recombinant intron flanked by exons 2 and 6 has a U12-dependent consensus branch point sequence (italicized) and a 3' AC dinucleotide (italicized) that serves as the cryptic splice site acceptor. This splicing event results in an "AG insertion" in the transcript. The region sequenced is indicated by the box that encompasses exons 2, 6 and intervening sequences including the single loxP site.

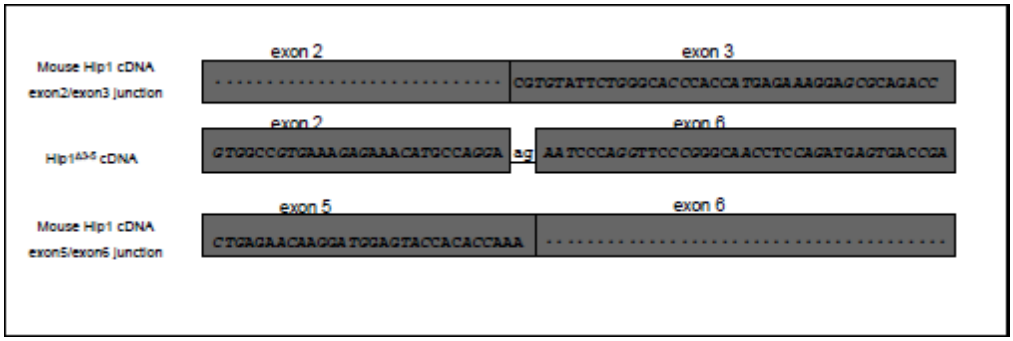

Figure 2.7: Partial *Hip1Δ3-5* cDNA sequence alignment with wild type mouse *Hip1* cDNA. Shown is an alignment of cDNA sequence from the nested PCR reaction with the exon 2/3 and exon 5/6 junctions of mouse *Hip1* mRNA reference sequence (NM_146001). Dots in the mouse *Hip1* mRNA reference sequence denote identity with the *Hip1 Δ3-5* cDNA sequence. Codons are represented by alternating bold/nonbold trinucleotide sequences. Note the AG dinucleotide insertion between exons 2 and 6 of the *Hip1 Δ3-5* cDNA sequence, which maintains the open reading frame of the transcript.

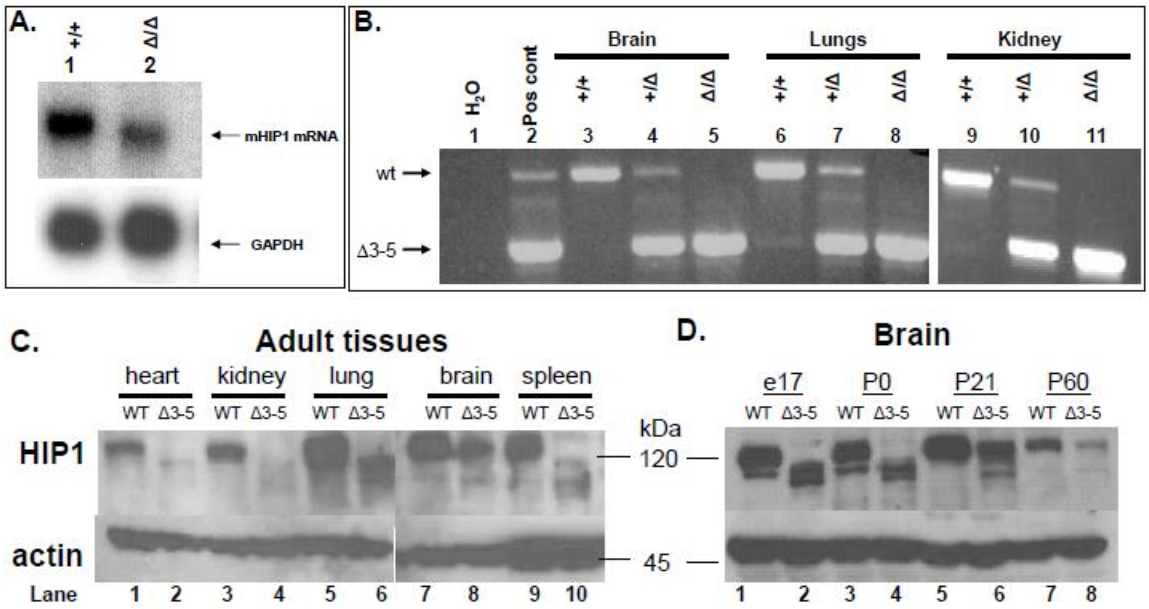

Figure 2.8: Expression patterns of the Δ3-5insAG mRNA and its putative protein product.

A. Northern blot analysis using a probe specific for the 5' end of the mouse *Hip1* mRNA (nucleotides 1-1260) demonstrated the presence of a significant amount of a slightly truncated product in the RNA of mouse embryonic fibroblast (lane 2 versus lane 1).

B. Primers specific to the exon 1/2 junction (forward) and the exon 13/14 junction (reverse primer) of murine *Hip1* cDNA were used to amplify the cDNA. The resulting products were separated on a 1.0% agarose gel. Water was used as the negative control (lane 1). RNA from a TRAMP prostate cancer cell line generated from the prostate tumor tissue of a mouse that was heterozygous for the $Hip1^{\Delta 3\text{-}5}$ allele was used as a positive control for both the wild type *Hip1* and $Hip1^{\Delta 3\text{-}5/insAG}$ mRNA transcripts (lane 2). A 1.6 kb band indicates the presence of wild type *Hip1* mRNA transcripts while a 1.3 kb band indicates the presence of the mutant $Hip1^{\Delta 3\text{-}5/insAG}$ mRNA transcripts. Brain, lung and kidney tissues from wild type *Hip1* mice (+/+) produced the 1.6 kb band but not a 1.3 kb band (lanes 3, 6 and 9). Similar tissues from heterozygous Δ3-5 mice (+/Δ) produced both a 1.6 kb band and a 1.3 kb band (lanes 4, 7 and 10). Only the 1.3 kb band was produced in brain, lung, and kidney tissues from homozygous Δ3-5 mice (Δ/Δ) (lanes 5, 8 and 11).

C. Expression of the truncated product was most prominent in lung tissue although lesser amounts are detected in all other tissues tested. Interestingly, brain tissue from Δ3-5 adult mice displayed significant amounts of a protein product that co-migrated with the wild type form. This co-migration was not observed in the extracts from embryonic brains (described in panel D). Actin blotting was performed using an anti-actin monoclonal antibody (Sigma) as a control.

D. Postnatal day zero brains (isolated immediately after birth) have HIP1 banding patterns similar to those of embryos. Pre-weaning stage brains have two distinct HIP1 bands, and the adult brains have a HIP1 band that co-migrates with the wild type band.

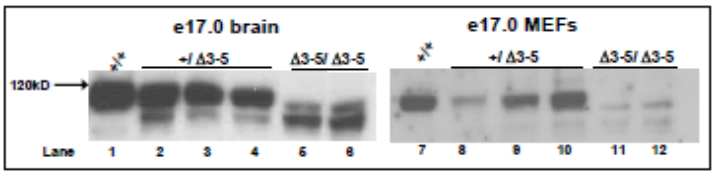

Figure 2.9: HIP1 Δ3-5/insAG 106 kDa protein is present in mouse embryonic brain and fibroblasts. Western blot analysis for HIP1 expression in the brains (left panel) and fibroblasts (right panel) of 17-day old mouse embryos of different genotypes demonstrated the presence of a slightly truncated HIP1 product. MEF cells of different genotypes were cultured from eleven individual embryos from the same mother. Only 5 samples are shown here but all demonstrated similar banding patterns as related to the distinct genotypes.

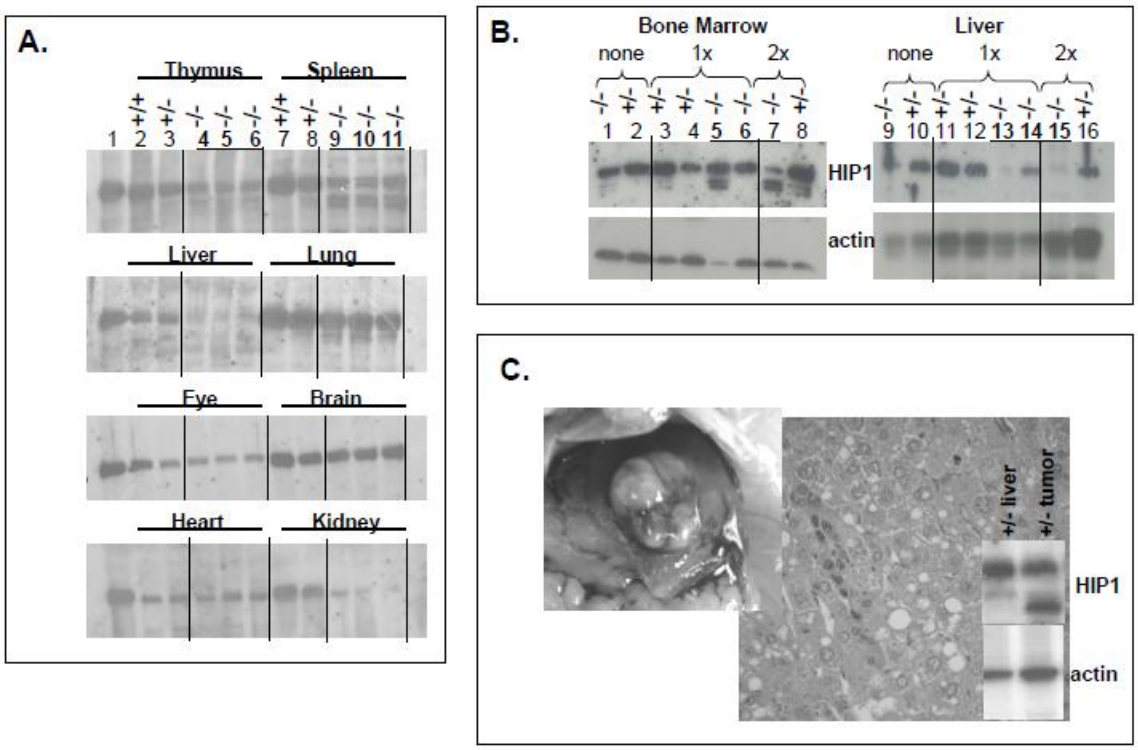

Figure 2.10: Conditional cre-mediated recombination of the floxed Hip1 allele leads to either HIP1 deficiency or expression of the truncated product depending on tissue analyzed.

A. Mx1-Cre transgenic mice carrying none (+//+; lanes 2 and 7), one (-/+; lanes 3 and 8) or two (-/-; lanes 4-6 and 9-11) of the floxed *Hip1* alleles were treated with 3 injections of pIpC at 8-12 weeks of age then were retreated at 20 weeks of age. Their organs were harvested at 28-32 weeks of age. Organ extracts were separated on 6% SDS-PAGE and analyzed for HIP1 expression by western blotting (using the UM354 (1:5000) antibody). An extract of a wild type brain (lane 1) was included as a positive control of HIP1 expression. Near complete recombination (resulting in the deficiency of HIP1 protein) was observed in liver and kidney but not in thymus and spleen where residual wild type HIP1 and truncated HIP1 (putative Δ3-5insAG product) was expressed. As expected, eye, brain, and heart tissue showed no evidence for recombination since Mx1-cre is not induced in these tissues [42]. A small amount of putative Δ3-5insAG truncated product was observed in lung tissue and may be a result of recombination in tissue macrophages, which are abundant in the lung tissue.

B. Mice were untreated (lanes 1, 2, 9 and 10) or treated at 6 weeks of age with pIpC (6 doses IP every other day; lanes 3-6 and Lanes 11-14). A small group was treated with pIpC again at 20 weeks of age (3 additional doses every other day; lanes 7, 8 and 15, 16). The mice were sacrificed at 6 months of age, and their tissues were analyzed for HIP1 expression by western blot (UM354). Complete deficiency of HIP1 was never observed in bone marrow despite continued pIpC injections whereas complete deficiency of HIP1 was achieved was maintained in the liver without repeated recombination. Interestingly, in the mouse without complete recombination in the liver (lane 14), there was no

truncated product in its cultured bone marrow (lane 6). A small amount of the truncated product was observed in cultured bone marrow from some untreated mice (*e.g.* lane 1), a finding consistent with the possibility that the endogenous production of interferon (*i.e.* in response to viral infections) can activate Mx1-cre expression at low levels in mice in the absence of pIpC treatment. As a loading control, actin blots were performed on 10% SDS-PAGE using a monoclonal anti-actin antibody (Sigma, St. Louis, MO).

C. Mice were treated with pIpC in two stages: first at 21 weeks of age (with 6 every other day doses) and second at 55 weeks of age (with 6 every other day doses). Six treated mice (3 heterozygous and 3 homozygous) and 5 untreated mice were necropsied. At necropsy, a previously undetected liver tumor was discovered in a treated heterozygous mouse, and it was harvested for histological and protein expression analysis. Increased amounts of truncated HIP1 expression were observed in the tumor tissue compared to surrounding "normal" liver tissue. Since this was a heterozygous mouse, expression from the wild type allele was also detected.

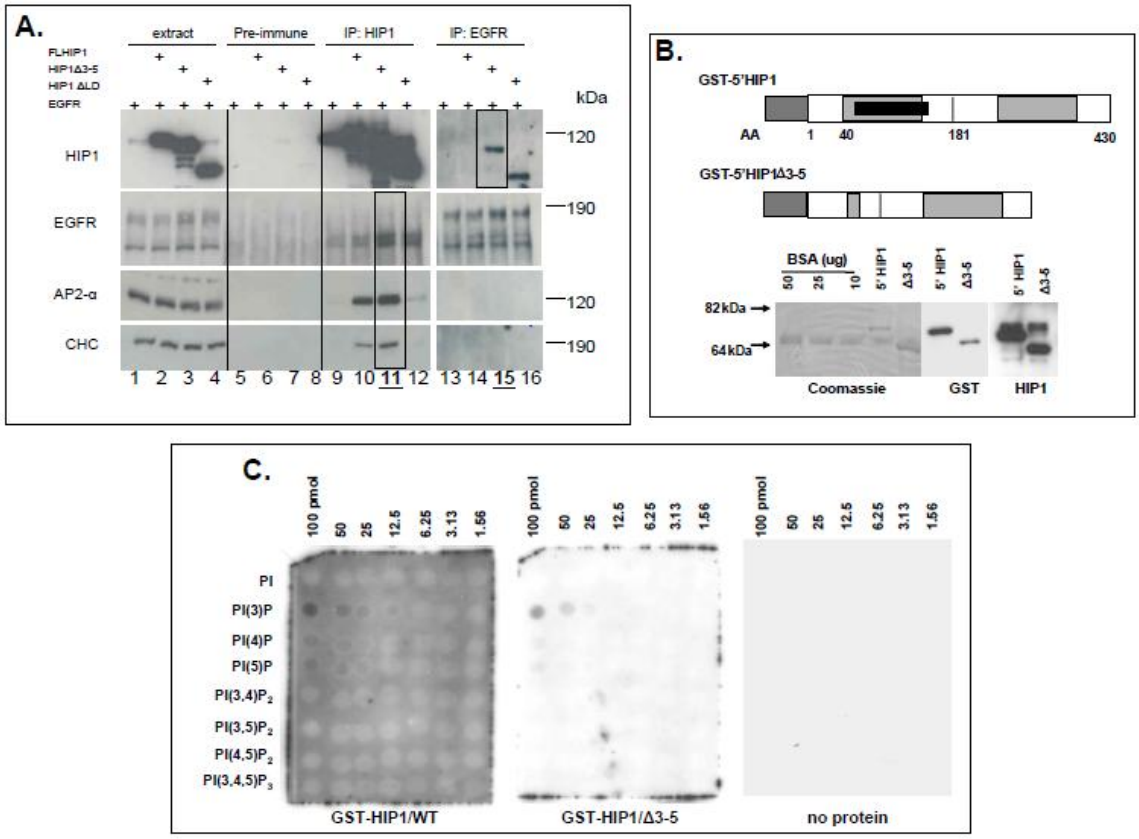

Figure 2.11: HIP1Δ3-5insAG association with clathrin, AP2, EGFR and lipids.
A. HEK 293T cells were transfected with EGFR and/or various HIP1 constructs. Cells were lysed 24 hours post-transfection and polyclonal anti-HIP1 (UM323) and anti-EGFR antibodies were used for immunoprecipitation. The immunoprecipitates were separated on 6% SDS-PAGE gels and transferred to nitrocellulose for western blot analysis using the indicated antibodies. Lanes 1-4: whole cell lysates. Lanes 5-8: Pre-immune immunoprecipitates. Lanes 9-12: anti-HIP1 immunoprecipitates. Lanes 13-16: anti-EGFR immunoprecipitates. Note the association of AP2, CHC, and EGFR with HIP1 is preserved despite deletion of sequences encoded by exons 3-5. Interestingly, the anti-EGFR antibody did not co-precipitate wild type HIP1 (top panel, lane 14) but did co-precipitate the HIP1Δ3-5 and HIP1ΔLD mutant proteins (top panel; lanes 15 and 16).
B. Schematic diagrams of GST-5'HIP1 and GST-5'HIP1/Δ3-5 fusion proteins are shown. Expression of these fusion proteins in *E. coli* BL21 was induced by treatment with 0.1 mM IPTG. The cells were pelleted and lysed, and the fusion proteins were purified from the resulting extracts using glutathione sepharose 4 beads. Ten microliters of a 1:10 dilution of the purified GST-5'HIP1 and GST-5'HIP1/Δ3-5 fusion proteins were run on a 10% polyacrylamide gel and immunoblotted with an anti-GST antibody (1:5000) or an anti-HIP1 antibody (UM354-1:2000) to ensure reaction of the proteins by the respective antibodies and to confirm their purity. Similar amounts were run on a separate 10% polyacrylamide gel along with various known concentrations of BSA, and the gel was Coomassie stained to estimate the concentrations of the purified fusion proteins.

C. Protein solutions containing 10 μg of either purified GST-5'HIP1 or GST-5'HIP1/Δ3-5 protein in TBST with 1% milk were incubated with PIP arrays (Echelon) containing various concentrations of different phosphoinositides. As with the PIP strips, both GST-5'HIP1 and GST-5'HIP1/Δ3-5 proteins bound preferentially to PtdIns(3)P. Lipid-protein interactions were detected using a polyclonal anti-GST antibody (Cell Signaling Technologies). No signal was detected using antibody alone.

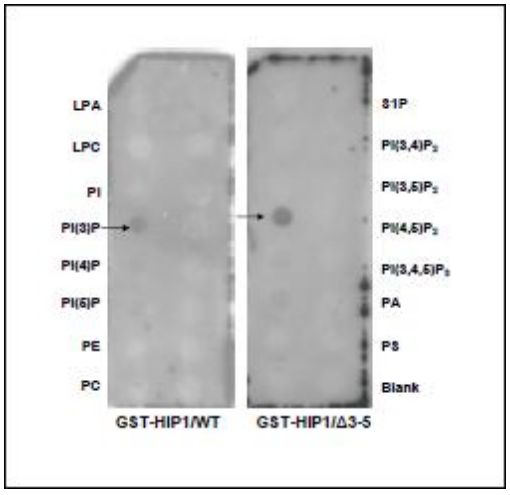

Figure 2.12: Comparison of lipid binding specificity and relative affinity GST-5'HIP1/Δ3-5 and GST-5'HIP1 using PIP strips. Protein solutions containing 10μg of either purified GST-5'HIP1 or GST-5'HIP1/Δ3-5 protein in TBST with 1% milk were incubated with PIP strips (Echelon) containing 15 different lipids at 100 pmol/spot. Lipid-protein interactions were detected using a polyclonal antibody (UM354) that recognizes both GST-5'HIP1 and GST-5'HIP1/Δ3-5 proteins. Both proteins bound preferentially to PI(3)P on the PIP strips.

CHAPTER 3

ALTERNATIVE HIP1 TRANSCRIPTS IN MOUSE AND HUMAN CELLS MAY ENCODE DIFFERENT HIP1 ISOFORMS

Summary

Huntingtin Interacting Protein 1 (HIP1) is a clathrin binding protein that is necessary for the *in vivo* maintenance of a subset of normal and neoplastic cells. Reports of the ability of HIP1 to induce or inhibit cell death are conflicting. One possible explanation for this is that different isoforms of HIP1 are expressed and these isoforms have different effects on cellular survival. Indeed, here we have identified a second *Hip1* mRNA that may encode a protein with potentially opposing effects on cellular survival than the originally characterized isoform. The two mRNAs differ only in their starting exons, designated exons 1a and 1b. The predicted protein products differ only slightly in their amino termini. However, an alternatively translated protein product is selectively produced by the exon1b-containing transcript, possibly the result of translational reinitiation. This product lacks the AP180 N-terminal homology (ANTH) domain and may induce apoptosis when exogenously expressed. Efforts are currently underway to determine if this is the case.

Introduction

HIP1 was originally identified as a protein that binds huntingtin, the protein whose gene is mutated in Huntington's disease [1, 2]. Subsequently, it was found to have domains that bind clathrin, AP2 [18-21], inositol lipids [14-16] and actin [46]. Knockout of *Hip1* alone [26, 37] or together with its only known relative, Hip1-related (*Hip1r*) [27], results in an adult mouse degenerative phenotype, which are rescued by heterologous expression of full-length HIP1 [28]. HIP1 was independently identified as the amino-terminal partner of a oncogenic fusion protein (HIP1/PDGFβR) that resulted

from a chromosomal translocation in bone marrow cells of a patient with leukemia [10]. Subsequently, HIP1 protein levels were found to be elevated in prostate, colon [9], breast [38], brain [5] and lymphoid [7] cancers and HIP1 expression in prostate cancer was prognostic [9]. Furthermore, HIP1 on its own transforms fibroblasts [38] and is necessary for prostate cancer progression in mice [6]. As a result of these data, it has been hypothesized that HIP1 is a novel type of oncogene that, when over-expressed, hijacks normal endocytic pathways to transform cells by increasing pro-growth and pro-survival signals from multiple receptors in parallel [47].

In contrast to its role in promoting cellular survival or growth, it has also been reported that HIP1 has pro-apoptotic functions that contribute to neurodegeneration [3, 4]. These functions have variably been dependent upon caspase 8 [4] and caspase 9 activation which is enhanced by the presence of the protein designated "HIP1 protein interactor" (HIPPI) [3]. Although, we have searched and not found any apoptotic activity upon exogenous expression of HIP1 in our laboratory using the same cells (293T), we have found that a mutant HIP1 construct that lacks the ANTH domain (HIP1/ΔANTH) does induce apoptosis [9, 16]. Furthermore, it was recently reported that there are two alternative forms of *Hip1* in *Drosophila* that have opposing roles in Notch-mediated neurogenesis and these forms are homologous to the full length HIP1 and the HIP1/ΔANTH form [30]. We have also observed by immunoblot analysis the presence of multiple isoforms of HIP1 in mouse tissues extracts [34] as well as in monocytic bone marrow cells induced to differentiate into osteoclasts [7].

To investigate the possibility that different forms of HIP1 have different functions as reflected by their pro- or anti-survival activities, we analyzed mammalian tissues and cells for the presence of alternative *Hip1* transcripts. We report here that there are at least two distinct *Hip1* mRNA transcripts that result from the use of alternative first exons and these transcripts may encode different protein products that have opposing pro- and anti-apoptotic activities. These data provide a possible explanation of prior data that appears "conflicting" in the literature [3, 4, 9].

Materials and Methods

5' Rapid Amplification of cDNA Ends (RACE) analysis

5' RACE analysis was performed using the GeneRacer™ kit (Invitrogen). All procedures were performed according to the manufacturer's suggestions. Five (5) µg of total RNA isolated from mouse brain and spleen was used as starting material for analysis. PCR amplified products generated in the last step of the 5'RACE procedure were separated on a 1% agarose gel run in 0.5X TBE running buffer. Bands of interest were extracted from agarose using the QIAquick® Gel Extraction kit (Qiagen) according to manufacturer's protocol. Purified cDNA was subcloned into the pCR® 4-TOPO® vector for sequencing. All sequencing was performed by the University of Michigan DNA sequencing core facility. Sequence analysis was performed using the UCSC BLAT Search Genome program (http://www.genome.ucsc.edu/cgi-bin/hgBlat)

HIP1 expression constructs

MycHis-tagged *HIP1A* construct (previously referred to as full-length HIP1), was generated as previously reported [16]. MycHis-tagged *HIP1B* construct was generated using reverse transcriptase PCR (RT-PCR) with HEK 293T cell RNA as the starting material. A 1.2Kb fragment was generated using the following primers: 5'-ATA AGA ATG CGA GAA ATG AAT TGA C-3' (forward) and 5'-CAG TTC TGC CCG CAG GAA TTC ACA C-3' (reverse). The resulting fragment was digested with NotI and EcoRI to generate overhangs at the 5' and 3' ends. This fragment was ligated into NotI and EcoRI-digested pcDNA3.1-*HIP1A*. To generate the various ATG mutant constructs, we used the QuickChange® XL Multi-Site-Directed Mutagenesis kit (Stratagene). The primers used were designed using the suggested primer design program at the Stratagene website.

Cell culture

All cell lines were obtained from A.T.C.C. unless stated otherwise. The 293T cell line was maintained in Dulbecco's Modified Eagle Medium High Glucose 1x (Gibco, Invitrogen - Cat. #11965) supplemented with 10% (v/v) fetal calf serum, 100 U/mL penicillin and 100 µg/mL streptomycin, at 37°C in a humidified atmosphere 5% CO_2/air. The RAW 264.7 cell line was maintained in Dulbecco's Modified Eagle Medium High Glucose 1x (Gibco, Invitrogen - Cat. #11995) supplemented with 10% (v/v) fetal calf

serum, 100 U/mL penicillin and 100 μg/mL streptomycin, at 37°C in a humidified atmosphere 5% CO_2/air.

Mouse embryo fibroblast establishment and culture

MEFs were isolated and cultured as previously described [27]. Briefly, DKO MEFs were prepared from a total of 4 pregnancies and 10, 14, 16 and 18 day old embryos were used. Following removal of the head and liver, embryos were rinsed several times with sterile phosphate buffered saline (PBS), minced with a scalpel and digested with trypsin (0.05% solution containing 0.53 mM EDTA) for 10 minutes at 37^{o}C, using 1 ml of solution per embryo and shaking vigorously every 1 min. The trypsin was inactivated by addition of DMEM supplemented with 10% FBS, 2 mM glutamine and plated repeatedly to generate lines [48]. Staining for phalloidin, transferrin update and PDGFβR half life were analyzed as described previously [27].

RAW cell differentiation

RAW cell differentiation to RAW-OC was performed by adding human recombinant RANKL (Sigma) at a final concentration of 35ng/mL. Following treatment with RANKL, cells were allowed to incubate under normal culture conditions for a total of 6 days. Media was changed after the first three days and every day thereafter.

DNA Transfections

Transfections of 293T cell lines were performed in 6-well plates using SuperFect® Transfection Reagent (Qiagen) according to the manufacturer's suggested protocol. Cells were plated in a six-well plate (2 mL per well) at about 2 x 10^5 cells/mL in triplicate and grown for 24 h before transfection. Two μg of the various pcDNA 3.1 expression constructs were transfected into cells.

Quantitative real time-PCR (qPCR)

Total RNA was isolated from cells and tissues using the RNeasy® RNA isolation kit (Qiagen). First strand cDNA for real time PCR was generated using the SuperScript First-Strand Synthesis System for RT-PCR kit (Invitrogen). Random hexamers were used for reverse transcription of cDNA. Concentration of resulting cDNA was quantified using a ND-4000 nanodrop spectrophotometer. Samples were diluted to a final concentration of 100ng/ul. A total of 100 ng of cDNA was used for each reaction and each reaction was

performed in triplicate. The real time PCR reactions were performed using a Mastercycler ep realplex (Eppendorf) according to the manufacturer's instructions. For relative expression calculations, expression values of target transcripts were normalized to glyceraldehyde 3-phosphate dehydrogenase (*GAPDH*). Primer efficiencies were determined prior to data analysis and these efficiencies were used to calculate relative expression using the Pfaffl method [49]. For determination of absolute transcript levels, a standard curve was generated individually for each transcript analyzed. Standard curves were generated using purified cDNA plasmids, which contained PCR-amplified inserts of each target transcript.

The primers used were designed to generate amplicons in the range of 150 to 200 bp with the exception of *GAPDH* primer (294bp). The primers used for each qPCR assay were as follows: *GAPDH* forward primer sequence was 5'-CTG GTG CTG AGT ATG TCG TG-3' and reverse primer sequence was 5'-CAG TCT TCT GAG TGG CAG TG-3'; Total *HIP1* forward primer sequence was 5'-GCT GGG GAG CCA CTG TCA T-3' and reverse primer sequence was 5'-GGT TGG GGC TGT CCT TAT CA; *HIP1A* forward primer sequence was 5'-GAG AGC TTC GAG CGG ACT CA-3' and reverse primer sequence was GGC AGA ACT TCC AGC AGA GC-3'; *HIP1B* forward primer sequence was 5'-CGG TCA TGG ATG TGA GCA AG-3' and reverse primer sequence was 5'-GGC AGA ACT TCC AGC AGA GC-3'.

Protein isolation and western blot analysis

Cells were washed with PBS and lysed using 100µl lysis buffer (50 mM Tris pH7.4, 150 mM NaCl, 1% Triton X-100, 1.5 mM MgCl2, 5 mM EGTA, and 10% Glycerol) containing protease phosphatase inhibitors mixture [30 mM sodium pyrophosphate, 50 mM sodium flavide, 100 µM sodium orthovanadate and 5 complete EDTA-free mini tablets (Roche)]. Cells were incubated on ice for 10 and centrifuged at 13,200 rpm for 15 min at 4°C. Supernatant was transferred to new tubes and protein concentrations were determined by Bradford assay (Bio-Rad). Forty µg of protein was loaded to 6% SDS-polyacrylamide Tris-glycine gels (SDS-PAGE) unless stated otherwise. Gels were electrotransferred onto nitrocellulose membranes and membranes were blocked for 1 hour in TBS-T containing 5% non fat milk. The resulting blocked membranes were and probed overnight at 4°C with either a rabbit polyclonal HIP1

antibody specific to the N-terminus (1:5,000, UM354), a rabbit polyclonal HIP1 antibody specific to the C-terminus (1:5,000; UM410) or a mouse monoclonal α-myc antibody (1:2000; Cell Signaling). The next day, membranes were washed 3 times in TBS-T for a total of 15 minutes and incubated with horseradish peroxidase (HRP)-conjugated secondary antibodies at room temperature for 1 hour. Membranes were developed with a homemade enhanced chemiluminescence reagent (ECL).

Results

An alternative *Hip1* transcript is identified in mouse cells

Moores *et a*l. recently reported two alternative *Hip1* cDNA clones in *Drosophila,* which differed in their starting exons [30]. These transcripts were predicted to generate different protein products, one of which lacked the key ANTH domain necessary for lipid binding. To explore the possibility of alternative *Hip1* transcripts in mammalian cells, we performed 5'RACE analysis on RNA isolated from mouse brain and spleen, two tissues known to express *Hip1* [26]. Two transcripts were repeatedly identified that differed in their starting exons (Figure 3.1). The first transcript (designated *Hip1a*) contained a 179-nucleotide sequence starting exon (exon 1a) and was the expected transcript that has been used consistently by our laboratory [9]. The second transcript (designated *Hip1b*) contained a 151-nucleotide sequence starting exon (exon 1b) and was located 56Kb downstream of exon 1a, within the originally identified 84Kb murine intron. The predicted protein starting from the first ATG in the exon 1a transcript is 1,030 amino acids and in the exon 1b mRNA is 996 amino acids.

Having identified these two distinct transcripts, we wondered whether one or the other predominated in different cell types. To analyze the absolute levels of each transcript, we first generated a standard curve using purified cDNAs plasmids that encoded either exon 1a- or exon 1b-containing transcripts (Figure 3.2). The standard curves were used to calculate the copy number of both transcripts present in multiple samples of undifferentiated RAW 264.7 cells. The absolute amount of the *Hip1b* transcript was 5-fold greater than *Hip1a* (Figure 3.3). Next we analyzed the transcript levels in intact mouse tissues relative to undifferentiated RAW cells to get an idea of the expression levels of the different *Hip1* transcripts in different tissues. The cortex, cerebellum, hippocampus, kidney, heart and lung all had *Hip1a* transcript levels higher

than *Hip1b* (Figure 3.4). Lung had the highest levels of *Hip1a* transcript as well as the largest difference between transcript expression levels with *Hip1a* levels over 15-fold higher than *Hip1b*. Interestingly, western blot analysis of tissue extracts taken from the same mice demonstrated a single slower migrating band in all of the tissues with varying intensities (Figure 3.5) compared to RAW cells lysates, which demonstrated two distinct bands of similar intensities. The slower-migrating band may represent the larger isoform of the HIP1 doublet we have observed previously [7] while the faster-migrating of the two bands observed in RAW cells may represent the smaller isoform. It appears that the transcript levels in different mouse tissues correlated with the western blot as the *Hip1a* transcript, which predicts for a larger protein, predominates in the tissues and only a larger protein is detected by western blot. However, there is no data (i.e. mass spectrometry analysis) at this point that confirms this slower-migrating band is indeed the predicted product of the *Hip1a* transcript.

Previously, we reported that Receptor Activator for NFκB Ligand (RANKL) stimulation of the RAW cells leads to increased expression of the larger isoform of HIP1 after 6 days in culture (Figure 3.6 - insert and [7]). Given that expression of this larger isoform of the HIP1 doublet in mouse tissues appears to correlate with *Hip1a* transcript levels, we wondered whether this phenomenon was due to induction of *Hip1a* mRNA. To answer this question, we performed quantitative PCR on differentiated RAW cells and compared the levels of *Hip1a* and *Hip1b* in these cells to that of undifferentiated RAW cells maintained in culture for the same period of time (6 days). We found that *Hip1a* transcript levels were 2-fold higher in differentiated RAW cells than in undifferentiated RAW cells cultured under the same conditions (Figure 3.7). This was not the case with *Hip1b* levels as they remained the same. These data further support the hypothesis that the *Hip1a* transcript generates the larger HIP1 isoform of the HIP1 doublet.

Up to this point, we had observed alternative *Hip1* transcript levels in 1) a single murine-derived cell line under normal culture conditions with our analysis of undifferentiated RAW cells, 2) normal murine tissues and 3) a cytokine-induced phenotypic change in a single murine-derived cell line with RANKL-stimulated RAW cells. To expand this list of conditions for which alternative *Hip1* transcript levels were observed, we turned to mouse embryonic fibroblast (MEF) cell lines. These cell lines can

be immortalized using the standard 3T3 immortalization protocol established by Todaro and Green [50]. MEF cell lines provide a nice system to study your gene of interest in which immortalized cells can be compared to non-immortalized cells. Hence, we wanted to examine whether changes in the expression levels of either transcript occurred upon immortalization.

To investigate whether alternative *Hip1* transcript levels changed upon immortalization, we isolated RNA from non-immortalized (passage 5) and immortalized (beyond passage 30) MEFs and used it for qPCR analysis. We analyzed the RNA for copies of both alternative transcripts similar to the process with undifferentiated RAW cells. The expression levels of both transcripts varied across the board with some cell lines having many more copies of both alternative *Hip1* transcripts than others. To better visualize the differences in transcript expression levels for all four cell lines, we analyzed the ratio of *Hip1a* to *Hip1b*. In three of the four cell lines that were analyzed, we observed ratios higher than 1 indicating the presence of more *Hip1a* than *Hip1b* (Figure 3.8). This is in stark contrast to undifferentiated RAW cells, which expressed 5-fold more *Hip1b* transcript than *Hip1a*. However, after immortalization the ratio of *Hip1a* to *Hip1b* decreased significantly in two of the four cell lines. In all four cell lines, the ratio decreased below 1 indicating that the amount of *Hip1b* transcript exceeded that of *Hip1a*. This shift in favor of *Hip1b* transcript levels is interesting given that RAW cells (an immortalized, transformed cell line) also express more of the *Hip1b* transcript whereas intact mouse tissues express more of the *Hip1a* transcript.

Hip1b transcript expressed in human cells as well

Having discovered an alternative *Hip1* transcript in mouse, we wondered if this transcript was expressed in human cells as well. Chopra *et al*. initially reported the presence of alternative transcripts in human brain as a result of alternative splicing [29]. However, the alternative transcripts were not well characterized and no subsequent work was done to expand on this finding. Therefore we decided to look for *HIP1B* expression in human cells. To accomplish this, we used the mouse *Hip1b* sequence to identify a homologous region in the human *HIP1* locus. We identified a highly conserved 152-nucleotide region and used the sequence in this region to generate primers for qPCR analysis. We isolated total RNA from HEK 293T cells cultured under normal conditions

and used this RNA to determine the copy number of *HIP1A* and *HIP1B.* As with analysis of the transcript levels in undifferentiated RAW cells, we generated a standard curve using purified cDNA plasmids specific to the human transcripts (Figure 3.9). Surprisingly, we found that the levels of *HIP1A* and *HIP1B* were equivalent (Figure 3.10).

We next decided to examine whether other cell lines expressed the *HIP1B* transcript as well. We have previously reported that HIP1 is expressed at high levels in multiple epithelial-derived cancer cell lines [9]. Additionally, we have observed that two HIP1 isoforms are detected in varying amounts by western blot analysis in some cancer cell lines (unpublished data). For instance, the ovarian cancer cell line SKOV3, only the larger isoform is detected whereas in the colon cancer cell line UACC257 both isoforms are detected but the smaller isoform is more intense (Figure 3.11 – insert). To test whether there was a relationship between the different protein isoforms and alternative *HIP1* transcript levels, we performed qPCR analysis on a small subset of cancer cell lines in which varied detection of the two isoforms was observed. In addition to the SKOV3 and UACC257 cell lines, we analyzed the DU145 (prostate cancer) and MDA-MB435 (breast cancer) cell lines. Similar levels of both HIP1 protein isoforms were detected in these two cell lines (Figure 3.11 – insert). *HIP1B* transcript was detected in all four cell lines (data not shown). However, unlike 293T cells that expressed equivalent levels of *HIP1A* and *HIP1B* transcripts, all four cancer cell lines analyzed expressed more *HIP1B* than *HIP1A* (data not shown). The results in the SKOV3 cell line were rather unexpected given only the larger-mass isoform was detected. We also observed that there appeared to be a correlation of the ratios of HIP1A to HIP1B with the ratios of the larger isoform to the smaller isoform on western blot. We decided to analyze the ratio of *HIP1A* to *HIP1B* transcript to see if this was in fact the case. We found that as the ratio of *HIP1A* to *HIP1B* decreased, so did the intensity of the larger-mass isoform relative to the smaller-mass isoform (Figure 3.11). As with the data presented earlier in this chapter regarding HIP1 isoform expression in mouse (Figures 3.4 and 3.5), caution must be used in interpreting this data. While it appears to indicate a connection between the alternative *HIP1* transcripts and the HIP1 isoforms observed on western blot, this connection must be

confirmed by either transcript-specific knockdown to show loss of the predicted isoform or N-terminal protein sequence data to show the predicted isoform sequence.

Mutational analysis demonstrates potential alternative translation initiation start sites in *HIP1B* transcript

It is possible, based on our analysis of alternative *HIP1* transcripts so far, that the *HIP1A* transcript encodes for the larger isoform of the HIP1 doublet in both mouse and human cells and the *HIP1B* transcript encodes for the smaller isoform. The open reading frame (ORF) for the *HIP1A* transcript in humans predicts a 1038-amino acid product with an approximate mass of 116 KDa while the ORF for the *HIP1B* transcript in humans predicts a 1003-amino acid product with an approximate mass of 113 KDa. With a difference in mass of only 3 KDa, it appeared unlikely that the lower-mass isoform was the predicted HIP1B product. Furthermore, the predicted HIP1B product retains a full ANTH domain, unlike the truncated isoform identified in *Drosophila* [30]. To determine the actual product produced by the *HIP1B* transcript, we generated a myc/His-tagged human *HIP1B* cDNA expression construct and transfected it into 293T cells. Twenty-four hours after transfection, we isolated protein lysates from transfected cells and ran them on a 6% SDS-PAGE gel. Western blot analysis of the samples revealed an intense band, which migrated slightly faster than the band produced by our previously generated *HIP1A* cDNA construct (Figure 3.12). Surprisingly, a second, faster-migrating product appeared in one of the two *HIP1B*-transfected samples probed with an α-myc antibody. To ensure that this product was not the result of proteolytic cleavage, we repeated the experiment and isolated protein directly from the cell dish using boiling Laemmli buffer (2% sodium dodecyl sulfate, 5% β-mercaptoethanol and 0.125M Tris HCl). Western blot analysis of these samples resembled the first experiment with a faster-migrating band observed in both *HIP1B*-transfected samples (data not shown). This band did not appear in any of the *HIP1A*-transfected samples we analyzed.

We began to wonder if this second band observed in *HIP1B*-transfected samples was the result of an alternative translation start site. Alternative translation mechanisms in eukaryotes have been reported to occur by “leaky scanning” when the predicted start AUG is in a suboptimal context [51, 52]. Additionally, translation reinitiation is a reported mechanism of alternative translation in which an upstream ORF (upORF)

encoding for a very small peptide allows the 40S ribosomal subunits to remain intact and continue to scan the transcript until it comes into contact with another AUG in an optimal context [51, 52]. This process often involves skipping an AUG codon in an optimal context. To determine whether this was the case with *HIP1B*, we examined the cDNA sequence for other ORFs both upstream and downstream of the predicted translation initiation site (TIS). We came across an upstream ORF consisting of only 8 codons (Figure 3.13), which fit the criteria for an upORF [52] suggesting that reinitiation was indeed a possibility. This was not the case with the *HIP1A* transcript as there were no upORFs (data not shown), which explains the lack of a second band in *HIP1A*-transfected samples. In terms of downstream ORFs, we identified three potential downstream AUGs: two within exon 4 and a third within exon 5 (Figure 3.13). Interestingly, the predicted products of two of these ORFs lacked the ANTH domain (Figure 3.14) and all had an approximate mass at least 14 KDa less than the predicted HIP1A product (Table 3.1). Any one of these predicted products could potentially be the lower HIP1 isoform of the observed HIP1 western blot doublet.

We next decided to begin to test the hypothesis that the smaller isoform was the product of translation reinitiation from the *HIP1B*. To do this, we generated multiple mutant constructs via PCR mutagenesis using the original *HIP1B* construct as a template. We mutated thymidines to cytosines in each of the putative ATG initiation start sites in the *HIP1B* transcript in different combinations. For the first construct, we mutated the ATGs at positions 134 to 136 and 149 to 151 in exon 1b to generate a construct that could not initiate translation from exon 1b (designated T135/150C). We hypothesized that this mutant would not express the original predicted product we observed in our original western blots. A second mutant construct consisted of mutations in the AUGs at positions 401 to 403 and 410 to 412 in exon 4 (designated T402/411C). Our final mutant construct consisted of a mutation in the ATG at positions 479 to 481 in exon 5 (designated T480C). We planned to use the final two mutants to determine which of the ATG start sites were responsible for the smaller isoform of the HIP1 doublet. Neither of the two ATG start sites in exon 4 was in the optimal surrounding context but the exon 5 ATG start site was in an optimal context. Therefore we hypothesized that the exon 5 ATG was the translation initiation start site of the smaller isoform of the HIP1 doublet. We transfected

all three mutant constructs into 293T cells individually and isolated protein from the transfected cells 24 hours later. We subsequently analyzed the samples by western blot. As expected we did not detect a band corresponding to the larger isoform of the HIP1 doublet in T135/150C-transfected cells (Figure 3.15). Additionally, we detected two faster-migrating bands, one of which appeared to correspond to the smaller isoform of the HIP1 doublet. It is possible that the slower-migrating band of the two represents a product translated from one of the exon 4 ATG start sites while the faster-migrating band represents a protein translated from the exon 5 ATG start site. Surprisingly, only the expected slower-migrating band was detected in the T402/411C and T480C mutant-transfected samples (Figure 3.15). The faster-migrating band which represents the smaller-mass isoform of the HIP1 doublet was not detected in the non-mutated *HIP1B*-transfected sample as well. Our continued experiments with these *HIP1B* constructs revealed that the faster-migrating band is not readily detected 100% of the time as is evident from Figure 3.12. This inconsistent expression of the smaller-mass isoform may be due to the fact that the *HIP1B* construct does not contain the complete 152-nucleotide sequence of exon 1b, hence it lacks the upORF. If reinitiation is the mechanism by which translation from the downstream AUGs in either exon 4 or exon 5 is possible, than one would predict that loss of the upORF decreases translation efficiency from these sites. It would be interesting to see if inclusion of the 5' sequence of exon 1b improves the translation efficiency of these downstream ORFs.

Discussion

In this study, we describe the characterization of an alternative *HIP1* transcript that is expressed in both mouse and human cells. The alternative transcript (designated *HIP1B*) uses an alternative starting exon (exon 1b) from the original *HIP1* transcript (*HIP1A*). This is the first known report of an alternative *Hip1* transcript in mouse and a characterization of an initially reported alternative *HIP1* transcript in humans [29]. This finding has the potential to help resolve conflicting reports of HIP1 and its role in cellular survival and tumorigenesis versus its role as a pro-apoptotic protein. We hypothesize that the two transcripts encode for two different HIP1 isoforms, which differ in their amino-termini similar to a recent report of multiple isoforms in *Drosophila* [30]. In this report, one of the isoforms lacked the ANTH domain and both isoforms were shown to have

contrasting effects on Notch-mediated neurogenesis when exogenously expressed in Drosophila. The newly discovered transcript we describe in this report potentially encodes for a HIP1 isoform that lacks the ANTH domain as well. This isoform could possibly induce apoptosis given our previous report in which a *HIP1* mutant cDNA construct lacking the ANTH domain induced apoptosis in 293T cells [9].

Our analysis of both *Hip1* transcripts in mouse RAW cells demonstrated that *Hip1b* transcript levels exceed *Hip1a* approximately 5-fold. However, when we stimulated RAW 264.7 cells with RANKL to induce differentiation into osteoclast-like RAW-OC cells, we observed a 2-fold induction of the *Hip1a* transcript but no change in the *Hip1b* transcript. This data is consistent with previously observed data in which expression of the larger isoform of the HIP1 doublet is detected in primary bone marrow cells 14 days after stimulation and increases in RAW cells 6 days after stimulation with RANKL [7]. This is the first report of selective induction of a *Hip1* transcript by stimulation with a cytokine. Both the RAW cell differentiation and the primary bone marrow cell differentiation models provide a useful tool for future study of *Hip1* transcriptional regulation, particularly *Hip1a* transcriptional regulation.

Our observations in RAW cells also provide us with more insight into the HIP1 doublet. Based on the changes in HIP1 expression following RANKL stimulation, it appears that that the *Hip1a* transcript encodes for the larger isoform of the HIP1 doublet. In addition to the observations in RAW cells, *Hip1a* expression levels were higher in most of the intact mouse tissues. This appears to correlate somewhat to expression of the HIP1 doublet as only the larger isoform was detected in the same mouse tissues. Both isoforms were detected in RAW cells and in equivalent amounts. It appears that translation of the encoded proteins does not occur in a linear manner. In other words, the transcript levels do not seem to correspond directly to the protein levels. Perhaps the expression levels of each isoform are regulated by a post-translational mechanism that depends on the ratio of both transcripts present. Indeed, when human cancer cell lines that express varying levels of both HIP1 isoforms were analyzed for their expression levels of *HIP1A* and *HIP1B*, HIP1 isoform expression appeared to correlate with the ratio of *HIP1A* to *HIP1B*. Basically, the greater the ratio of *HIP1A* to *HIP1B*, the higher the expression of the larger isoform of the HIP1 doublet relative to the smaller isoform.

Another intriguing possibility that may explain the lack of corresponding transcript and protein levels comes in the form of translational regulation of HIP1 similar to the classic example of *GCN4* in yeasts [53]. *GCN4* mRNA contains four small ORFs upstream of the Gcn4p coding sequences. Deletion of these ORFs or mutations in their start codons increases *GCN4* translation without changing mRNA levels [54]. Individual mutational analysis of the upORFs demonstrated that upORF1 acts as a positive regulatory element of Gcn4p induction under amino acid starvation conditions while upORFs 2, 3 and 4 act as negative regulatory elements [55]. *GCN4* translation is regulated The *HIP1B* transcript contains an upORF, which could potentially act as a regulatory element allowing translation of the dORF in either exon 4 or exon 5 under certain conditions or in certain types of cells. This possibility should be investigated in future studies.

It is also possible that the antibody used for western blot analysis of these mouse tissues has a weak affinity for the smaller isoform. Although the antibody used was generated against the C-terminus of HIP1, which is similar in both proteins, there could be conformational changes in the smaller isoform that render the epitope less accessible and only high levels of expression of the isoform can be detected. This could explain the apparent equivalent levels of both isoforms in undifferentiated RAW cells despite a 5-fold difference in transcript levels. More work is needed to understand this phenomenon.

One could make the argument for post-translational modification of the HIP1 protein as a reasonable alternative explanation for the HIP1 doublet. The smaller band of the doublet may be modified by a mechanism such as phosphorylation or ubiquitinylation leading to detection of a larger band. However, this appears unlikely given the fact that only one band is detected in protein samples isolated from HIP1A-transfected 293T cells when using the α-myc antibody and this band appears to resemble the larger band of the doublet. Previous observations regarding protein samples from HIP1A-transfected 293T cells using different HIP1 antibodies produce similar results.

We also observed that the *Hip1a* transcript is expressed at higher levels than the *Hip1b* transcript in non-immortalized MEFs. However, the expression levels seem to shift in favor of the *Hip1b* transcript upon immortalization. The ratio of *Hip1a* to *Hip1b* transcript decreases significantly in two of the four cell lines analyzed with the other two

cell lines trending towards a shift in favor of *Hip1b* expression. I would hypothesize that a certain ratio of *Hip1a* to *Hip1b* must be maintained in certain cells in order for the expression of the larger isoform to occur. A decrease in the ratio of *Hip1a* to *Hip1b* may lead to a decrease in, or altogether loss of, expression of the larger isoform of the HIP1 doublet. Furthermore a decrease or loss of expression of the larger isoform may contribute to susceptibility to immortalization. However, more data from multiple different cells must be collected before this hypothesis can be substantiated.

Far more uncertain is the phenomenon that regarding expression of the smaller isoform of the HIP1 doublet. The smaller isoform of the HIP1 doublet may be the product of an alternative mechanism of translation known as reinitiation [51, 52]. In short, this mechanism involves the translation of a small open reading frame (ORF) upstream of a predicted translation initiation site (TIS). These small ORFs typically consist of no more than 30 codons with the smaller ORFs being more effective. Translation of this upstream ORF reduces the translation efficiency of the predicted TIS and allows for alternative translation of downstream ORFs. Additionally, the distance between the termination code of the upstream ORF and the downstream ORF affects the translation efficiency of the downstream ORF with larger distances equating to higher translation efficiencies. The *HIP1B* transcript meets these criteria. It has an upstream ORF of 8 codons with a fairly large distance between the termination code of the upstream ORF and the AUG codons in exons 4 and 5. This is not the case with the *HIP1A* transcript, which could explain why we have not observed additional bands in cells transfected with *HIP1A* cDNA.

Indeed, when we mutated the ATG codons in exon 1b we were unable to detect the slower-migrating band originally observed in *HIP1B*-transfected cells but we did detect two faster-migrating bands. The bands are likely the products of translation initiated from AUG codons in both exon 4 and exon 5. Both bands appear to be similar to the smaller isoform of the HIP1 doublet detected endogenously in 293T cells but it is unclear which of the two bands corresponds to the smaller isoform. We also observed that the faster-migrating band is not always detected in *HIP1B*-transfected cells. This may be due to lower translation efficiency of the downstream ORF in the *HIP1B* construct as it was originally designed. The construct lacks most of the 5' end of exon 1b, which may support the idea that the lower band is the result of reinitiation. However, it is

also possible that this smaller isoform is regulated in a manner similar to GCN4 as mentioned above and loss of the upORF affects proper regulation of translation from the dORF. Regardless of the potential mechanism involved, the data presented in this chapter suggest that the *HIP1B* transcript may be responsible for the smaller isoform of the HIP1 doublet. Efforts involving selective siRNA-mediated knockdown of each transcript are currently underway to confirm if this is or is not the case.

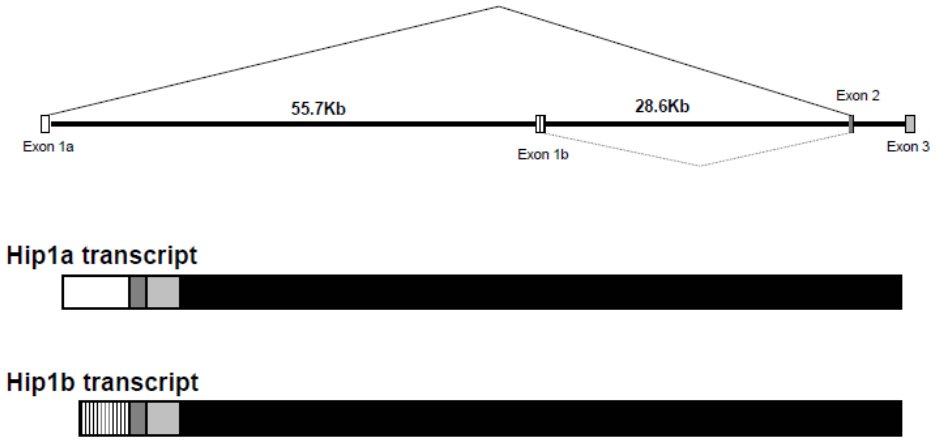

Figure 3.1: Diagram of alternative *Hip1* transcripts in mouse. 5' RACE analysis was performed on RNA isolated from mouse brain and spleen. Analysis revealed two alternative Hip1 transcripts (termed *Hip1a* and *Hip1b*). The transcripts only differ in their initial exon. Exon 1a is 179 nucleotides long and exon 1b is 151 nucleotides long. Transcript 1a is predicted to produce a 1030-aa product while transcript 1b predicts a 996-aa product.

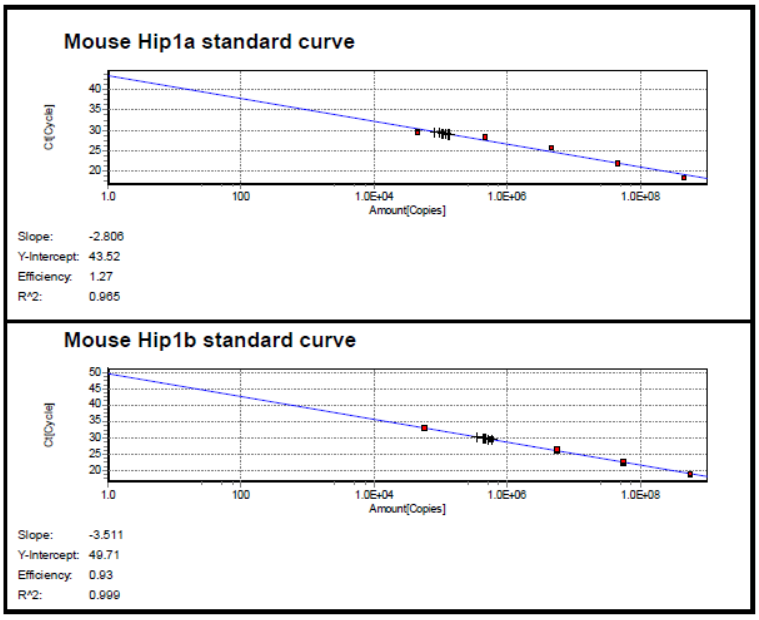

Figure 3.2: Standard curve for mouse Hip1a and Hip1b transcript analysis. Purified cDNA plasmids containing a PCR-amplified insert of either *Hip1a* or *Hip1b* transcript were serially diluted ten-fold starting from a copy number of 1.10×10^8 to generate a standard curve for determination of copy number in each sample. Five points were used for each curve. Primer efficiencies and R^2 values are provided to show the accuracy of the curve.

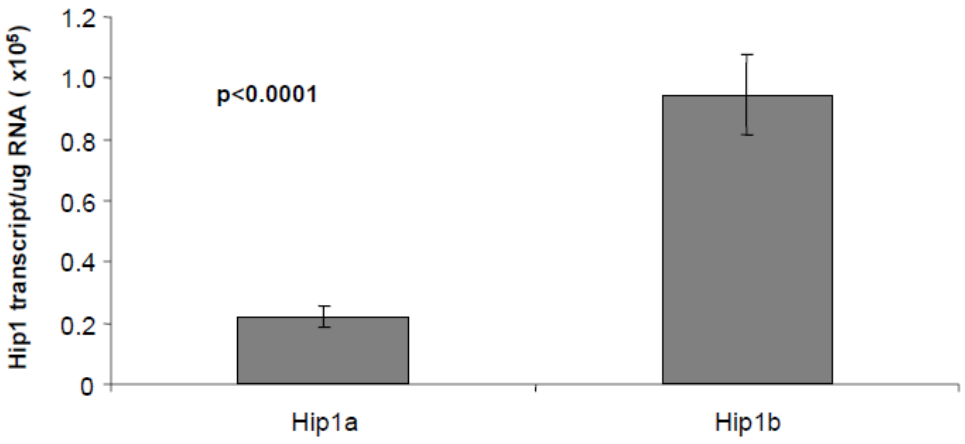

Figure 3.3: Absolute *Hip1* transcript levels in undifferentiated RAW cells. Total RNA was isolated from undifferentiated RAW cells cultured under normal conditions and used to generate cDNA for quantitative PCR analysis. Absolute transcript levels were calculated as indicated in Materials and Methods and normalized to the starting amount of RNA used. This graph is representative of 3 independent experiments. Error bars represent standard deviations.

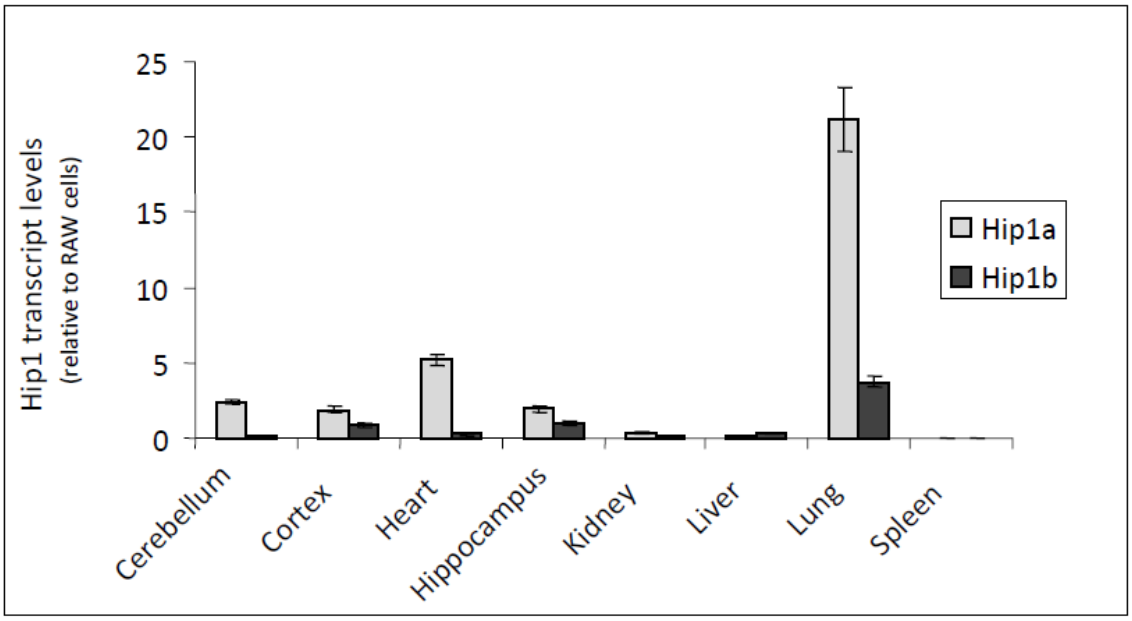

Figure 3.4: Relative *Hip1a* and *Hip1b* transcript levels in various mouse tissues. Total RNA was isolated from various mouse tissues as indicated in Materials and Methods. Five (5) µg of total RNA was used to generate cDNA for qPCR analysis. Expression levels were normalized to *Gapdh*. Values represent Hip1a expression levels relative to undifferentiated RAW cells. This graph is representative of 3 independent experiments using 3 separate mice six to eight weeks in age. Error bars represent standard deviations.

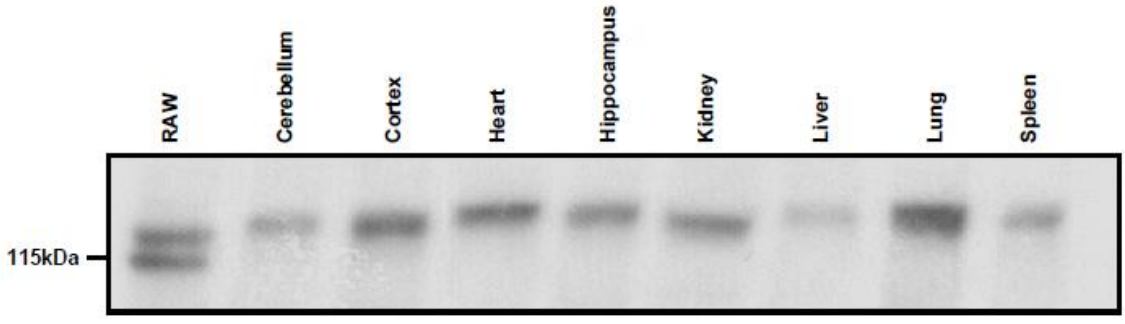

Figure 3.5: Western blot analysis of mouse tissues. Various tissues were isolated from 6-week old mice and protein was isolated from these tissues as indicated in the Materials and Methods section. Protein lysates were run on a 6% SDS-PAGE gel and transferred to nitrocellulose membrane for western blot analysis. Samples were probed with a polyclonal Hip1 antibody (UM354 – 1:5000 dilution).

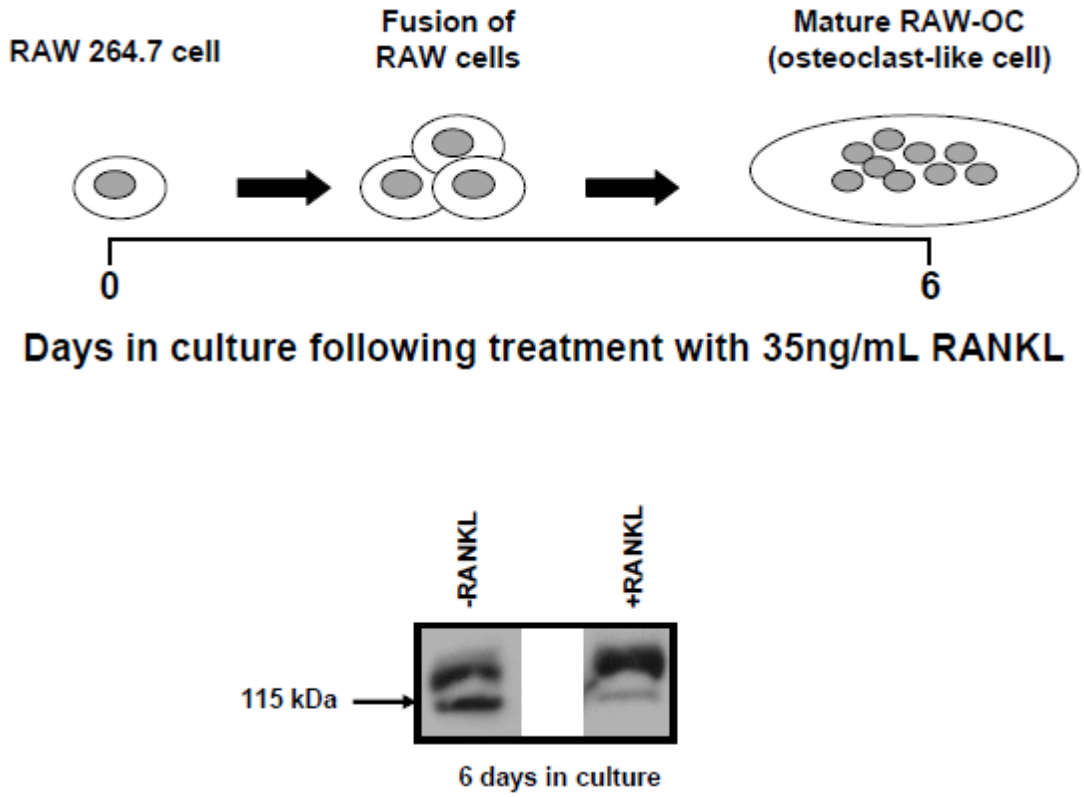

Figure 3.6: RAW cell differentiation into RAW-OC leads results in an induction of higher molecular weight protein. RAW 264.7 cells differentiate into osteoclast-like cells 6 days after treatment with RANKL. RAW cells were cultured under normal conditions for 6 days after treatment with 35ng/mL of human recombinant RANKL. Media was changed after 3 days in culture and then everyday thereafter. On the sixth day after treatment with RANKL, RAW cells were harvested and protein was isolated. Protein lysate was prepared as indicated in Materials and Methods. The polyclonal Hip1 anti-body, UM354 was to detect HIP1 expression.

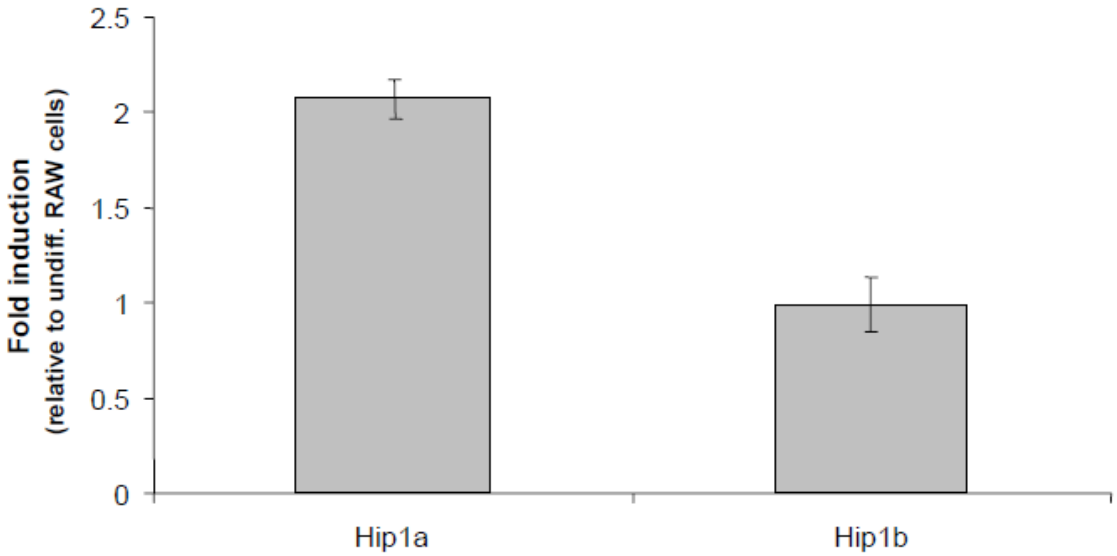

Figure 3.7: Relative *Hip1* transcript levels in differentiated RAW-OC cells. RAW cells were cultured under normal conditions for 6 days after treatment with 35ng/mL of human recombinant RANKL. Media was changed after 3 days in culture and then everyday thereafter. On the sixth day after treatment with RANKL, RAW cells were harvested and total RNA was isolated as indicated in Materials and Methods. Five (5) µg of total RNA was used to generate cDNA for quantitative PCR analysis. Expression levels were normalized to *Gapdh*. Values represent fold induction relative to untreated RAW cells cultured for 6 days. This graph is representative of 3 independent experiments. Error bars represent standard deviations.

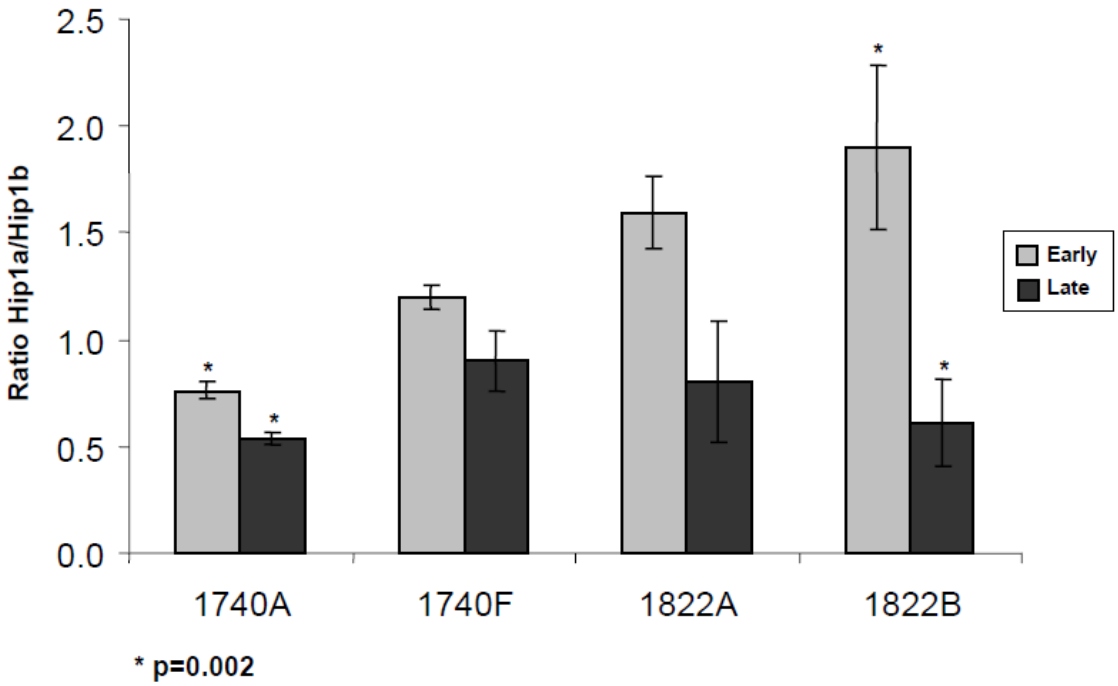

Figure 3.8: Ratio of *Hip1a* to *Hip1b* transcript levels in immortalized and non-immortalized mouse embryonic fibroblasts (MEFs). Total RNA was isolated from both immortalized (late passage) and non-immortalized (early passage) MEFs cultured as indicated in Materials and Methods. Eight hundred (800) ng of total RNA was used to generate cDNA for quantitative PCR analysis. Absolute transcript levels were calculated as indicated in Materials and Methods and normalized to the starting amount of RNA used. Values reflect the *Hip1a* copy number divided by the *Hip1b* copy number. This graph is representative of 3 independent experiments. Error bars represent standard deviations.

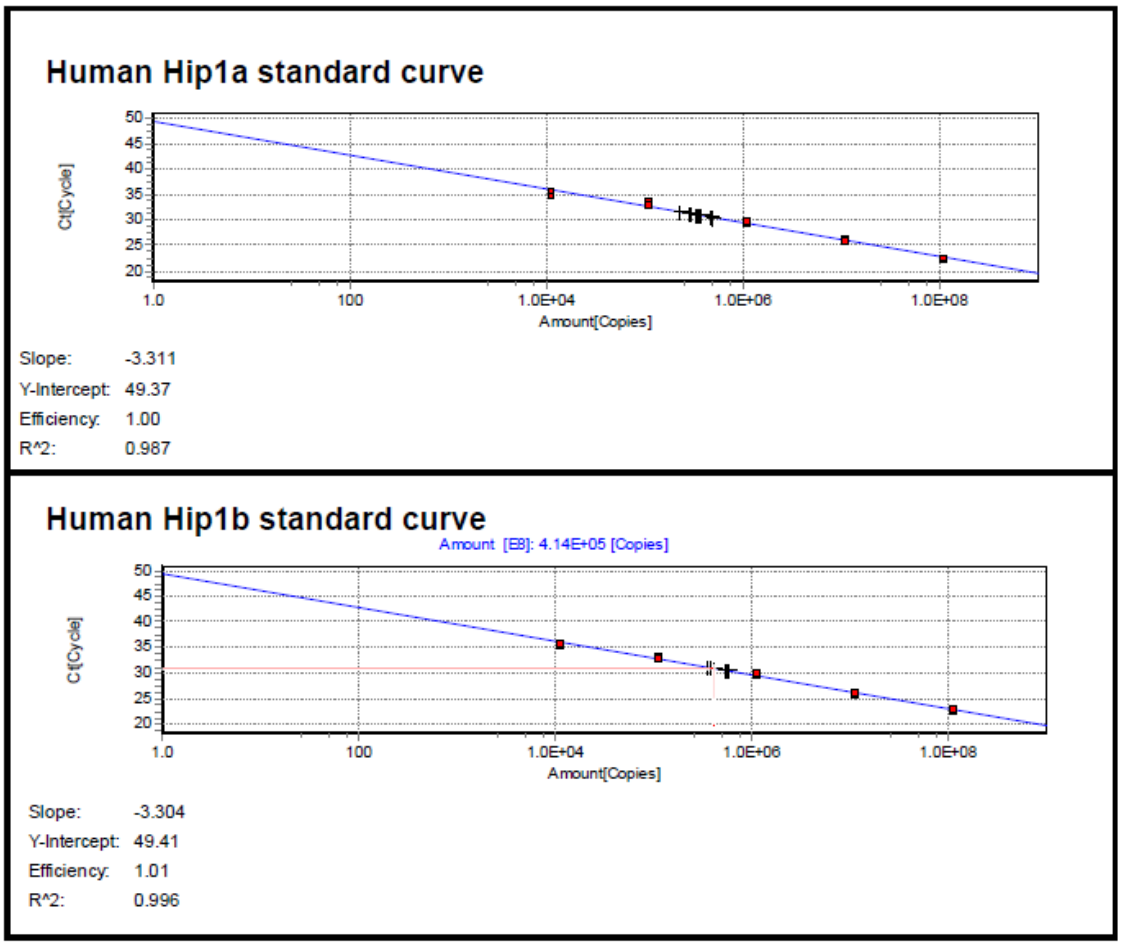

Figure 3.9: Standard curve for human *HIP1A* and *HIP1B* transcript analysis. Purified cDNA plasmids containing a PCR-amplified insert of either *HIP1A* or *HIP1B* transcript were serially diluted ten-fold starting from a copy number of 1.10×10^8 to generate a standard curve for determination of copy number in each sample. Five points were used for each curve. Primer efficiencies and R^2 values are provided to show the accuracy of the curve.

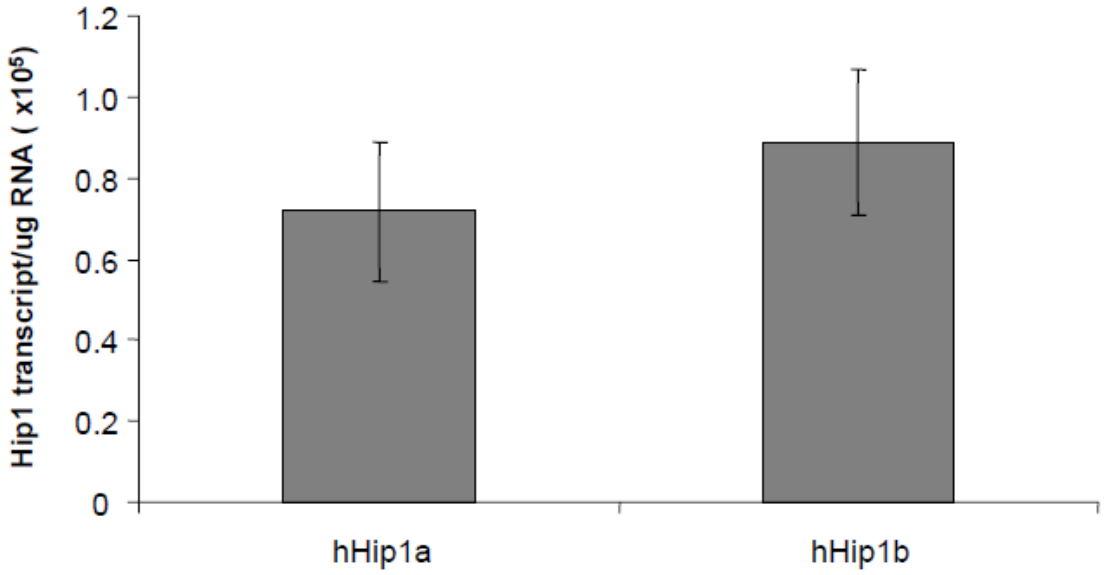

Figure 3.10: Absolute *HIP1* transcript levels in HEK 293T cells. Total RNA was isolated from HEK 293T cells cultured under normal conditions and used to generate cDNA for quantitative PCR analysis. Absolute transcript levels were calculated as indicated in Materials and Methods and normalized to the starting amount of RNA used. This graph is representative of 3 independent experiments. Error bars represent standard deviations.

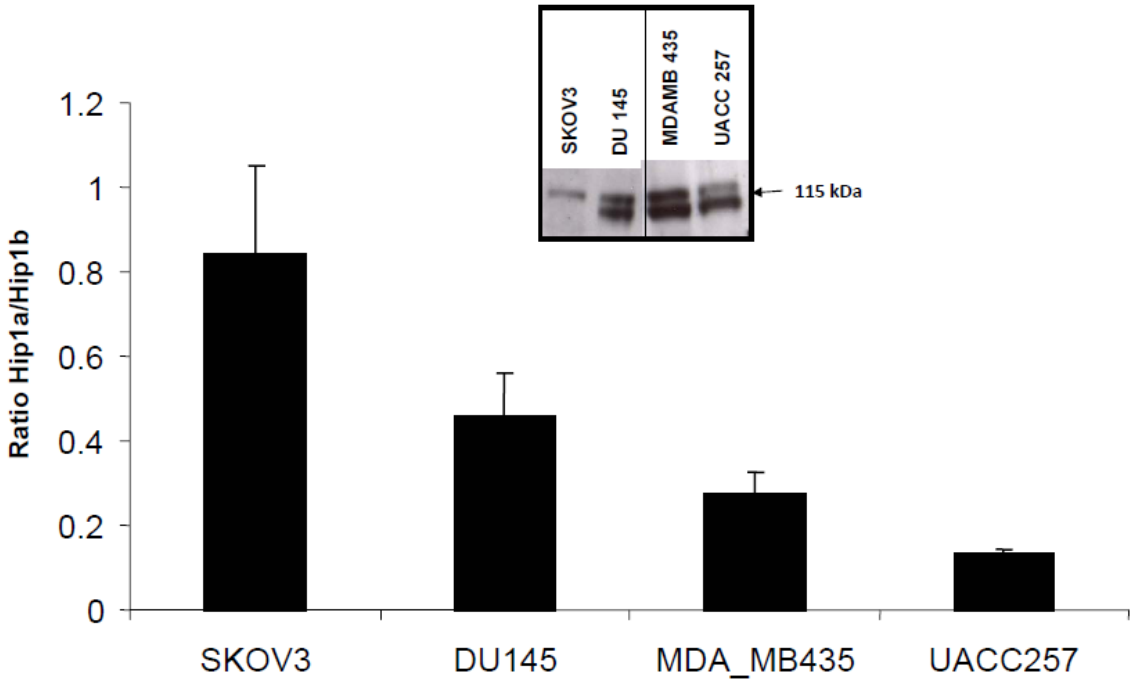

Figure 3.11: Ratios of *HIP1A* to *HIP1B* in selected cancer cells lines. Cancer cell lines with different HIP1 expression profiles were selected for quantitative analysis of both *HIP1A* and *HIP1B* transcripts. Total RNA was obtained from the National Cancer Institute and 800 ng of total RNA was used to generate cDNA for quantitative PCR analysis. Absolute transcript levels were calculated as indicated in Materials and Methods and normalized to the starting amount of RNA used. Values reflect the *HIP1A* copy number divided by the *HIP1B* copy number. This graph is representative of 3 independent experiments. Error bars represent standard deviations.

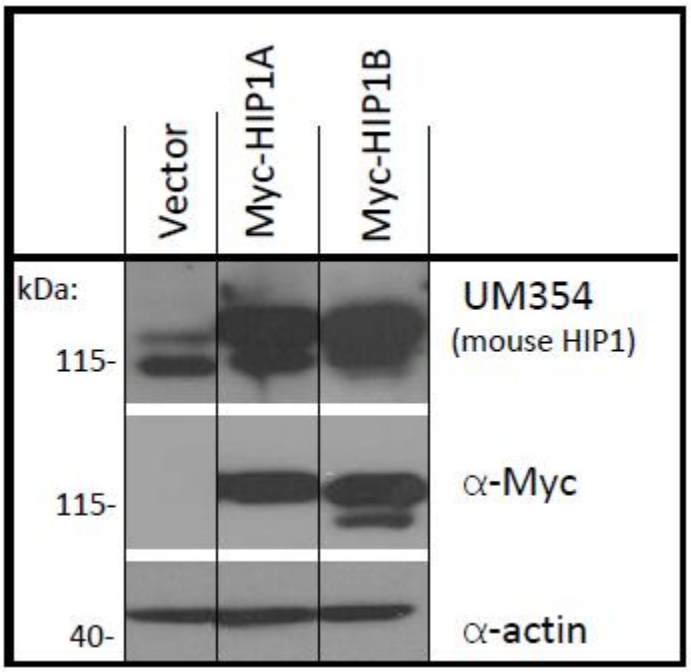

Figure 3.12: Exogenous expression of *HIP1B* AUG mutants in HEK 293T cells. HEK 293T cells were cultured under normal conditions and transfected with one of the indicated cDNA plasmids. Twenty-four hours after transfection, cells were harvested and protein was isolated using the procedures indicated in the Materials and Methods section. Proteins were run on a 6% SDS-PAGE gel and transferred to nitrocellulose membrane. Membranes were blotted overnight with the one of the following antibodies: 1) Hip1 polyclonal antibody (UM354), 2) monoclonal α-myc antibody or polyclonal α-actin antibody. Note the presence of a faster-migrating band in one of the *HIP1B*-transfected samples.

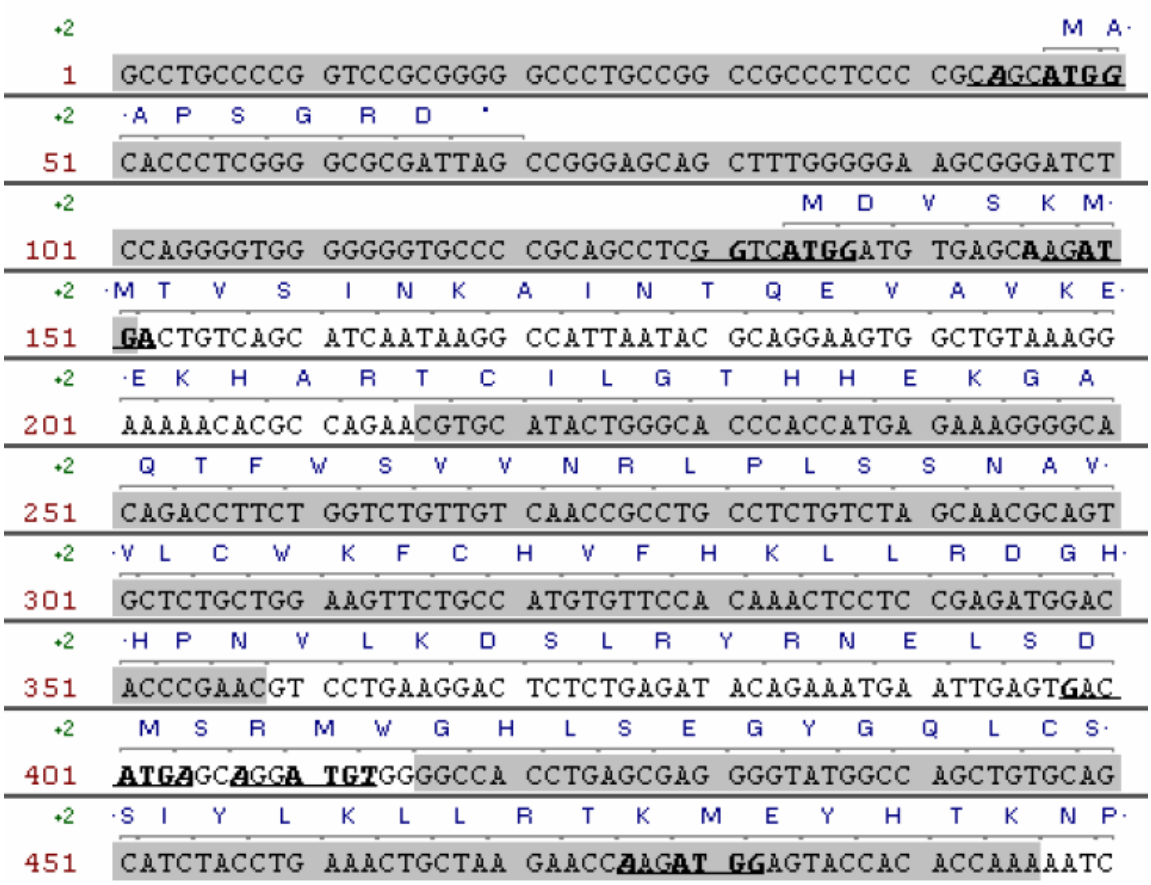

Figure 3.13: Putative open reading frames (ORFs) in *HIP1B* transcript. The 5' portion of the human *HIP1B* transcript is displayed along with potential upstream and downstream ORFs. Translation initiation sites (TIS) are represented in bold font. Kozak sequences are underlined and bases at positions -3 and +4, the most essential positions, are in bold italics. Odd-numbered exons are shaded gray beginning with exon 1b. The *HIP1B* has an upstream ORF of 8 codons, which is not present in the *HIP1A* transcript (not shown).

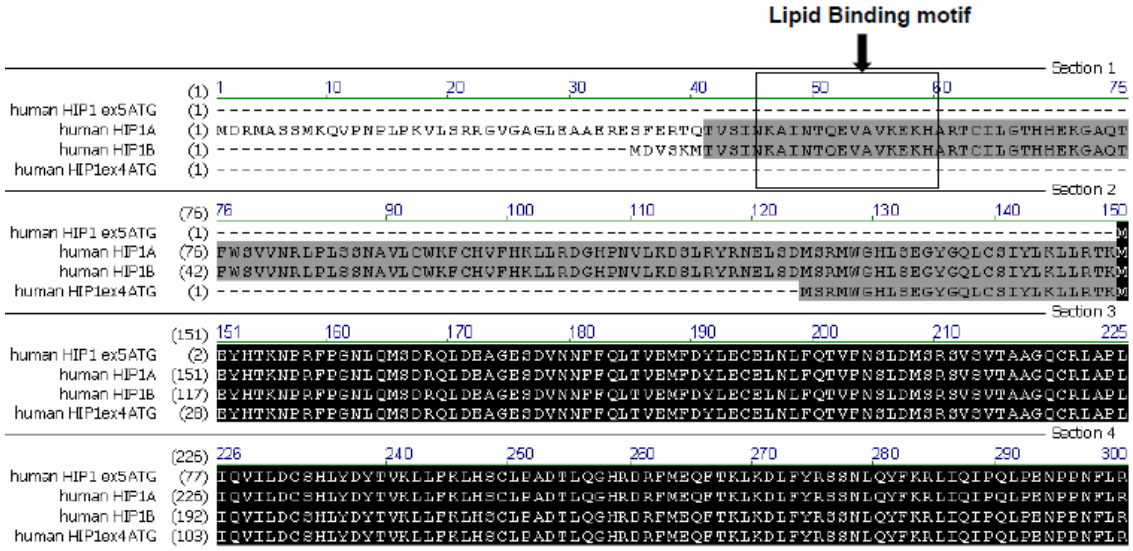

Figure 3.14: Alignment of predicted protein sequences. The predicted protein sequences of HIP1A and HIP1B were aligned with the potential protein products translated from downstream translation start sites in exon 4 and exon 5. Note the key lipid-binding motif for the AP180 N-Terminal Homology domain (ANTH) is absent in exon 4 and exon 5 potential products. Gray-shaded sequence indicates conservation between at least two potential products. Black-shaded sequence indicates complete identity between all 4 potential products.

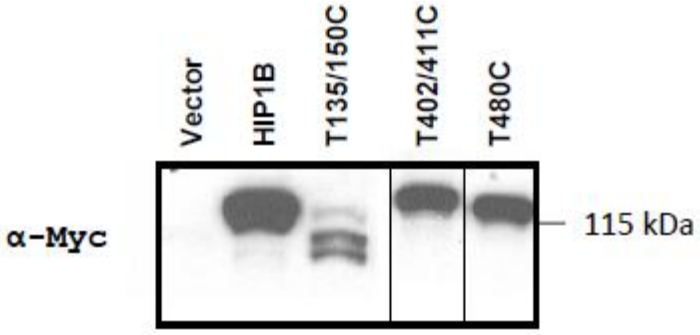

Figure 3:15: Western blot analysis of mutant Hip1b-transfected cells. HEK 293T cells were transfected with the indicated Hip1 cDNA plasmid. Twenty-four hours after transfection, cells were harvested and protein was isolated. Protein lysates were prepared as indicated in Materials and Methods and run on a 6% SDS-PAGE gel. Gels were transferred to nitrocellulose membrane and probed with α-myc antibody at a dilution of 1:2000 overnight. The next day, membranes were washed and probed with HRP-conjugated mouse secondary antibody. Lane assignments – 1) vector; 2) *HIP1B*; 3) t135/150c mutant; 4) t402/411c mutant; 5) t480c mutant.

	Predicted protein product	ANTH domain intact
Human HIP1A	1038 aa (116 kDa)	Yes
Human HIP1B	1004 aa (113 kDa) 3 kDa difference	Yes
Human HIP1B_ex4ATG	915 aa (102 kDa) 14 kDa difference	No
Human HIP1B_ex5ATG	889 aa (993 kDa) 23 kDa difference	No

Table 3.1: Comparison of predicted HIP1 proteins.

CHAPTER 4

ANALYSIS OF THE *HIP1A* PROMOTER

Summary

We have recently shown that two forms of Huntingtin Interacting Protein (HIP1) are expressed in both mouse and human cells. One form, HIP1A, has been studied extensively in the past and has been characterized as a clathrin binding protein involved in receptor trafficking. Additionally, HIP1 has been described as a pro-survival protein primarily on the basis of studies that have focused on the HIP1A isoform. Exogenous expression of HIP1A has been reported to transform fibroblasts and the mechanism believed to be responsible is stabilization of receptor tyrosine kinases such as epidermal growth factor (EGF) receptor and fibroblast growth factor (FGF) receptor 4. This poses the question: Is aberrant HIP1A expression observed in cancer linked to transcriptional de-regulation? To begin to answer this question, we have investigated a putative promoter sequence 5' of exon 1a. Our investigation has uncovered multiple κB sites within the promoter. However, NF κB activation does not appear to have a direct effect on HIP1 transcription in the system used.

Introduction

The Huntingtin Interacting Protein (*HIP1)* gene is quite complex. The mouse *Hip1* gene maps on chromosome 5 at position 5qG2 in humans, and covers over 139 Kb. The human gene maps to chromosome 7 at position 7q11.23 and covers over 204 Kb. Both genes contain disproportionately large first introns relative to the rest of the gene. Intron 1 of the human *HIP1* gene comprises over 139 Kb (roughly 68% of the gene) while intron 1 of the mouse *Hip1* gene consists of over 89 Kb (about 64%). The existence of such a large intron suggests the possibility of an alternative promoter leading to expression of an additional transcript. Both human and mouse mRNA transcripts consist

of 31 exons, which suggests the possibility of multiple *HIP1* transcripts through alternative splicing. Large 3' untranslated regions (3' UTR) of over 6kb in both mouse and human suggest additional regulatory mechanisms. Given this data it appears that the HIP1 gene may be highly regulated at the transcriptional and post-transcriptional levels. Our lab recently reported the presence of a unique U12-dependent intron, which leads to a cryptic splicing event in genetically-modified mice that lack exons 3 through 5 [34]. Surprisingly, the resulting hypomorphic protein is only expressed in certain tissues despite the presence of the mRNA transcript in non-protein expressing tissues. Given this data it appears that the HIP1 gene may be highly regulated at the transcriptional and post-transcriptional levels.

To this point, we demonstrated in the previous chapter of this thesis that alternative *HIP1* mRNA transcripts are expressed in both humans and mice. These transcripts differ only in their starting exons. One transcript (*HIP1A*) uses a 179-bp starting exon (exon 1a) and translates a predicted protein product of 1038 amino acids. A second transcript (*HIP1B*) uses a 152-bp starting exon and encodes for a protein of 1003 amino acids. The *HIP1B* transcript appears to encode a protein that lacks much of the AP180 N-terminal homology (ANTH) domain. This includes studies done by our laboratory suggesting HIP1A protein possesses transforming abilities. Exogenous expression of *HIP1A* cDNA(previously referred to as full length *HIP1*) transforms fibroblasts [8]. The mechanism believed to be responsible for this transformation is stabilizing of epidermal growth factor (EGF) receptor [8, 16]. Additionally, we have reported elevated levels of HIP1 in multiple cancers including brain, breast, colon, prostate and lymphoid cancers [5, 7, 9]. The particular form of HIP1 elevated in these cancers was not determined nor was the mechanism responsible for elevated expression uncovered.

This study poses the question: Is aberrant HIP1A expression linked to transcriptional de-regulation observed in cancer? To answer this question, we subcloned a 958-bp sequence upstream of exon1a into the pGL3 luciferase reporter vector and have shown it has promoter activity. Additionally we have identified the minimal sequence required for optimal promoter activity. Further analysis of the promoter revealed multiple putative NFκB consensus sites (known as κB sites, which were tested for functional

significance). However, there does not appear to be a direct effect of NFκB activation on *HIP1A* transcription in this system.

Materials and Methods

HIP1 promoter constructs

The numbering chosen considers as -1 the nucleotide preceding the translation start site (ATG) located in the first exon. A region corresponding to the *HIP1A* promoter (-917 to +148 bp) was originally amplified by PCR using primers containing adaptors and cloned into the pcDNA3 vector inside the *EcoR*I site. This fragment was then digested with *Sac*I and *EcoR*V and ligated into the pGL3-basic vector (Promega) digested with *Sac*I and *Sma*I. In order to delete the region +42 to +148, we used the QuickChange® XL Site-Directed Mutagenesis kit (Stratagene) with phosphorylated primers surrounding the region to delete. The final product was termed the -917/+41 promoter construct. The 5' truncated promoter mutant constructs, with the exception of the -331/+41 construct and the -240/+41 construct, were amplified by PCR with primers containing adaptors, using the -917/+41 promoter construct as a DNA template, and cloned between *Mlu*I and *Bgl*II. The -331/+41 construct and the -240/+41 construct were obtained by deletion of the -487/+41 construct using the QuickChange® XL Site-Directed Mutagenesis kit, and phosphorylated primers.

Generation of the region of interest (ROI) deletion mutant was obtained by PCR amplification of a 218-bp fragment just 3' of the region of interest and an *Xho*I site at its 5'end. The primers used for this reaction were 5'-AAG CTC GAG TCT GGA AGA CTG GCA GAA CTC ACA-3' (forward) and 5'-AGT ACC GGA ATG CCA AGC TTA CTT AGA T-3' (reverse). The resulting PCR product was gel purified and the digested with *Xho*I to produce overhangs at both ends of the fragment. The -917/+41 promoter construct was digested with *Xho*I as well to remove the region of interest and additional 3' sequence and the *Xho*I-treated PCR fragment was ligated into the vector using T4 ligase (Roche). The resulting ligation product was propagated using DH5α cells (Invitrogen).

Mutagenesis of the NFκB site in the -331/+41 construct was performed with the QuickChange® XL Site-Directed Mutagenesis kit, according to the manufacturer

protocol, using the forward primer 5'-GGG CGG GCG GCG GCG CCG TCT TTC GAA G-3' and the reverse primer 5'-GGG GCC CTC GGC TGC CCC CTT CGA AA-3'.

The PCR products were purified using the QIAquick Gel Extraction Kit (Qiagen). All the plasmids were prepared and purified using the QIAprep Spin Miniprep and HiSpeed Plasmid Maxi Kits (Qiagen), and sequencing analysis were performed by the University of Michigan DNA sequencing core, using an ABI model 3730 sequencer (Applied Biosystems).

Promoter analysis of putative *cis*-acting elements

The *HIP1A* promoter sequence was analyzed for putative *cis*-acting elements using the TFSEARCH program [56].

Cell culture

All cell lines were obtained from A.T.C.C. unless stated otherwise. The 293T cell line was maintained in Dulbecco's Modified Eagle Medium High Glucose 1x (Gibco, Invitrogen - Cat. #11965) supplemented with 10% (v/v) fetal calf serum, 100 U/mL penicillin and 100 μg/mL streptomycin, at 37°C in a humidified atmosphere 5% CO_2/air.

The RAW 264.7 cell line was maintained in Dulbecco's Modified Eagle Medium High Glucose 1x (Gibco, Invitrogen - Cat. #11995) supplemented with 10% (v/v) fetal calf serum, 100 U/mL penicillin and 100 μg/mL streptomycin, at 37°C in a humidified atmosphere 5% CO_2/air.

The K562 cell line was maintained in RPMI-1640 media with L-Gln 2mM (Cellgro – Cat#10-040-CM) supplemented with 10% (v/v) fetal calf serum, 100 U/mL penicillin and 100 μg/mL streptomycin, at 37°C in a humidified atmosphere 5% CO_2/air.

DNA Transfections

Transfections of 293T, K562 and RAW264.7 cell lines were performed in 6-well plates using SuperFect® Transfection Reagent (Qiagen) according to the manufacturer's suggested protocol. Cells were plated in a six-well plate (2 mL per well) at about 2 x 10^5 cells/mL in triplicate and grown for 24 h before transfection. Five hundred ng of the various pGL3 promoter constructs were transfected into cells along with 50ng of pRL-CMV.renilla construct, which was used as a transfection efficiency control. In the case of

κB repeat construct, 500ng of DNA was transfected into cells along with 50ng of pRL-CMV.renilla construct.

Reporter gene assay

Reporter gene assays were performed using the Dual-Luciferase Reporter Assay System (Promega) with slight modification to manufacture's protocol. Twenty four hours after transfection, cells were washed with PBS. Five hundred μL of passive lysis buffer was added to each well and incubated at room temperature for 15 minutes. Cell lysates were collected and centrifuged at 13,200rpm for 30 seconds at 4^{o}C. Ten μL of each lysate was added to individual wells of a white, opaque 96-well plate (Corning-Costar). Luciferase activity was measured using a Veritas microplate luminometer (Turner Biosystems). Firefly luciferase activity readings were normalized to the *Renilla* luciferase activity readings.

Induction of NFκB activity

NFκB activity was induced in 293T cells using human recombinant TNFα (Sigma) at a final concentration of 10ng/mL. Following treatment with TNFα, cells were incubated under normal culture conditions for a total of 6 hours unless indicated otherwise.

NFκB activity in RAW 264.7 cells was induced using human recombinant RANKL (Sigma) at a final concentration of 35ng/mL. Following treatment with RANKL, cells were incubated under normal culture conditions for a total of 6 hours.

Quantitative real time-PCR (qPCR)

The 293T cells used for NFκB induction analysis were cultured in 6-well plates, treated with 10ng/mL TNFα and allowed to incubate under normal culture conditions for the times indicated. Total RNA was isolated from 293T cells using the RNeasy® RNA isolation kit (Qiagen). First strand cDNA for real time PCR was generated using the SuperScript First-Strand Synthesis System for RT-PCR kit (Invitrogen). Random hexamers were used for reverse transcription of cDNA. Concentration of resulting cDNA was quantified using a ND-4000 nanodrop spectrophotometer. Samples were diluted to a final concentration of 100ng/ul. A total of 100 ng of cDNA was used for each reaction and each reaction was performed in triplicate. The real time PCR reactions were

performed using a Mastercycler ep realplex (Eppendorf) according to the manufacturer's instructions. The RNA content of samples compared by qPCR was normalized based on the amplification of glyceraldehyde 3-phosphate dehydrogenase (*GAPDH*).

The primers used were designed to generate amplicons in the range of 150 to 200 bp with the exception of *GAPDH* primer (294bp). Primer efficiencies were determined prior to data analysis and these efficiencies were used to calculate relative expression using the Pfaffl method [49]. The primers used for each qPCR assay were as follows: *GAPDH* forward primer sequence was 5'-CTG GTG CTG AGT ATG TCG TG-3' and reverse primer sequence was 5'-CAG TCT TCT GAG TGG CAG TG-3'; *HIP1A* forward primer sequence was 5'-GAG AGC TTC GAG CGG ACT CA-3' and reverse primer sequence was 5'-GGC AGA ACT TCC AGC AGA GC-3'.

Immunoblot analysis

The 293T cells used for NFκB induction analysis were cultured in 6-well plates, treated with 10ng/mL TNFα and allowed to incubate under normal culture conditions for the times indicated. Cells were washed with PBS and lysed using 100μl lysis buffer (50 mM Tris pH7.4, 150 mM NaCl, 1% Triton X-100, 1.5 mM $MgCl_2$, 5 mM EGTA, and 10% Glycerol) containing protease phosphatase inhibitors mixture [30 mM sodium pyrophosphate, 50 mM sodium flavide, 100 μM sodium orthovanadate and 5 complete EDTA-free mini tablets (Roche)]. Cells were incubated on ice for 10 min and centrifuged at 13,200 rpm for 15 min at 4°C. Supernatant was transferred to new tubes and protein concentrations were determined by Bradford assay (Bio-Rad). Forty (40) μg of protein was loaded to 6% SDS-polyacrylamide Tris-glycine gels (SDS-PAGE). Gels were electrotransferred onto nitrocellulose membranes and membranes were blocked for 1 h in TBS-T containing 5% non fat milk. Membranes were then probed overnight at 4°C with either the mouse monoclonal HIP1 antibody (1:2000, 4B10) or the mouse monoclonal IκBα antibody (1:10,000; Cell Signaling). The next day, membranes were washed 3 times in TBS-T for a total of 15 minutes and incubated with horseradish peroxidase (HRP)-conjugated secondary antibodies at room temperature for 1 hour. Membranes were developed with a homemade enhanced chemiluminescence reagent (ECL).

Results

Minimal promoter identified for human *HIP1A* promoter

The mechanisms involved in the transcriptional regulation of the *HIP1* gene have not been studied. To understand more about *HIP1A* transcriptional regulation in particular, we subcloned a 958-base pair sequence, which includes 917 base pairs immediately 5' of exon 1a along with the first 41 base pairs of exon 1a into the pGL3 luciferase reporter gene construct. This segment was selected with the intent of analyzing a 950-base pair region 5' of the predicted translation initiation site (TIS) of the *HIP1A* transcript. Analysis of this sequence demonstrated presence of a canonical CAAT box and absence of a TATA box indicating the likelihood that this sequence functions as a TATA-less promoter [57] (Figure 4.1). We transfected the newly generated *HIP1A* promoter (-917/+41) construct into 293T cells and checked for promoter activity. As expected, promoter activity of the -917/+41 fragment registered much higher than the pGL3 promoter-less vector (data not shown). Surprisingly, -917/+41 activity was also higher than that of the SV40-containing reporter construct (data not shown). These data confirm that the 958-base pair sequence cloned and identified here does function as a promoter.

To determine the minimal amount of sequence necessary for optimal promoter activity, we generated a series of 5' truncated promoter constructs via PCR mutagenesis using the -917/+41 construct as a template (Figure 4.2). We transfected these constructs individually into 293T cells and measured luciferase activity 24 hours after transfection. Luciferase activity of the first four truncated promoter constructs was similar to the -917/+41 construct (Figure 4.3). However, luciferase activity of the -107/+41 construct exhibited a significant drop in promoter activity.

To confirm these results, we transfected either the -107/+41, the -917/+41 or the -240/+41 construct into the K562 cell line. K562 cell line was established from the pleural effusion of a 53-year-old female with chronic myelogenous leukemia in terminal blast crises. This cell line is one of the few leukemia-derived cell lines that expressed high levels of the HIP1 protein [9]. Luciferase activity of the *HIP1A* promoter constructs in K562 cells mimicked the activity observed in 293T cells (Figure 4.4). From this data, we

concluded that the minimal sequence necessary for optimal promoter activity consists of the sequence corresponding to bases -240 to +41.

Importance of bases -240 to -108 examined

Given the fact that promoter activity decreased substantially with the loss of bases -240 to -108, we wondered whether this "region of interest" (ROI) was necessary for promoter activity. We analyzed this region for homology using the University of California-Santa Cruz (UCSC) genome browser (http://genome.ucsc.edu/) and observed "moderate conservation" between 27 vertebrae species specifically in the sequence -181 to -108 compared to the rest of the promoter (data not shown). We hypothesized that this region may be important for promoter activity.

It is also possible that the decrease in promoter activity observed in the -107/+41 promoter construct was due to a substantial loss of required promoter sequence for optimal activity to occur. This construct retained only 148 bp from the original promoter construct. Perhaps there are compensatory elements upstream of the ROI and loss of these elements in addition to the loss of the ROI leads to diminished promoter activity. To test the hypothesis that the ROI is important for promoter activity, we generated a deletion construct, which lacked bases -181 to -108 (Figure 4.5) and transfected it into both 293T and K562 cells. Twenty-four hours after transfection, we collected protein lysates and measured luciferase activity in the samples. We observed no significant difference in the luciferase activity of cells transfected with the deletion mutant construct when compared to the -917/+41 construct (Figure 4.6). Based on these results, we concluded that the region -181 to +41 is not essential to *HIP1A* promoter activity but rather loss of such a substantial portion of promoter sequence affects optimal promoter activity.

Analysis of human Hip1 promoter reveals multiple κB sites

Sequence analysis of the *HIP1A* promoter sequence also demonstrated four putative κB binding sites (Figure 4.1). This was particularly intriguing given that our lab has reported HIP1 overexpression in both Hodgkin's disease and non-Hodgkin's lymphoma [7]. More specifically, Reed-Sternberg cells, considered to be the neoplastic cell in Hodgkin's disease, stain positive for HIP1 expression. Strong constitutive

activation of NFκB is a characteristic of these Reed-Sternberg cells [58]. Additionally, we reported a change in HIP1 protein expression levels [7] as well as a significant increase in *Hip1a* transcript levels (chapter 3 of this thesis) following RAW 264.7 cell differentiation into RAW-OC, an osteoclast-like cells. Since this differentiation process is initiated by the activation of the Receptor Activator of NFκB (RANK) by its ligand, RANKL, the identification of these putative κB sites seemed to suggest a role of NFκB in *HIP1A* transcriptional regulation.

To test whether these putative binding sites were functional, we used two of the 5' truncations of the -917/+41 construct (Figure 4.7). One of the constructs lacked the first two κB site (-487/+41) and the other maintained only the κB site at positions -10 to -1 (-331/+41). This κB site was 100% conserved between the mouse and human *HIP1A* promoter sequences (data not shown), thus it was predicted to be the most important. We transfected the -917/+41 construct (all 4 κB sites), the -487/+41 promoter construct (3 κB sites) and the -331/+41 promoter construct (only one κB site) into 293T cells. Twenty-four hours after transfection, cells received 10ng/ml of TNFα to induce NFκB activity. Six hours later, the cells were harvested, protein lysates were collected and luciferase activity was measured. Luciferase activity of cells transfected with the -917/+41 construct and treated with TNFα was reduced compared to the luciferase activity of uninduced cells (Figure 4.8). Cells transfected with the -487/+41 and the -331/+41 promoter constructs and treated with TNFα exhibited the same pattern. A κB-luciferase construct was used as a positive control for NFκB activation and as expected, luciferase activity of 293T cells transfected with this construct was highly elevated 6 hours after treatment with TNFα (Figure 4.8 - insert). This apparent repression of the human *HIP1A* promoter was unexpected given the increase in *Hip1a* transcript levels observed in differentiated RAW cells. To test whether this repression was real, we mutated the κB site at positions -10 to -1 in the -331/+41 construct (Figure 4.9). As stated earlier, this site is the most highly conserved of the 4 κB sites. We selected the -331/+41 construct as a template because it lacked the other three κB sites yet it still exhibited a similar decrease in promoter activity. The mutated construct was transfected into 293T cells and repression of luciferase activity following NFκB induction was compared to cells transfected with

the non-mutated construct. Cells transfected with the mutated κB construct experienced a similar reduction in promoter activity as the non-mutated promoter construct (Figure 4.10).

To confirm the results observed in 293T cells treated with TNFα, we decided to analyze our reporter constructs in RAW cells induced with RANKL. This system seemed like a logical choice given that we observe an increase in *Hip1a* transcript in RAW cells in culture for 6 days following RANKL treatment (chapter 3). We transfected RAW cells with the non-mutated -331/+41 construct as well as the -331/+41 construct with the mutated kB site. Twenty-four hours later we treated cells with RANKL (35ng/mL) and incubated them in culture for a total of 6 days following RANKL treatment. Unfortunately, both firefly and *Renilla* luciferase activity (used as a transfection efficiency control) in all samples collected was similar to non-transfected cells, suggesting that the cells that remained in culture no longer expressed the transfected constructs. To circumvent this issue, we studied promoter responsiveness to NFκB short-term in RAW cells by measuring luciferase activity 6 hours after treatment with RANKL (similar to 293T analysis). Luciferase activity in RAW cells following treatment with RANKL was essentially the same compared to non-treated RAW cells in both the non-mutated and mutated -331/+41 constructs (Figure 4.11). In contrast, the κB positive control was significantly increased following RANKL treatment. The conflicting data obtained from the promoter analysis in RAW cells coupled with no difference in promoter activity between the mutated and non-mutated promoter constructs following NFκB induction led me to question whether the apparent repression observed in 293T cells was a true indication of HIP1A promoter responsiveness to NFκB. To explore whether NFκB activation plays a physiological role in *HIP1A* transcriptional regulation, we decided to measure the effect of NFκB induction on *HIP1A* mRNA transcript levels. To do this, we treated 293T cells with TNFα and isolated RNA from these cells at various timepoints following induction. The isolated RNA was used to generate first-strand cDNA for subsequent quantitative PCR analysis. Quantitative PCR analysis of these samples revealed no significant changes in the levels of *HIP1A* transcripts relative to *HIP1A* levels in untreated 293T cells (Figure 4.12).

Additionally, HIP1 protein levels did not change as determined by western blot analysis (Figure 4.13). IκB degradation was analyzed to confirm that NFκB was activated and indeed it was. Taken together, this data suggests that NFκB does not act directly on the *HIP1A* promoter.

Discussion

Despite the extensive work that has gone into analyzing the HIP1 protein, very little work has been invested in understanding the transcriptional regulation of the gene. In particular, no work has been done to decipher differences in regulation of alternative *Hip1* transcripts. This study attempted to gain more insight into transcriptional regulation of the *HIP1A* transcript primarily based on the hypothesis that this transcript may potentially be de-regulated in cancer. The hypothesis is grounded in the fact that only the *HIP1A* cDNA has been shown to transform cells [8] and lead to plasma cell neoplasms *in vivo* [7].

DNA sequence 5' of the transcriptional start site of the *HIP1A* transcript was isolated to determine whether it functions as an adequate promoter. As expected, the sequence exhibited strong promoter activity exceeding activity of an SV40-driven reporter construct. Further analysis of this sequence revealed that the minimal amount of sequence required for this optimal promoter activity was bases -240 to +41. Bases -240 to -108 initially appeared to be necessary for promoter activity as loss of these bases led to a substantial loss of promoter activity. However, when bases -181 to -108 were removed from the original -917/+41 promoter construct, activity was essential similar to the unmodified form of the promoter. This data suggests these nucleotides are not necessary for optimal activity to occur. It's possible that there are multiple regulatory *cis*-elements present in the promoter sequence that are compensatory in nature. Loss of some of the elements alone may not be enough to diminish promoter activity but their combined loss dramatically affects overall promoter activity. The minimal amount of promoter activity that remained in the -107/+41 promoter construct is likely to be due to the CAAT box present in this minimal sequence. It would be interesting to see whether mutation of this regulatory element would indeed abrogate promoter activity completely.

Analysis of the *HIP1A* promoter also revealed the presence of four putative κB binding sites. The presence of these sites was encouraging given the association of NFκB and lymphoid malignancies [59]. We have previously reported HIP1 overexpression in Hodgkin's disease and non-Hodgkin's lymphoma [7]. In particular, Reed-Sternberg cells stain positive for HIP1. Reed-Sternberg cells are considered the neoplastic cell in Hodgkin's disease and they have constitutive NFκB activation [58]. We have also reported in chapter 3 of this thesis that *Hip1a* transcript levels are elevated in RAW cells following their treatment with RANKL. RANKL is a known inducer of the NFκB pathway. The effect of NFκB activity on *HIP1A* transcriptional regulation was explored using the luciferase reporter gene system and quantitative PCR analysis. Initially, it appeared that *HIP1A* promoter activity was repressed by the activation of NFκB in 293T cells as treatment with TNFα led to a decrease in promoter activity. However, further analysis of promoter activity in RAW cells treated with RANKL showed no change. Additionally, there does not appear to be any direct physiologically significant response to activation of NFκB in 293T cells. Under the same induction conditions used for the reporter gene assay, essentially no changes in *HIP1A* transcript levels or HIP1 protein levels were detected. Taken together, these data suggest no involvement of the NFκB signaling pathway in *HIP1A* transcriptional regulation. These data also suggest that the induction of *Hip1a* transcript levels observed in differentiated RAW cells is unlikely a direct result of NFκB signaling on *Hip1a* transcriptional regulation. It is worth noting that the NFκB signaling cascade is not the only one activated with RANKL stimulation. There are at least four other signaling cascades that have been reportedly activated due to RANKL stimulation: 1) c-Jun N-terminal kinase (JNK), 2) p38, 3) extracellular signal-regulated kinase (ERK) and 4) Src [60]. Preliminary analysis of the *HIP1A* promoter sequence did not reveal any response elements associated with these signaling pathways. However, this does not rule out the possibility of their involvement in *Hip1a* transcriptional regulation. More work must be done to determine the mechanisms involved in the observed induction of *Hip1a* in differentiating RAW cells.

Figure 4.1: Human *HIP1A* promoter sequence. The 917-base pair sequence immediately 5' of exon 1a as well as the first 41 base pairs of exon 1a were PCR amplified and subcloned into the pGL3 Firefly luciferase reporter gene construct. Analysis of this sequence revealed the presence of 4 NFκB sites (shaded gray) and the typical CAAT box (underlined). The sequence is numbered with the transcription start site (TSS) as +1. Exon 1a sequence is in bold font.

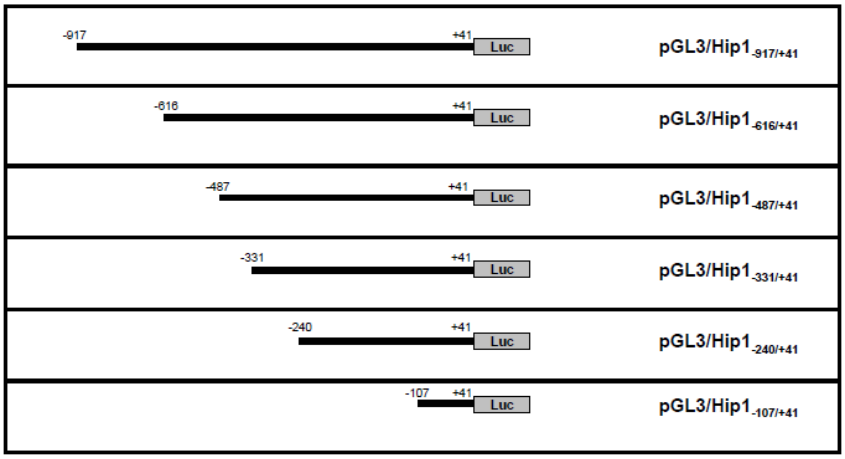

Figure 4.2: Diagram of various promoter constructs. Multiple 5' truncations of the original *HIP1A* promoter construct were generated in order to determine the minimal sequence necessary for optimal promoter activity.

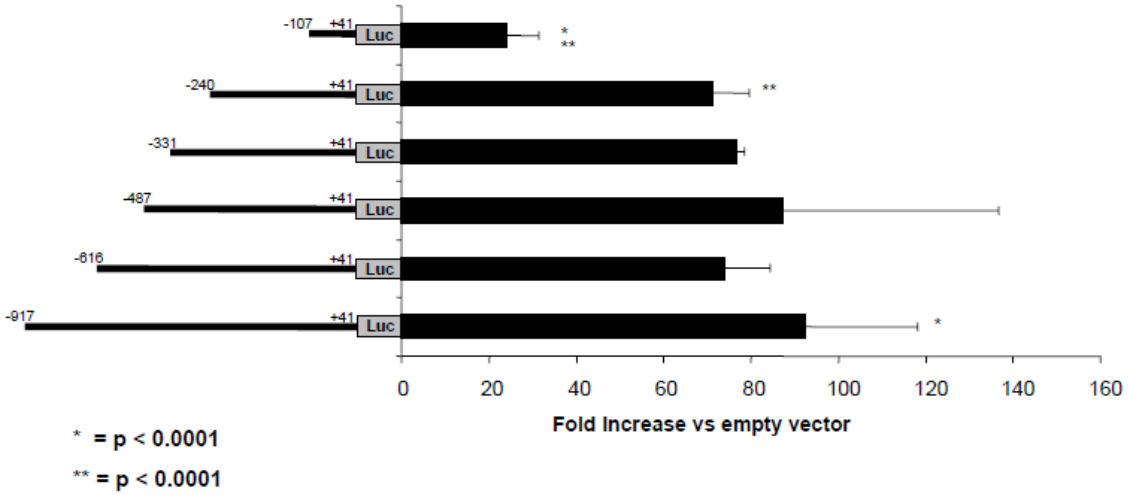

Figure 4.3: Human HIP1A promoter activity in 293T cells. The various promoter constructs were transfected into HEK 293T cells along with *Renilla* luciferase constructs (transfection efficiency control) and protein lysates were collected 24 hours after transfection in order to measure luciferase activity. Firefly luciferase readings were normalized to *Renilla* luciferase readings. This graph shows the fold increase of normalized luciferase activity compared to the promoter-less pGL3 basic vector.

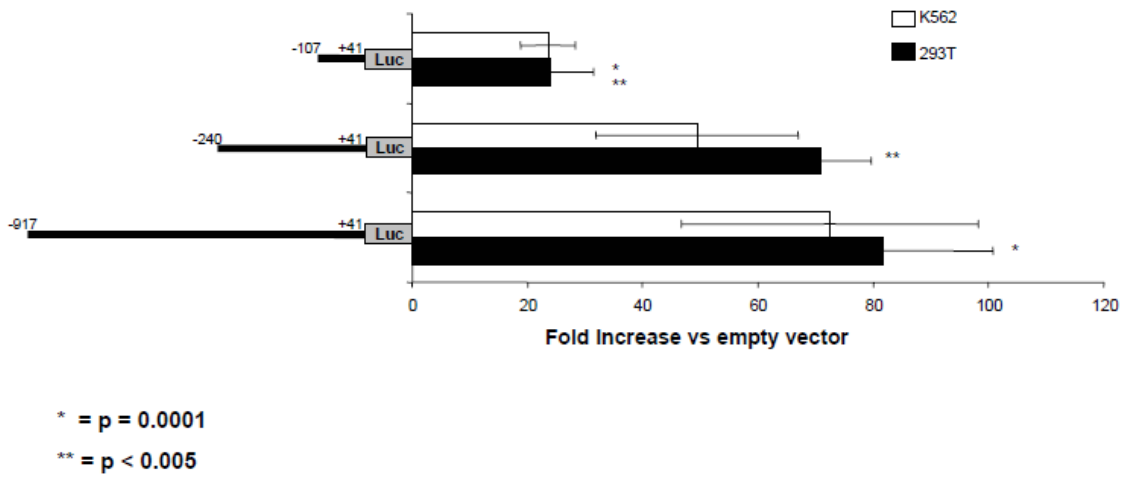

Figure 4.4: Human *HIP1A* promoter activity in both HEK 293T and K562 cells. Three of the promoter constructs were transfected into both HEK 293T cells and K562 cells along with *Renilla* luciferase constructs (transfection efficiency control). Protein lysates were collected 24 hours after transfection in order to measure luciferase activity. Firefly luciferase readings were normalized to *Renilla* luciferase readings. This graph shows the fold increase of normalized luciferase activity compared to the promoter-less pGL3 basic vector.

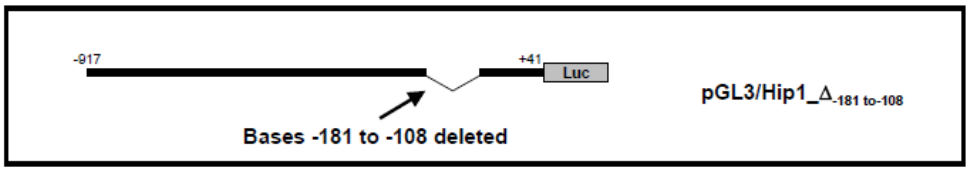

Figure 4.5: Diagram of the "region of interest" deletion mutant construct. The human *HIP1A* promoter sequence from -181 to -108 was deleted from the original promoter construct by PCR mutagenesis in order to analyze whether this region was necessary for promoter activity.

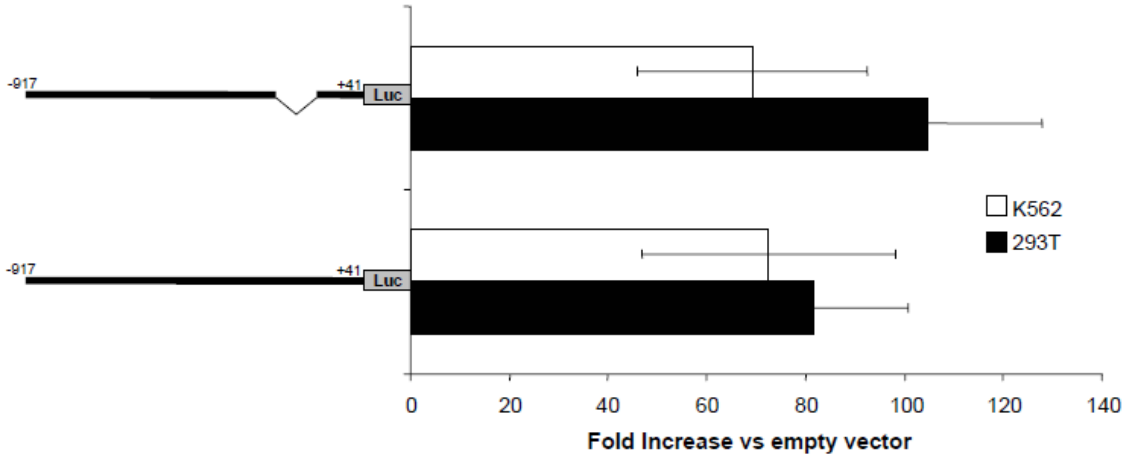

Figure 4.6: Promoter activity of -181/-108 deletion mutant in HEK 293T and K562 cells. Both the original promoter construct and the -181/-108 deletion mutant construct were transfected into HEK 293T and K562 cells along with *Renilla* luciferase constructs (transfection efficiency control). Protein lysates were collected 24 hours after transfection in order to measure luciferase activity. Firefly luciferase readings were normalized to *Renilla* luciferase readings. This graph shows the fold increase of normalized luciferase activity compared to the promoter-less pGL3 basic vector.

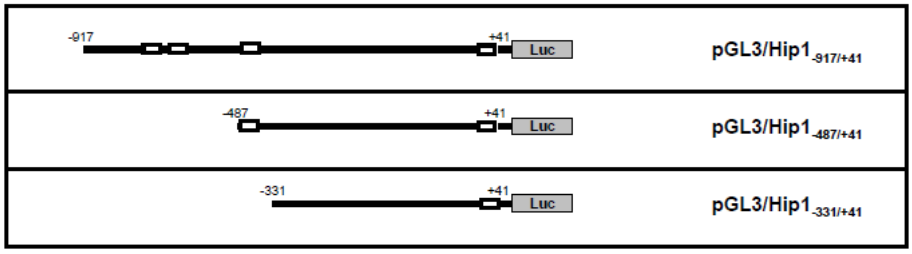

Figure 4.7: Diagram of promoter constructs with κB sites. A total of 4 κB sites (white bars) were identified through sequence analysis of the original promoter sequence. The -487/+41 promoter construct contains 2 of the 4 κB sites and the -331/+41 promoter construct contains only one of the κB sites. This single κB site is the most conserved of the 4 (100% identical) when compared to mouse and very highly conserved among multiple species. These 3 constructs were used in NFκB induction assays (see figure 3B).

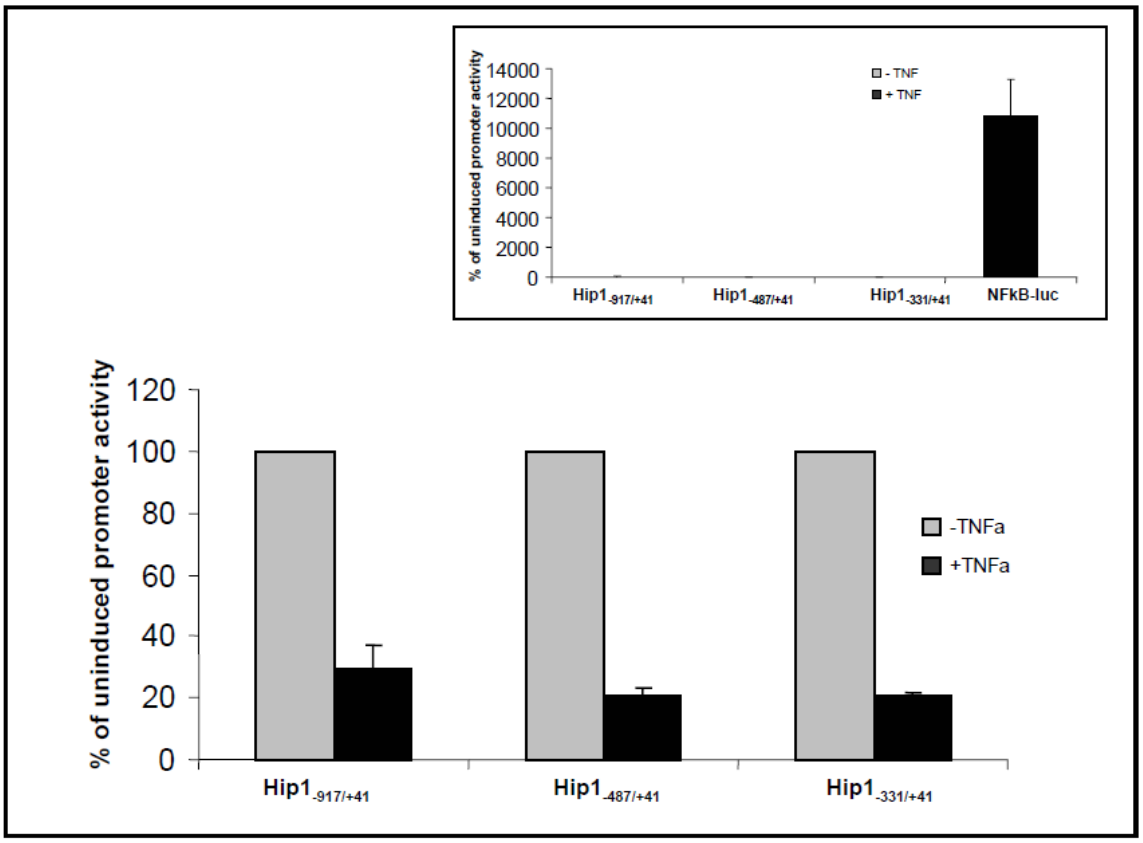

Figure 4.8: Human *HIP1A* promoter activity in HEK 293T cells following NFκB induction with TNFα. The three promoter constructs identified in figure 4.7 were transfected into HEK 293T cells along with *Renilla* luciferase constructs (transfection efficiency control). Twenty-four (24) hours later cells were treated with 10ng/mL of human recombinant TNFα and protein lysates were collected 6 hours later in order to measure luciferase activity. Firefly luciferase readings were normalized to *Renilla* luciferase readings. Promoter activity of TNF-treated cells is represented as a percentage of the normalized promoter activity of untreated cells. A κB-luciferase construct was used as a control for NFκB activity (insert).

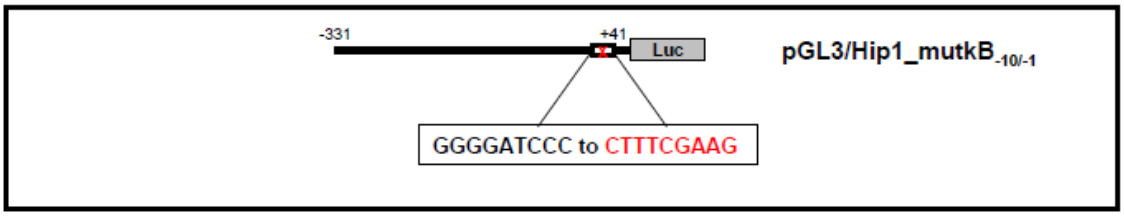

Figure 4.9: Diagram of the NFκB mutant construct. The NFκB site in the -331/+41 promoter construct was mutated by PCR mutagenesis in order to analyze whether the site is functional.

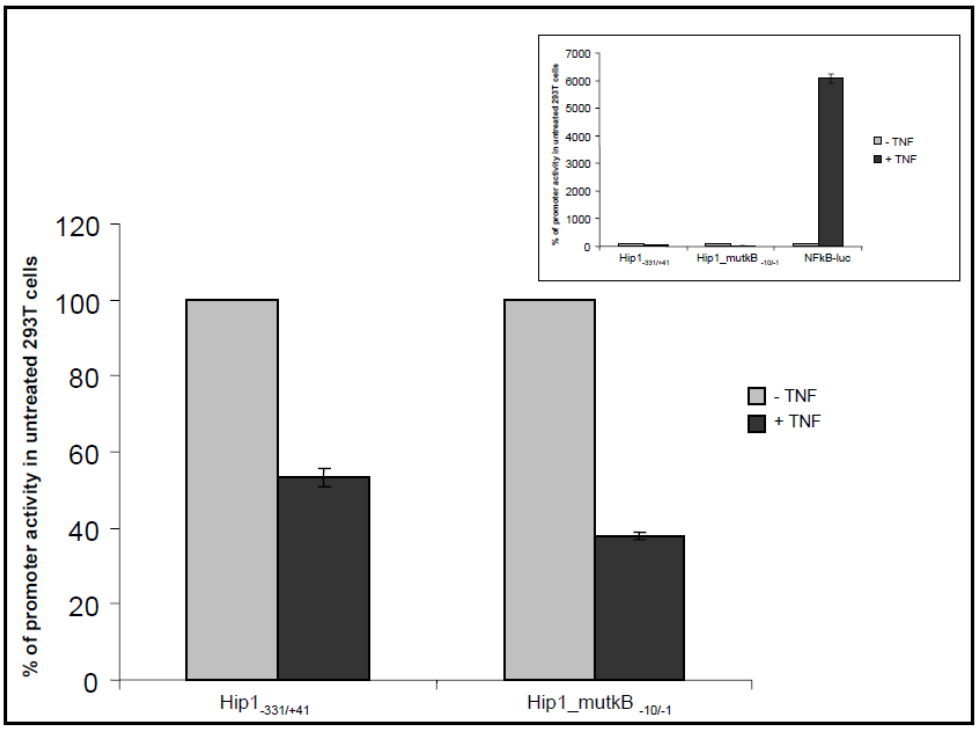

Figure 4.10: NFκB mutant promoter activity in HEK 293T cells following NFκB induction with TNFα. Promoter activity of the -331/+41 promoter construct, which contains the highly conserved κB site, was compared to the κB mutant construct indicated in figure 4.9. Both promoters were transfected into HEK 293T cells along with *Renilla* luciferase constructs (transfection efficiency control). Twenty-four (24) hours later cells were treated with 10ng/mL of human recombinant TNFα and protein lysates were collected 6 hours later in order to measure luciferase activity. Firefly luciferase readings were normalized to *Renilla* luciferase readings. Promoter activity of TNF-treated cells is represented as a percentage of the normalized promoter activity of untreated cells. A κB-luciferase construct was used as a control for NFκB activity (insert).

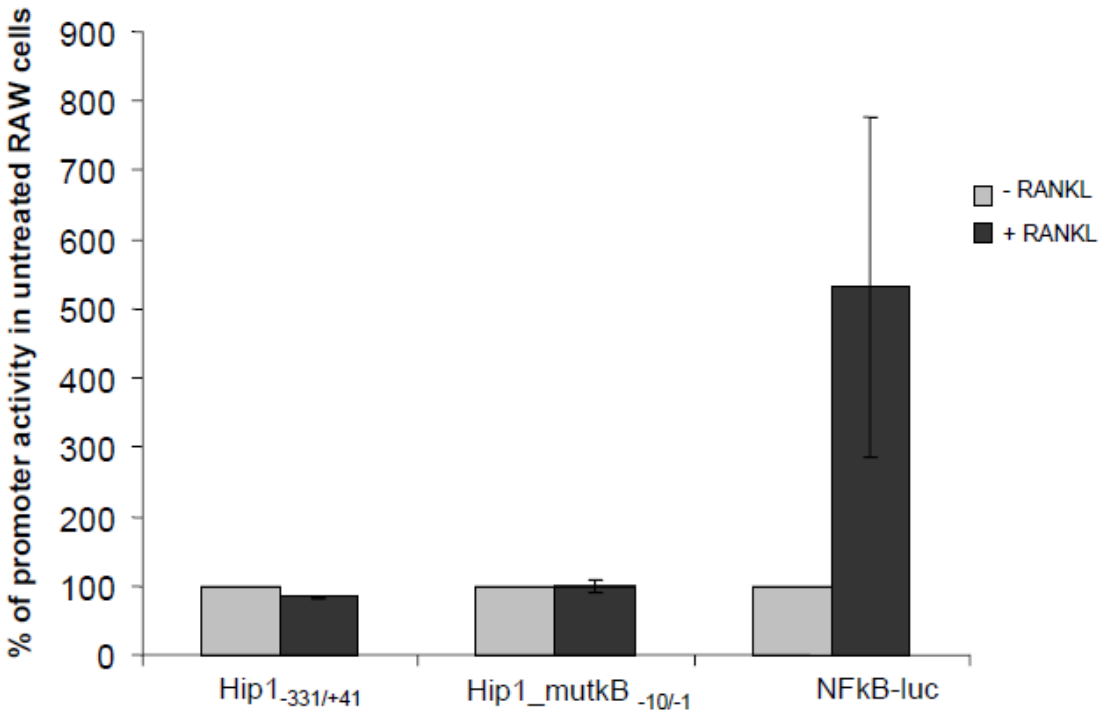

Figure 4.11: Human *HIP1A* promoter activity in RAW 264.7 cells following NFκB induction with RANKL. Promoter activity of the -331/+41 promoter construct, which contains the highly conserved κB site, was compared to the κB mutant construct indicated in Figure 4.9. Both promoters were transfected into RAW 264.7 cells along with *Renilla* luciferase constructs (transfection efficiency control). Twenty-four (24) hours later cells were treated with 35ng/mL of human recombinant RANKL and protein lysates were collected 6 hours later in order to measure luciferase activity. Firefly luciferase readings were normalized to *Renilla* luciferase readings. Promoter activity of RANKL-treated cells is represented as a percentage of the normalized promoter activity of untreated cells. A κB-luciferase construct was used as a control for NFκB activity.

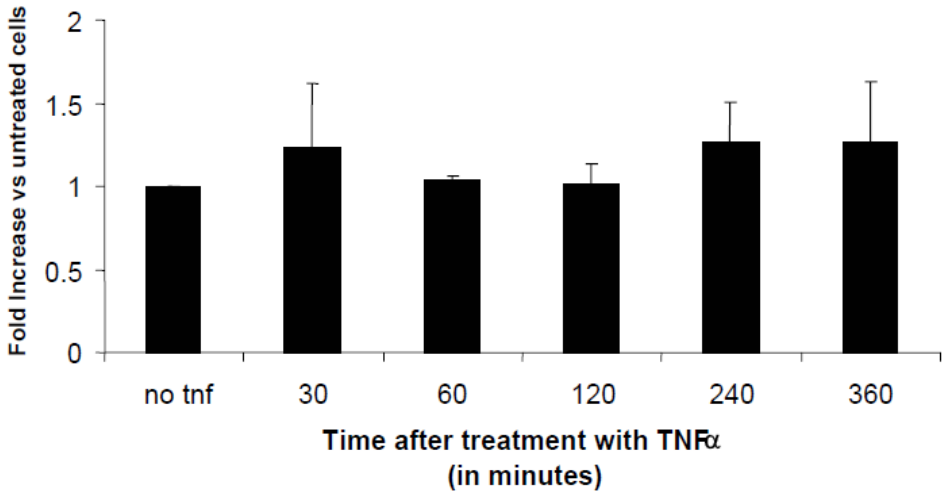

Figure 4.12: *HIP1A* transcript levels following NFκB induction. HEK 293T cells were treated with 10ng/mL of human recombinant TNFα and harvested at the various timepoints indicated. Five (5) ug of total RNA was isolated from the cells and used to generate cDNA for quantitative PCR analysis. Relative expression levels were determined as described in the Materials and Methods section. Values represent expression levels relative to untreated HEK 293T cells.

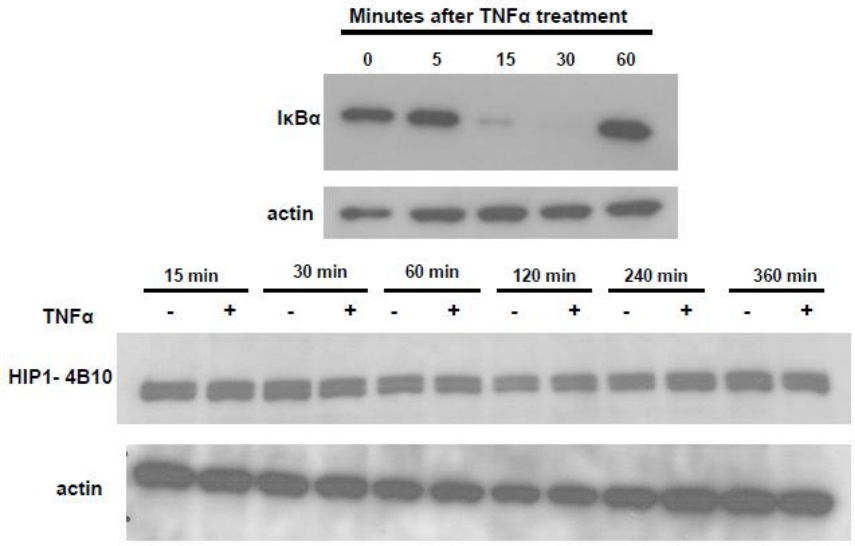

Figure 4.13: HIP1 protein levels following NFκB induction. HEK 293T cells were treated with 10ng/mL of human recombinant TNFα and harvested at the various timepoints indicated. Protein was isolated from the cells and western blot analysis was performed as described in Materials and Methods and run on a 6% SDS-PAGE gel. Western blot analysis of IκBα was done to confirm NFκB activation.

CHAPTER 5

CONCLUSION

The major goal of this thesis project was to provide insight into the transcriptional and post-transcriptional regulation of the *HIP1* gene. The previous three chapters describe the studies aimed at accomplishing this goal. This chapter summarizes the major conclusions drawn from these studies.

Partially functional HIP1 product suggests multiple isoforms with separate cellular functions

In chapter 2, we describe a novel form of HIP1 that is expressed *in vivo* as the result of a novel cryptic splicing event between a 5' AT-AC intron (intron 2) and a 3' GT-AG intron (intron 5). Our initial intent was to generate a "third generation" *Hip1* knockout mouse allele (the $Hip1^{\Delta 3\text{-}5}$) that does not provide the confounding issues associated with the previously generated spontaneous "null" allele [26] and could be conditionally deleted. We planned to use this mouse to extend our analysis of HIP1 involvement in tumorigenesis [6]. We were surprised to find that $Hip1^{\Delta 3\text{-}5/\ \Delta 3\text{-}5}$ mice, when crossed with tumor prone mice, are equally, if not more, prone to the development of prostate and breast tumors than *Hip1* wild type mice. Further analysis demonstrated that the tumor cells from the $Hip1^{\Delta 3\text{-}5/\ \Delta 3\text{-}5}$ genetic background expressed a truncated form of the HIP1 protein (HIP1Δ3-5insAG protein) as a result of the novel cryptic splicing event described above. Additionally, HIP1Δ3-5insAG protein is selectively expressed in brain and lung examined from $Hip1^{\Delta 3\text{-}5/\ \Delta 3\text{-}5}$ mice but not kidney or spleen. This type of cellular natural selection provides us with the first clue that multiple HIP1 isoforms may be expressed differentially in various tissues and these isoforms may have separate cellular functions.

The second clue comes from the observation that the resulting protein product from the Δ3-5 mice slightly rescues the phenotype observed in *Hip1* single knockout mice [26]. While homozygous Δ3-5 mice still develop spinal defects and testicular degeneration, they do not develop cataracts. Furthermore, the Δ3-5 protein still binds lipids, clathrin, AP2 and EGFR. It is possible that the mutant protein expressed in homozygous mice is similar enough to the wildtype protein involved in normal endocytic functions that it can partially compensate. Similarly, we conclude that the HIP1 protein responsible for normal spinal and testicular development and/or maintenance cannot be generated in the Δ3-5 mice. As I will discuss later in this chapter, one of the HIP1 isoforms observed may be the result of a downstream ATG translation initiation site in either exon 4 or exon 5. Both of these exons are absent in the truncated *Hip1Δ3-5insAG* mRNA transcript. This mutant mouse provides an intriguing model to study *Hip1* gene regulation more extensively.

Alternative transcripts may code for different isoforms

The study described in chapter 3 explores the possibility of the use of alternative *HIP1* transcripts for generation of HIP1 isoforms with different cellular functions. In this work we describe the discovery of an alternative *HIP1* transcript (*HIP1B*) in mouse and human. This is the first report of an alternative *Hip1* transcript in mouse and a more rigorous characterization of an initially reported alternative *HIP1* transcript in human [29]. The alternative transcripts are expressed in varying amounts in different mouse cells. For instance, the newly identified *Hip1b* transcript is expressed more predominantly in RAW 264.7 cells cultured under normal conditions (by approximately 5-fold). In contrast, the *Hip1a* transcript is predominantly expressed in intact mouse tissues and non-immortalized mouse embryonic fibroblasts (MEFs), with most tissues expressing more *Hip1a* than *Hip1b*. The most dramatic difference in transcript levels was observed in lung, which had *Hip1a* levels 15-fold higher than *Hip1b*.

Our analysis of these alternative transcripts has uncovered two situations in which original expression patterns change. The first situation involves stimulation of RAW cells with the cytokine, receptor activator of NFκB ligand (RANKL). RANKL stimulation of RAW cells leads to differentiation into osteoclast-like cells, RAW-OC, 6 days after

stimulation. During this process, the *Hip1a* transcript is selectively induced by 2-fold while *Hip1b* transcript levels remained unchanged. This selective induction correlates to an increase in expression of the larger-mass isoform of the HIP1 doublet previously reported [7]. This finding provides us with the first reported *Hip1*-inducible system for further analysis of *Hip1* transcriptional analysis and protein expression. In the second situation, the ratio of *Hip1a* transcript to *Hip1b* transcript decreases upon immortalization of (MEFs). This observation requires more detailed characterization before any definitive conclusions can be made but the possible implications for study of the role of HIP1 in immortalization and transformation are exciting.

The alternative transcripts differ only in their starting exons but this difference allows for potential translation from a downstream open reading frame (dORF). We hypothesize that downstream translation occurs through an alternative translation mechanism known as reinitiation [51, 52]. Exon 1b of the *HIP1B* transcript contains a small upstream open reading frame (upORF) of 8 codons just upstream of the predicted translation initiation site (TIS) that encodes for a 1003-amino acid protein. The *HIP1A* transcript does not encode any upORFs. Reinitiation at downstream ATGs typically occurs because small upORFs allow the 40S ribosomal complex to occasionally skip ATG codons that are in an optimal context when close to the upORF and initiate translation at more dORF in an optimal context. A classic example of this type of alternative translation is seen with *GCN4* in yeast in which four upORFs play a regulatory role [53-55]. We have shown through mutational analysis that a band similar in migration, by SDS-PAGE, to the smaller-mass isoform of the HIP1 doublet is detected when the exon 1b ATG codons are disrupted. It is not known which of the downstream ATGs are responsible for the product most similar in migration to the smaller isoform. It is possible that both are translated as we have occasionally observed a HIP1 triplet, although far less frequently.

We also cannot say definitively that the smaller isoform is indeed a product of one of these dORFs. It is possible that the HIP1 doublet is the result of post-translational modification of a single HIP1 protein. HIP1 may be phosphorylated, ubiquitinylated or modified in some other fashion and the larger band of the HIP1 doublet may be the result of this occurrence. However, this possibility seems less likely given that only one band is

detected in protein samples from HIP1A-transfected 293T cells when using α-myc antibody to detect the cDNA product. As of yet, we have not detected both bands in HIP1A-transfected 293T cells using α-myc antibody or a HIP1 antibody specific to human HIP1 protein. Our data seem to support the hypothesis that the *HIP1B* transcript may encode for a different HIP1 protein than *HIP1A*.

The data presented in chapter 3 provide the first evidence that HIP1 isoforms with distinct cellular roles exist in humans and mice. The predicted products of the dORFs in *HIP1B* each lack the AP180 N-terminal homology (ANTH) domain, which is necessary for lipid binding [14-16]. We have previously shown that exogenous over-expression of HIP1 with a functional ANTH domain transforms fibroblasts [38] and heterologous expression of this form of HIP1 leads to plasma cell neoplasms *in vivo* [7]. In contrast, HIP1 than lacks the ANTH domain induces apoptosis [9]. Others have shown that alternative *Hip1* transcripts are expressed in *Drosophila* and these transcripts encode for two different isoforms, one of which lacks the ANTH domain [30]. These different isoforms exhibit contrasting effects on Notch-mediated neurogenesis when exogenously expressed in *Drosophila*. Preliminary studies regarding exogenous expression of the *HIP1A* mutant with disrupted exon 1b ATG codons in HEK 293T cells suggest that the expressed products induce apoptosis.

Transcriptional regulation of *HIP1A* is complex

In chapter 4, I report the identification and characterization of the *HIP1A* promoter. Our analysis revealed that the minimal sequence required for optimal promoter activity includes bases -240 to +41 with +1 designated as the transcription start site (TSS). We observed a dramatic drop in promoter activity when bases -240 to -108 were deleted from a 5' truncated promoter construct. Sequence analysis of this region ("region of interest" or ROI) demonstrated moderate conservation between 27 different species from bases -180 to -108. To determine if these bases were necessary for promoter activity, we deleted this region from the original *HIP1A* promoter construct and measured luciferase activity. Surprisingly, promoter activity was similar to the original promoter construct suggesting that this region is not necessary for promoter activity. Perhaps there are *cis*-acting elements 5' of this region that can compensate for the loss of this region. This would explain why promoter activity in the -107/+41 promoter construct is

dramatically reduced. Clearly there are elements 5' of this sequence, which are necessary for optimal promoter activity. More work will be done to identify the putative *cis*-acting elements necessary for *HIP1A* transcription.

My analysis of the *HIP1A* promoter sequence also revealed 4 putative κB sites. Aberrant NFκB activity has been tied to multiple lymphoid malignancies including Hodgkin's disease [59]. We have previously reported that HIP1 expression is elevated in both Hodgkin's disease and non-Hodgkin's lymphoma [7]. Additionally, we observed induction of the *Hip1a* transcript (reported in chapter 3) and increased expression of the larger mass HIP1 isoform [7] 6 days after RAW cells have been treated with RANKL, a known inducer of NFκB activity. Therefore, we examined whether the *HIP1A* promoter is regulated by NFκB. Promoter analysis in both 293T and RAW cells suggests that this is not the case. Promoter activity in 293T cells initially appeared to decrease after treatment with TNFα but a similar decrease in activity was observed when the most conserved κB site was mutated in the HIP1A promoter construct that lacked the other 3 κB sites. No change was observed in promoter activity when RAW cells were treated with RANKL under the same conditions. Furthermore, no change was observed in *HIP1A* transcript levels or HIP1 protein levels in 293T cells after treatment with TNFα.

These results were somewhat surprising given the observed increases in *Hip1a* transcript and the larger HIP1 protein isoform (which may be the translated product of the *Hip1a* transcript) in RAW cells treated with RANKL. However, it is worth noting that binding of RANKL to its receptor target, RANK, triggers multiple signaling cascades responsible for lineage commitment as well as osteoclast activation, survival, cytoskelatal rearrangement and motility [60, 61]. In addition to activation of the NFκB signaling pathway, at least four other signaling cascades are reportedly activated: 1) c-Jun N-terminal kinase (JNK), 2) p38, 3) extracellular signal-regulated kinase (ERK) and 4) Src [61]. Any one of these signaling cascades could potential be involved in increased expression of *Hip1a* transcript. Future efforts will focus on identifying the mechanisms responsible the selective increase in *Hip1a* expression.

The future of HIP1

The work involved in this project has provided exciting new insight to the field of HIP1. Although we initially intended to design a conditional *Hip1* knockout allele, we

generated an allele that encodes for a mutant form of Hip1 lacking exons 3 through 5. Mice homozygous for this mutant allele can serve as a model for investigating tissue-specific expression of HIP1 protein. These mice selectively express the mutant HIP1 protein and expression of HIP1 in the brains of these mice changes throughout development. Additionally, the mutant mRNA is incapable of generating products from the exon 4 and exon 5 AUG start codons. If the smaller band of the HIP1 doublet is another HIP1 isoform than further analysis of these mice may provide valuable insight into regulation of this product.

We have also identified a second *HIP1* transcript in humans and mice. The preliminary data presented in this thesis suggests the possibility that the two *HIP1* transcripts may encode for two isoforms with distinct cellular roles. The obvious next step is to confirm that these transcripts do encode for the different forms of HIP1 observed by western blot. This can be accomplished by N-terminal sequence of the two bands detected by western blot analysis. An alternative approach to confirming the connection between the two transcripts and their apparent products is selective siRNA knockdown of the individual *HIP1* transcripts. If the transcripts do encode for the two isoforms then loss of *HIP1A* transcript should result in loss of the larger isoform and knockdown of the *HIP1B* transcript should result in the loss of the smaller isoform. This approach could also provide insight into the distinct functions of the two isoforms. I would predict that knockdown of the *HIP1A* transcript would lead to decreased cellular survival and increased sensitivity to cellular stress. Knockdown of the *HIP1B* transcript may lead to increased susceptibility to transformation because of a lack of the HIP1 form perceived to be involved in apoptosis. A more ambitious goal would be to generate mutant mice that lack expression of either transcript. We know from our experience with the delta 3-5 mice, that this will be difficult. However, if these mice were successfully generated the resulting phenotypes would no doubt be informative.

In terms of transcriptional regulation of *HIP1*, we have only scratched the surface. We have a model for selective induction of *Hip1a* transcript in the RAW cell differentiation model. Although the data generated from this model and other systems we used in this thesis project do not support our hypothesis that the *HIP1A* promoter is regulated by NFκB, we cannot completely ruled out this possibility. However, it may be

worth investigating other signaling cascades activated by RANKL signaling. There are at least four other signaling cascades mentioned earlier in this chapter that can and should be explored. Future studies should focus on these signaling cascades individually to improve our understanding of *HIP1A* transcriptional regulation. Additionally, generating a stable RAW cell line that has the *HIP1A* promoter construct may be worth pursuing. This would allow for a more accurate analysis of the *HIP1A* promoter using our inducible model.

Finally, we would like to answer the question, "Which of the two transcripts is elevated in cancer?" This is really a fascinating question and it's ultimately why we do the work we do. It would be interesting to compare expression levels in normal tissue to that of tumor tissue and see if any notable changes are present. I would predict that *HIP1A* is elevated in cancer based on our previous observations that *HIP1A* cDNA transforms NIH3T3 fibroblasts [38]. Over-expression of *HIP1A* cDNA in vivo also leads to plasma cell neoplasms [7] although this phenomenon is a bit more complex due to random integration of the cDNA. If this is the case, targeted therapies can be designed for cancer that express high levels of HIP1 particularly prostate cancer. Such therapies may lead to improved prognosis. Indeed the future of HIP1 study is bright.

BIBLIOGRAPHY

1. Kalchman, M.A., et al., *HIP1, a human homologue of S. cerevisiae Sla2p, interacts with membrane-associated huntingtin in the brain.* Nat Genet, 1997. **16**(1): p. 44-53.
2. Wanker, E.E., et al., *HIP-I: a huntingtin interacting protein isolated by the yeast two-hybrid system.* Hum Mol Genet, 1997. **6**(3): p. 487-95.
3. Gervais, F.G., et al., *Recruitment and activation of caspase-8 by the Huntingtin-interacting protein Hip-1 and a novel partner Hippi.* Nat Cell Biol, 2002. **4**(2): p. 95-105.
4. Hackam, A.S., et al., *Huntingtin interacting protein 1 induces apoptosis via a novel caspase-dependent death effector domain.* J Biol Chem, 2000. **275**(52): p. 41299-308.
5. Bradley, S.V., et al., *Huntingtin interacting protein 1 is a novel brain tumor marker that associates with epidermal growth factor receptor.* Cancer Res, 2007. **67**(8): p. 3609-15.
6. Bradley, S.V., et al., *Serum antibodies to huntingtin interacting protein-1: a new blood test for prostate cancer.* Cancer Res, 2005. **65**(10): p. 4126-33.
7. Bradley, S.V., et al., *Aberrant Huntingtin interacting protein 1 in lymphoid malignancies.* Cancer Res, 2007. **67**(18): p. 8923-31.
8. Rao, D.S., et al., *Altered receptor trafficking in Huntingtin Interacting Protein 1-transformed cells.* Cancer Cell, 2003. **3**(5): p. 471-82.
9. Rao, D.S., et al., *Huntingtin-interacting protein 1 is overexpressed in prostate and colon cancer and is critical for cellular survival.* J Clin Invest, 2002. **110**(3): p. 351-60.
10. Ross, T.S., et al., *Fusion of Huntingtin interacting protein 1 to platelet-derived growth factor beta receptor (PDGFbetaR) in chronic myelomonocytic leukemia with t(5;7)(q33;q11.2).* Blood, 1998. **91**(12): p. 4419-26.
11. Ross, T.S. and D.G. Gilliland, *Transforming properties of the Huntingtin interacting protein 1/ platelet-derived growth factor beta receptor fusion protein.* J Biol Chem, 1999. **274**(32): p. 22328-36.
12. Wesp, A., et al., *End4p/Sla2p interacts with actin-associated proteins for endocytosis in Saccharomyces cerevisiae.* Mol Biol Cell, 1997. **8**(11): p. 2291-306.
13. Legendre-Guillemin, V., et al., *ENTH/ANTH proteins and clathrin-mediated membrane budding.* J Cell Sci, 2004. **117**(Pt 1): p. 9-18.
14. Ford, M.G., et al., *Simultaneous binding of PtdIns(4,5)P2 and clathrin by AP180 in the nucleation of clathrin lattices on membranes.* Science, 2001. **291**(5506): p. 1051-5.
15. Itoh, T., et al., *Role of the ENTH domain in phosphatidylinositol-4,5-bisphosphate binding and endocytosis.* Science, 2001. **291**(5506): p. 1047-51.
16. Hyun, T.S., et al., *HIP1 and HIP1r stabilize receptor tyrosine kinases and bind 3-phosphoinositides via epsin N-terminal homology domains.* J Biol Chem, 2004. **279**(14): p. 14294-306.
17. Lemmon, M.A., *Phosphoinositide recognition domains.* Traffic, 2003. **4**(4): p. 201-13.

18. Metzler, M., et al., *HIP1 functions in clathrin-mediated endocytosis through binding to clathrin and adaptor protein 2.* J Biol Chem, 2001. **276**(42): p. 39271-6.
19. Mishra, S.K., et al., *Clathrin- and AP-2-binding sites in HIP1 uncover a general assembly role for endocytic accessory proteins.* J Biol Chem, 2001. **276**(49): p. 46230-6.
20. Rao, D.S., et al., *Huntingtin interacting protein 1 Is a clathrin coat binding protein required for differentiation of late spermatogenic progenitors.* Mol Cell Biol, 2001. **21**(22): p. 7796-806.
21. Waelter, S., et al., *The huntingtin interacting protein HIP1 is a clathrin and alpha-adaptin-binding protein involved in receptor-mediated endocytosis.* Hum Mol Genet, 2001. **10**(17): p. 1807-17.
22. Engqvist-Goldstein, A.E., et al., *The actin-binding protein Hip1R associates with clathrin during early stages of endocytosis and promotes clathrin assembly in vitro.* J Cell Biol, 2001. **154**(6): p. 1209-23.
23. Legendre-Guillemin, V., et al., *HIP1 and HIP12 display differential binding to F-actin, AP2, and clathrin. Identification of a novel interaction with clathrin light chain.* J Biol Chem, 2002. **277**(22): p. 19897-904.
24. Metzler, M., et al., *Disruption of the endocytic protein HIP1 results in neurological deficits and decreased AMPA receptor trafficking.* Embo J, 2003. **22**(13): p. 3254-66.
25. Monks, A., et al., *Feasibility of a high-flux anticancer drug screen using a diverse panel of cultured human tumor cell lines.* J Natl Cancer Inst, 1991. **83**(11): p. 757-66.
26. Oravecz-Wilson, K.I., et al., *Huntingtin Interacting Protein 1 mutations lead to abnormal hematopoiesis, spinal defects and cataracts.* Hum Mol Genet, 2004. **13**(8): p. 851-67.
27. Hyun, T.S., et al., *Hip1-related mutant mice grow and develop normally but have accelerated spinal abnormalities and dwarfism in the absence of HIP1.* Mol Cell Biol, 2004. **24**(10): p. 4329-40.
28. Bradley, S.V., et al., *Degenerative phenotypes caused by the combined deficiency of murine HIP1 and HIP1r are rescued by human HIP1.* Hum Mol Genet, 2007. **16**(11): p. 1279-92.
29. Chopra, V.S., et al., *HIP12 is a non-proapoptotic member of a gene family including HIP1, an interacting protein with huntingtin.* Mamm Genome, 2000. **11**(11): p. 1006-15.
30. Moores, J.N., et al., *Huntingtin interacting protein 1 can regulate neurogenesis in Drosophila.* Eur J Neurosci, 2008. **28**(3): p. 599-609.
31. Sun, Y., et al., *Interaction of Sla2p's ANTH domain with PtdIns(4,5)P2 is important for actin-dependent endocytic internalization.* Mol Biol Cell, 2005. **16**(2): p. 717-30.
32. Jan, Y.N. and L.Y. Jan, *Genetic control of cell fate specification in Drosophila peripheral nervous system.* Annu Rev Genet, 1994. **28**: p. 373-93.
33. Ramain, P., et al., *Novel Notch alleles reveal a Deltex-dependent pathway repressing neural fate.* Curr Biol, 2001. **11**(22): p. 1729-38.

34. Graves, C.W., et al., *Use of a cryptic splice site for the expression of huntingtin interacting protein 1 in select normal and neoplastic tissues.* Cancer Res, 2008. **68**(4): p. 1064-73.
35. Engqvist-Goldstein, A.E., et al., *An actin-binding protein of the Sla2/Huntingtin interacting protein 1 family is a novel component of clathrin-coated pits and vesicles.* J Cell Biol, 1999. **147**(7): p. 1503-18.
36. Legendre-Guillemin, V., et al., *HIP1 and HIP12 display differential binding to F-actin, AP2, and clathrin: Identification of a novel interaction with clathrin-light chain.* J Biol Chem, 2002.
37. Metzler, M., et al., *Disruption of the endocytic protein HIP1 results in neurological deficits and decreased AMPA receptor trafficking.* Embo J, 2003. **22**(13): p. 3254-3266.
38. Rao, D.S., et al., *Altered receptor trafficking in Huntingtin Interacting Protein 1-transformed cells.* Cancer Cell, 2003. **3**(5): p. 471-82.
39. Greenberg, N.M., et al., *Prostate cancer in a transgenic mouse.* Proc Natl Acad Sci U S A, 1995. **92**(8): p. 3439-43.
40. Leder, A., et al., *Consequences of widespread deregulation of the c-myc gene in transgenic mice: multiple neoplasms and normal development.* Cell, 1986. **45**(4): p. 485-95.
41. Higuchi, M., et al., *Expression of a conditional AML1-ETO oncogene bypasses embryonic lethality and establishes a murine model of human t(8;21) acute myeloid leukemia.* Cancer Cell, 2002. **1**(1): p. 63-74.
42. Kuhn, R., et al., *Inducible gene targeting in mice.* Science, 1995. **269**(5229): p. 1427-9.
43. Patel, A.A. and J.A. Steitz, *Splicing double: insights from the second spliceosome.* Nat Rev Mol Cell Biol, 2003. **4**(12): p. 960-70.
44. Gu, H., et al., *Deletion of a DNA polymerase beta gene segment in T cells using cell type-specific gene targeting.* Science, 1994. **265**(5168): p. 103-6.
45. Burge, C.B., R.A. Padgett, and P.A. Sharp, *Evolutionary fates and origins of U12-type introns.* Mol Cell, 1998. **2**(6): p. 773-85.
46. Senetar, M.A., S.J. Foster, and R.O. McCann, *Intrasteric inhibition mediates the interaction of the I/LWEQ module proteins Talin1, Talin2, Hip1, and Hip12 with actin.* Biochemistry, 2004. **43**(49): p. 15418-28.
47. Hyun, T.S. and T.S. Ross, *HIP1: trafficking roles and regulation of tumorigenesis.* Trends Mol Med, 2004. **10**(4): p. 194-9.
48. Todaro, G. and H. Green, *Quantitative Studies of the Growth of Mouse Embryo Cells In Culture and Their Development Into Established Lines.* J Cell Biol, 1963. **17**: p. 299-313.
49. Pfaffl, M.W., *A new mathematical model for relative quantification in real-time RT-PCR.* Nucleic Acids Res, 2001. **29**(9): p. e45.
50. Todaro, G.J. and H. Green, *Quantitative studies of the growth of mouse embryo cells in culture and their development into established lines.* J Cell Biol, 1963. **17**: p. 299-313.
51. Kochetov, A.V., *Alternative translation start sites and hidden coding potential of eukaryotic mRNAs.* Bioessays, 2008. **30**(7): p. 683-91.

52. Kozak, M., *Regulation of translation via mRNA structure in prokaryotes and eukaryotes.* Gene, 2005. **361**: p. 13-37.
53. Hinnebusch, A.G., *Translational regulation of GCN4 and the general amino acid control of yeast.* Annu Rev Microbiol, 2005. **59**: p. 407-50.
54. Hinnebusch, A.G., *A hierarchy of trans-acting factors modulates translation of an activator of amino acid biosynthetic genes in Saccharomyces cerevisiae.* Mol Cell Biol, 1985. **5**(9): p. 2349-60.
55. Mueller, P.P. and A.G. Hinnebusch, *Multiple upstream AUG codons mediate translational control of GCN4.* Cell, 1986. **45**(2): p. 201-7.
56. Heinemeyer, T., et al., *Databases on transcriptional regulation: TRANSFAC, TRRD and COMPEL.* Nucleic Acids Res, 1998. **26**(1): p. 362-7.
57. Suzuki, Y., et al., *Identification and characterization of the potential promoter regions of 1031 kinds of human genes.* Genome Res, 2001. **11**(5): p. 677-84.
58. Bargou, R.C., et al., *Constitutive nuclear factor-kappaB-RelA activation is required for proliferation and survival of Hodgkin's disease tumor cells.* J Clin Invest, 1997. **100**(12): p. 2961-9.
59. Jost, P.J. and J. Ruland, *Aberrant NF-kappaB signaling in lymphoma: mechanisms, consequences, and therapeutic implications.* Blood, 2007. **109**(7): p. 2700-7.
60. Wada, T., et al., *RANKL-RANK signaling in osteoclastogenesis and bone disease.* Trends Mol Med, 2006. **12**(1): p. 17-25.
61. Boyle, W.J., W.S. Simonet, and D.L. Lacey, *Osteoclast differentiation and activation.* Nature, 2003. **423**(6937): p. 337-42.